DEPARTAMENTO DE CIÊNCIAS DA VIDA

FACULDADE DE CIÊCNCIAS E TECNOLOGIA
UNIVERSIDADE DE COIMBRA

Structural, Physicochemical and Photophysical Studies of New Cyclen Derivatives and Evaluation of Their Potential as MRI and MRI/NIR Probes

Dissertação apresentada à Universidade de Coimbra para cumprimentos dos requisitos necessários à obtenção do grau de Mestre em Bioquímica, realizada sob a orientação do Professor Doutor Carlos F.G.C. Geraldes (Universidade de Coimbra)

Henrique F. Carvalho

2011

Problems in science are sometimes made easier by adding complications.

Daniel C. Dennett

Agradecimentos

Este trabalho marca o final de uma importante etapa no meu percurso académico e pessoal e portanto não posso deixar de agradecer a todos aqueles que de alguma forma estão envolvidos na sua concretização.

Ao Professor Doutor Carlos F.G.C. Geraldes por proporcionar as condições necessárias à realização deste trabalho no grupo de Bioquímica Inorgânica e Imagem Molecular do CNC, pela sua orientação e apoio crítico na realização de tarefas e discussão de resultados, e ainda pelos seus conselhos e transmissão de conhecimentos que contribuíram fortemente para o meu desenvolvimento pessoal e académico.

À Professora Doutora Maria Margarida C. A. Castro pela sua prestabilidade na resolução de problemas com que naturalmente me deparei e também pelo seu desempenho nas actividades e assuntos relativos ao nosso grupo de investigação.

Ao Doutor Emeric Wasielewski pela formação e apoio que me prestou na Unidade de RMN do CNC.

À Doutora Éva Tóth por me ter recebido na unidade "Metal Complexes for Biomedical Applications" e aos restantes elementos da sua equipa pelo seu supervisionamento.

Ao André Martins, João Teixeira e Sara Figueiredo pelo apoio e aconselhamento que me prestaram e por serem para mim bons exemplos de aspiração científica e pessoal.

Aos meus colegas Rui Carvalho, Rui Lopes e David Dias pela companhia que me proporcionaram, pela troca de ideias e por contribuírem de forma importante para o desenvolvimento do meu espírito critico. Quero agradecer ainda à Joana Gomes, Cátia Melo e Neuza Domingues pela companhia e também pela oportunidade importante de poder aprender e ensinar.

Por último, mas não menos importante, gostaria de agradecer a todos os meus amigos e familiares mais próximos, a única razão pelo qual não enumero os seus nomes é porque acredito seriamente que a sua importância dispensa qualquer tipo de referência. Posso apenas afirmar que sem ele(a)s este trabalho não existiria sequer.

Resumo

Imagem por Ressonância Magnética (IRM) é uma modalidade de imagem onde um mapa multi-dimensional de sinais de Ressonância Magnética Nuclear (RMN) de ^{1}H pertencentes a uma dada amostra é gerado. É bastante utilizada em investigação biomédica e em prática clínica pela sua capacidade de obter imagens de elevada resolução espacial de tecidos moles. Nestas, sinais RMN de ^{1}H pertencentes a tecidos constitutivos são mapeados, principalmente os de ^{1}H pertencentes a moléculas de água, dada a sua elevada abundância natural e sensibilidade da técnica ao sinal proveniente destes núcleos.

Tem havido um grande interesse em melhorar a qualidade das imagens obtidas por IRM desde a sua implementação, nomeadamente através do aumento de contraste obtido entre unidades de volume. Isto é conseguido através da administração de Agentes de Contraste (AC), compostos que modulam a intensidade de sinal das imagens obtidas. Complexos de Gd^{III} baseados em poliaminocarboxilatos cíclicos ou lineares são a classe de AC mais estudada e todos os AC disponíveis comercialmente são baseados neste tipo de complexos. No entanto, é possível aumentar a eficácia destes compostos.

Este trabalho foca-se na caracterização físico-química, fotofísica e estrutural de dois tipos de sistemas. O primeiro tipo, consistindo em derivados de cicleno com três braços pendentes metilfosfonato – DO3P, DO3P1Pr e DO3P1ol – e os seus respectivos complexos de Ln^{III} foram estudados de forma a determinar o seu potencial como AC para IRM e também para determinar qual o efeito de um braço pendente adicional nas suas propriedades físico-químicas e estruturais. Os estudos realizados permitiram avaliar qual o esquema de coordenação apresentado por estes complexos, em particular que um braço pendente adicional propionato ou propanol não estão envolvidos na coordenação do ião Ln^{III} central quando outros três braços pendentes metilfosfonato o estão.

O segundo tipo de sistema, consistindo em derivados de cicleno com braços pendentes piridina-*N*-óxido – DO2A-*trans*-$(py^{NO})_2$ – e respectivos complexos de Ln^{III} foram também estudados e as suas propriedades físico-químicas, fotofísicas e estruturais foram analisadas. O potencial destes complexos como sondas de imagem para IRM e infra-vermelho próximo foram avaliados, nomeadamente a sua eficácia como AC de IRM e a capacidade sensibilizar luminescência de lantanídeos. Os resultados obtidos indicam que este sistema é um candidato potencial para estas aplicações uma vez que apresenta estabilidades termodinâmica e cinética favoráveis e que apresenta a capacidade de sensibilizar luminescência de iões Ln^{III} (Ln^{III} = Eu^{III}, Tb^{III}, Yb^{III}, Nd^{III}, Ho^{III} and Pr^{III}).

Abstract

Magnetic Resonance Imaging (MRI) is an imaging modality where a multi-dimensional map of ^{1}H Nuclear Magnetic Resonance (NMR) signals from a given sample is generated. It is widely used in biomedical research and clinical practice due to its ability to obtain high spatial resolution imaging of soft tissues. Here, ^{1}H NMR signals from constitutive tissues are mapped, mainly the ones from water molecules, due to their high natural abundance in soft tissues and high relative sensibility of their NMR signal.

There has been a great interest in increasing the quality of the obtained MRI images since its implementation as an imaging modality, namely through contrast enhancement between volume units. This can be done by administration of Contrast Agents, compounds that modulate the signal intensity of the obtained images. Gd^{III} complexes based on macrocyclic or linear aminocarboxylates are the most studied class of CAs and all the commercially-available CAS are based on these complexes. However, there is the possibility of increasing their efficiency and much effort has been made in this direction.

This work is focused on the structural, photophysical and physicochemical properties of two types of systems. The first type, cyclen derivatives with three methylphosphonate pendant arms - DO3P, DO3P1Pr and DO3P1ol – and their respective Ln^{III} complexes were studied in order to determine their potential as MRI CAs and also to determine the role of additional pendant arms in their structural and physicochemical properties. The studies performed allowed for determination of the coordination scheme presented by these complexes, namely that an additional propionate and propanol pendant arms do not participate in central Ln^{III} ion coordination when three methylphosphonate pendant arms are also involved.

The second type, a cyclen derivative with pyridine-*N*-oxide pendant arms – DO2A-*trans*-$(py^{NO})_2$ – and its respective Ln^{III} complexes were also studied and their physicochemical, photophysical and structural properties analyzed. The potential of these complexes as bimodal MRI and Near-Infrared Imaging probes was evaluated, namely its efficiency as a MRI CAs and the capacity to sensitize lanthanide luminescence. The obtained results indicate that this system is a potential candidate for such applications since its shows suitable thermodynamic and kinetic stabilities and the ability to efficiently sensitize Ln^{III} luminescence (Ln^{III} = Eu^{III}, Tb^{III}, Yb^{III}, Nd^{III}, Ho^{III} and Pr^{III}).

Keywords: MRI CONTRAST AGENTS; LANTHANIDE(III) COMPLEXES; IMAGING PROBES

Contents

CHAPTER 1

General Introduction

1.1 - Magnetic Resonance Imaging

Magnetic Resonance Imaging (MRI) is an imaging modality where a map of ^{1}H Nuclear Magnetic Resonance (NMR) signals from a given sample is generated. It is widely used in biomedical research due to its ability to obtain high spatial resolution imaging of soft tissues.[1]. Here, ^{1}H NMR signals from constitutive tissues are mapped, mainly the ones from water molecules. The water ^{1}H nuclei are easily detected due to their high natural abundance in soft tissues and high relative sensibility of their NMR signal, given by:

$$\omega = \gamma_H B_0 \quad (1)$$

where ω is their Larmor frequency, which is dependent on the proton giromagnetic ratio γ_H and on the applied homogenous magnetic field B_0. The three dimensional spatial encoding is obtained through the application of linearly induced magnetic field gradients over the main homogenous magnetic field, thus for each proton nucleus in the sample we have:

$$\omega = \gamma_H(B_0 + G.r_i) \quad (2)$$

where r_i represents the position of a given nucleus and G the vector representing the total gradient amplitude and direction (either G_x, G_y or G_z). This can be used for selectively obtain images from a slice portion of the sample. The two-dimensional image can then be obtained by either Back Projection Imaging or Fourier Transform Imaging, the latter being most commonly used.[2]

In order to obtain clearly visible structures it is necessary to generate contrast between two image volume units (voxels). The Signal Intensity (SI) of each image voxel after each spin-echo sequence is dependent on four main factors: ^{1}H nuclei density (ρH), longitudinal (T_1) and transversal (T_2) relaxation times and the water diffusion coefficient *f*(v). A simplified expression is given by:

$$SI = \rho H f(v)\left[1 - exp\left(\frac{-TR}{T1}\right)\right] exp\left(\frac{-TE}{T2}\right) \quad (3)$$

where TR is the time between two successive repetitions of the spin echo pulse sequence and TE is the time between the first 90° pulse and the maximum of the acquired echo.[3] By varying these two parameters the resulting image has different contributions of T_1 or T_2 and therefore

it is possible to obtain either T_1-weighted (with shorter TR values) or T_2-weighted (increased TE values) Images. Conventional T_1- and T_2-weighted Imaging modalities can be used to detect certain pathological processes, since either T_1 or T_2 times of a specific tissue can change as a result of certain biochemical events, such as variations in pH, temperature, salt or fat content. It is also possible to obtain T_2* images with Gradient Echo Sequences (T_1 and T_2 images are obtained with Spin Echo Sequences). These three types of image are the most common in clinical practice, but there are also other variants such as: Magnetic Resonance Angiography for observation of the circulatory system; Spin Density-Weighted Imaging, with the resulting SI reflecting local ρH or; Diffusion Imaging where water diffusion rates *f*(v) are measured (Fig. 1. 1).[4]

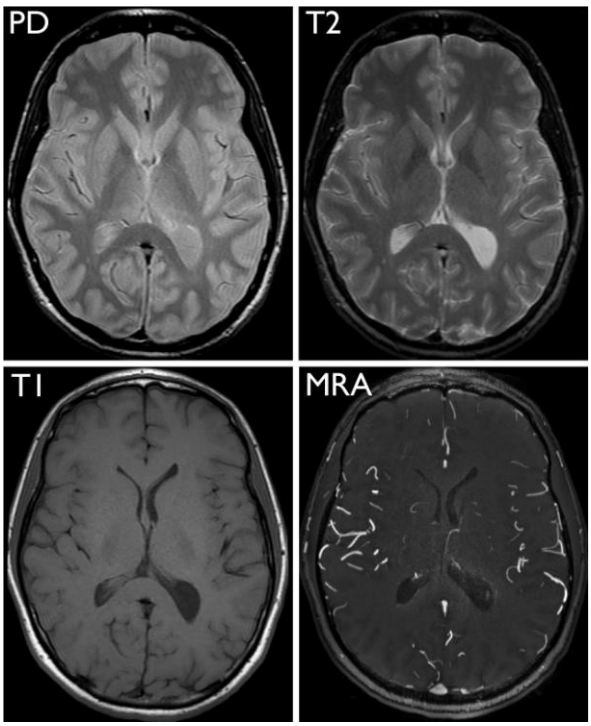

Fig. 1. 1: MRI of human brain. PD – Spin Density-Weighted Imaging; T1 – T_1-weigthed Imaging; T2 - T_2-weigthed Imaging; MRA – Magnetic Resonance Angiograph (Adapted).[2]

Another very important type of MRI is Functional Magnetic Resonance Imaging (fMRI), where physiological processes are observed *in vivo* (Fig. 1. 2). It is possible, for example, to measure the hemodynamic response related to neural activity in the central nervous system. This technique is responsible for major developments in the field of Neuroimaging, being currently the main technique employed in the field of brain mapping and Pharmacological MRI (phMRI), together with Electroencephalography (EEG) and Positron Emission Tomography (PET).[5] The underlying principle is the Blood-Oxygen-Level Dependence (BOLD) effect that

leads to changes in T_1 or T_2* images due to variations in deoxyhemoglobin levels.[6] These are mainly related to increased metabolic rate in regions of active neurons with concomitant increased blood-flow. In the case of phMRI, the pharmacological properties of a specific drug if measured with variations in the BOLD effect.[7]

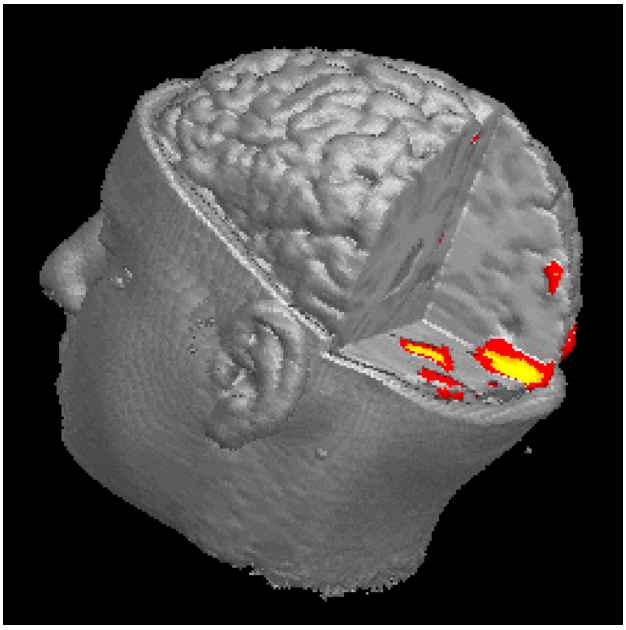

Fig. 1. 2: 3D fMRI image of human brain activation (adapted).[8]

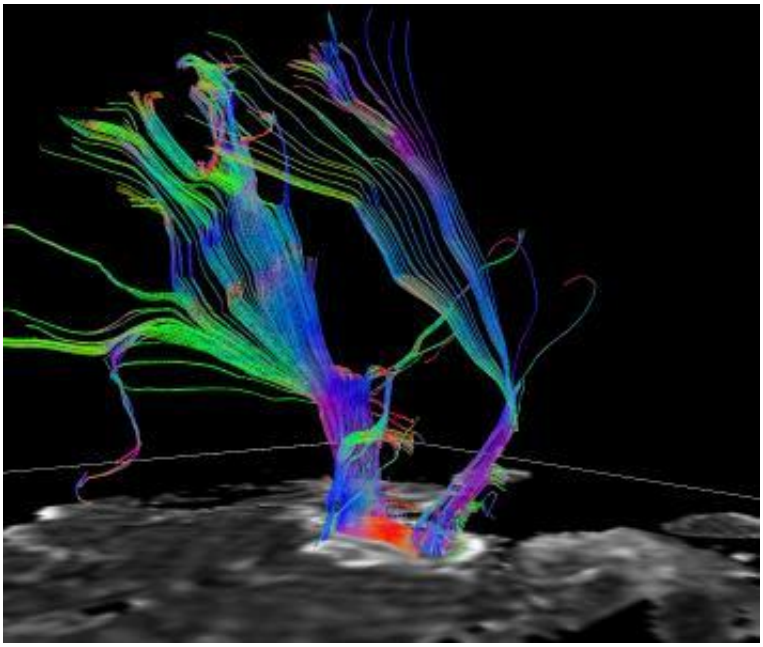

Fig. 1. 3: Visualization of a DTI measurement of a human brain (adapted).[9]

fMRI is usually associated only the BOLD effect, but other techniques are also used, such as: Magnetic Resonance Spectroscopic Imaging (MRSI),[10] where spectroscopic analysis is

performed on each voxel; Diffusion tensor Imaging,[11] a recently developed type of Diffusion imaging where water diffusion anisotropies are detected, allowing for brain tractography or (Fig. 1. 3); Real-Time Metabolic Imaging, where direct detection of metabolites is performed (Fig. 1. 4).[12]

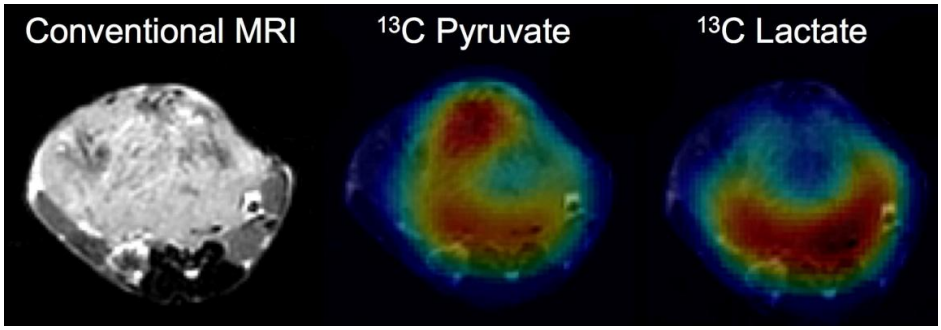

Fig. 1. 4: Metabolic Imaging of hyperpolarized ^{13}C pyruvate.[13]

1.2 – Gd^{III} Complexes as MRI Contrast Agents

I) General Features

There has been a great interest in increasing the quality of the obtained MRI images since its implementation as an imaging modality. Since the observed SI is dependent on the relaxometric properties of the water protons, one of the most common approaches has focused on their manipulation. Other strategies have focused on the technical aspects of this imaging modality, such as the development of higher imaging fields, and will not be discussed here.

A paramagnetically-induced relaxation of water protons is one way to decrease its relaxation times. This can be achieved by the presence of paramagnetic agents in the vicinity of water molecules such as solute metal cations. This type of compounds are designated T_1-Contrast Agents (CA), as they have an effect mainly on the longitudinal relaxation rates of water molecules (Fig. 1. 5). The list of candidates has been based on metal ions that contain high magnetic moments and suitable relaxation times of the respective unpaired electrons, such as the Gd^{III} ion (the theoretical aspects dealing with the relaxometric properties of Gd^{III} ions will be discussed in section II). However, it cannot be administrated as a free ion in clinical applications due to its severe toxicity, since its size is very similar to the Ca^{II} ion but with an higher charge, leading to a disruption of Ca^{II}-mediated signaling.[14,15]

One way to overcome the toxicity of free Gd^{III} ions is to bind them to compounds that act as strong chelates to form Gd^{III} complexes. For safety reasons, this complexes need to be stable for a long period of time when injected, so that the amount of released Gd^{III} remains minimal during circulation and excretion time. However, the conjugation of Gd^{III} with polydentante ligands leads to a decrease in its efficiency to transmit magnetic information to the bulk water molecules. This has led to the a large expansion in the field of CAs, since there is a need to create new compounds that can be as safe as effective in enhancing the image quality of MRI images.

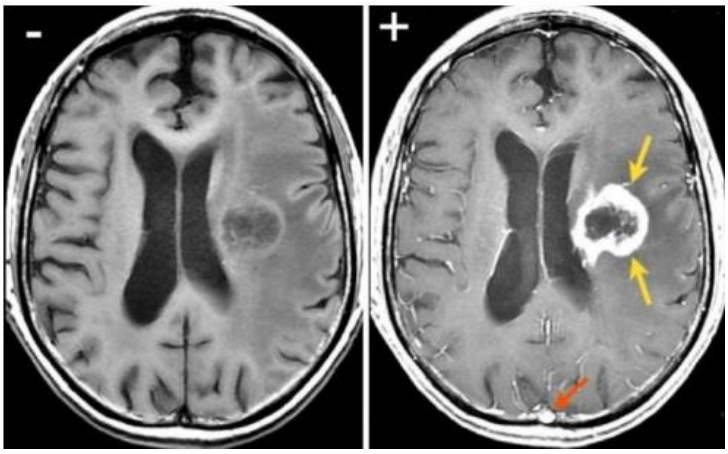

Fig. 1. 5: Brain tumor images in the absence (-) or presence (+) of CAs. Yellow arrows indicate blood brain barrier disruption (Adapted).[2]

So far, the majority of commercially-available T_1-CAs are based on Gd^{III} complexes (Fig. 1. 6). These compounds show desirable thermodynamic stability and kinetic inertness and can help in the diagnosis of certain kinds of pathologies. However, their efficiency is very low in relation to the theoretical upper bound for the current magnetic fields used in biomedical hardware.[16] The structure of commercially-available CAs is based on two types of polydentate aminocarboxylate ligands, acyclic (DTPA and DTPA-like ligands - Diethylenetriaminepentaacetic acid) and macrocyclic (DOTA and DOTA-like ligands - 1,4,7,1 O-tetraazacyclododecane-N,N',N",N'"-tetraacetic acid). Their structural properties have been extensively studied, leading to a better understating of the parameters involved in their efficiency as CAs. Parallel studies focused on new classes of compounds have also produced interesting and important results, such as AAZTA (6- amino-6-methylperhydro-1,4-diazepine-1,4,N^6,N^6 -tetraacetic acid) and HOPO (3-hydroxy-2-oxo-1,2-dihydropyridine- 4-carboxyamide) ligands.[17,18] Due to the scope of this work, in section III and IV, special emphasis will be given only to the structural and physicochemical properties of macrocyclic ligands such as DOTA and DOTA analogues and their

respective metal complexes. Difficulties in the design of new CAs arise in terms of the thermodynamic stabilities of such compounds, and even more important, their kinetic inertness.[15] These properties are closely linked to the possibility of transmetallation/transchelation processes, where the Gd^{III} can either be replaced by an endogenous ion (such as Zn(II) or Ca(II)) or bind to other chelating species (such as citrate, transferrin, phosphates, etc).[14] The encountered difficulties led to a more rational approach in the design of new CAs and will be discussed in section V.

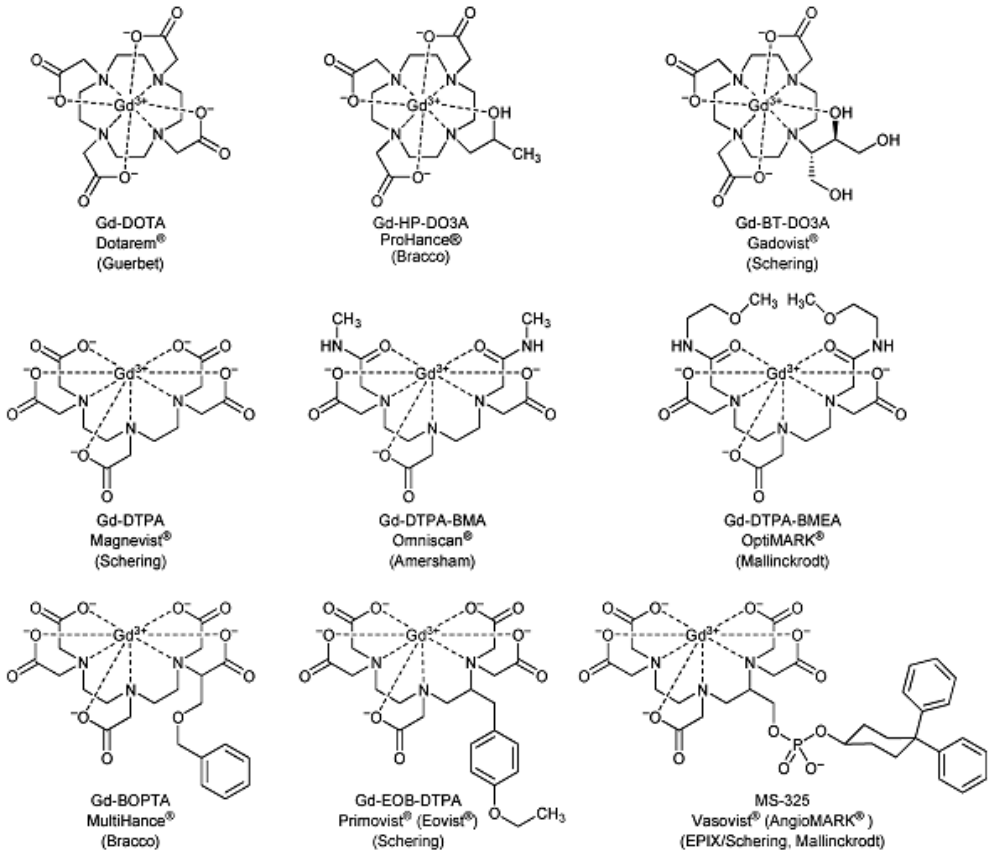

Fig. 1. 6: Commercially-available CAs (adapted).[16]

II) Parameters governing relaxivity

The efficiency of a CA is measured in terms of a parameter named relaxivity (r_i), defined as the capacity of a CA to decrease the relaxation times of water protons. Formally, the addition of a paramagnetic solute causes an increase of longitudinal and transversal relaxation rates of the solvent nuclei:[19]

$$\left(1/T_1\right)_{obs} = \left(1/T_i\right)_p + \left(1/T_i\right)_d = r_i[M] + \left(1/T_i\right)_d \quad (4)$$

where T_{iobs} is the observed longitudinal (i=1) and transversal (i=2) relaxation time, T_{ip} and T_{id} are the paramagnetic and diamagnetic contributions, respectively, [M] is the concentration (in mM) of the paramagnetic species. The longitudinal (r_1) or transversal (r_2) relaxivity is defined as the slope of R_{ip} ($R_{ip} = 1/T_{ip}$) as a function of the paramagnetic species concentration, [M]. Special emphasis is given here to longitudinal relaxivity (expressed in $mM^{-1}s^{-1}$) that corresponds to the capacity of 1 mM of a CA (*e.g.* Gd^{III}-DOTA) to increase the longitudinal relaxivity of water protons. The relaxivity of a CA is dependent not only on its concentration but also on the mechanisms governing the transmission of the paramagnetic information to bulk solvent molecules.

The transmission of magnetic information from the metallic centre to the nuclei of water molecules is the result of a magnetic hyperfine interaction between the nuclear spins **I** and the electron spin **S**, with the corresponding Hamiltonian being:

$$\mathcal{H}_{hf} = IAS \quad (5)$$

where A is the operator corresponding to the hyperfine coupling tensor. This interaction involves two components (*i*) the dipole-dipole interaction between the nuclear magnetic moment and the electrons outside the nucleus and (*ii*) the scalar interaction between the nuclear magnetic moment and the electron spin density at the nucleus.[20] The relaxation rates of the nuclear spin are caused by time-dependent fluctuations of the hyperfine interaction due to (*i*) rotational motion of the molecule bearing both paramagnetic centre and observed nucleus (intramolecular relaxation) and (*ii*) translational motion between the paramagnetic centre and the nucleus in different molecules (intermolecular relaxation).

The intramolecular relaxation, or *inner-sphere* relaxation, is characterized by a rotational correlational time and the equations used to describe it are based on the Generalized Solomon-Bloembergen-Morgan (GSBM) model. The intermolecular motion is based on the translational diffusion, or *outer-sphere* relaxation, and is characterized by a translational correlation time. The equations dealing with this parameter were developed by Freed and Ayant.[20]

Taken together, the total relaxivity r_i (i= 1, 2) is the sum of inner-sphere relaxivity r_i^{is} and outer-sphere relaxivity r_i^{os} (Fig. 1. 7):

$$r_i = r_i^{is} + r_i^{os}(+r_i^{2nd}) \qquad (6)$$

The inner-sphere contribution corresponds to the water molecules directly bound to the metallic centre in exchange with the bulk solvent and the outer-sphere contribution corresponds to the unbound water molecules. In some cases a second-sphere contribution r_i^{2nd} has to be considered, corresponding to water molecules that are bound to the complex through hydrogen bonds.[21] However, a more formal approach to this contribution is difficult since it cannot be easily differentiated from the outer-sphere contribution.

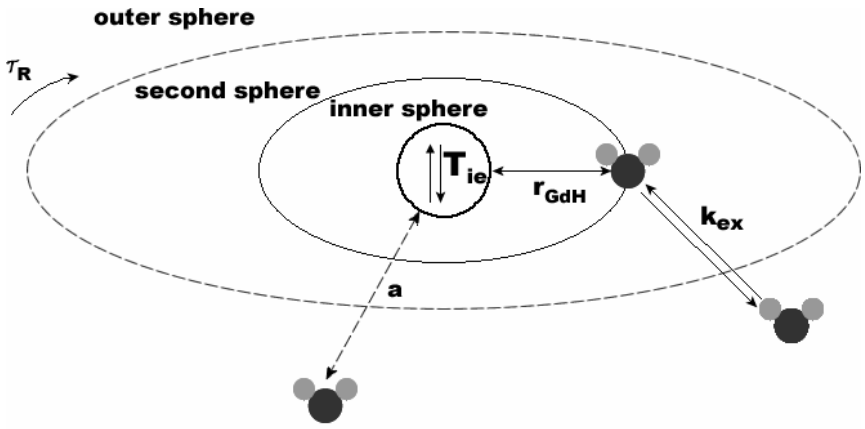

Fig. 1. 7: Schematic representation of the parameters involved in longitudinal relaxivity.

The equations contained in the GSBM model provide a simple analytical treatment of the relaxivity rates of Gd(III) complexes (despite some recent modifications and refinements) and are widely used to explain the physical properties of small complexes such as Gd^{III}-DOTA at current imaging fields. They can provide a good approximation to the underlying mechanisms when the inner-sphere contribution is predominant to the total relaxivity, as it is the case of these complexes.[20]

Considering the inner-sphere contribution to the total longitudinal relaxation r_1^{is}, the main parameters involved are: the number of water molecules coordinated to the metallic ion (q); the rotational correlation time of the molecule (τ_R) (molecular tumbling) and; the residence time of water molecules in the first coordination sphere (τ_M) or water exchange rate k_{ex} (k_{ex} = $1/\tau_M$). Therefore:

$$r_1^{is} = \frac{1}{1000} \times \frac{q}{55.55} \times \frac{1}{(T_{1M}^H + \tau_M)} \qquad (7)$$

where T_{1M}^{H} is the proton longitudinal relaxation time in the inner-sphere that is dependent on dipole-dipole T_{1M}^{dd} and scalar T_{1M}^{sc} interactions as well as on the "Curie relaxation" T_{1M}^{curie} (in systems with fast electron relaxation and slow molecular tumbling):

$$\frac{1}{T_{1M}^{H}} = \frac{1}{T_{1M}^{dd}} + \frac{1}{T_{1M}^{sc}} + \frac{1}{T_{1M}^{curie}} \qquad (8)$$

With,

$$\frac{1}{T_{1M}^{dd}} = \frac{2}{15}\left(\frac{\hbar^2\gamma_I^2\gamma_S^2 S}{r_{IS}^6}\right) S(S+1)\left(\frac{\mu_0}{4\pi}\right)^2 \times [3J(\omega_I, \tau_{d1}) + 7J(\omega_S, \tau_{d2})] \qquad (9)$$

$$\frac{1}{T_{1M}^{sc}} = \frac{2S(S+1)}{3}\left(\frac{A}{\hbar}\right)^2 J(\omega_S, \tau_{sc2}) \qquad (10)$$

$$\frac{1}{T_{1M}^{curie}} = \frac{\frac{\omega_I^2 {\mu_{eff}}^4 \left(\frac{\mu_0}{4\pi}\right)^2}{(3k_B T)^2}}{5r_{IS}^6}(4J(0, \tau_2) + 3J(\omega_I, \tau_R)) \qquad (11)$$

where r_{IS} is the internuclear electron spin-nuclear spin distance, $A/\hbar$ the scalar coupling constant (rad.s^{-1}), γ_I and γ_S the nucleus and electron giromagnetic constants, respectively, S the spin quantum number of the metallic ion (for Gd^{III} S= 7/2) and ω_I and ω_S the Larmor frequencies of the nucleus and the electronic spin. The spectral density is given by $J(\omega_I, \tau_R) = \frac{\tau}{1+\omega^2\tau^2}$ and the effective magnetic moment in the case of Ln^{III} ions corresponds to $\mu_{eff} = g_e\mu_B\sqrt{S(S+1)}$. The correlation time τ_{di} and τ_{sci} (i=1, 2) are defined as:

$$\frac{1}{\tau_{d1}} = \frac{1}{\tau_R} + \frac{1}{\tau_M} + \frac{1}{T_{ie}} \qquad (12)$$

$$\frac{1}{\tau_{sci}} = \frac{1}{\tau_M} + \frac{1}{T_{ie}} \qquad (13)$$

Where T_{ie} is the longitudinal (i=1) and transversal (i=2) electron spin relaxation rate:

$$\frac{1}{T_{1e}} = \frac{2\Delta^2}{50}(4S(S+1) - 3)\left(\frac{\tau_v}{1+\omega_S^2\tau_v^2} + \frac{4\tau_v}{1+\omega_S^2\tau_v^2}\right) \qquad (14)$$

$$\frac{1}{T_{2e}} = \frac{2\Delta^2}{50}(4S(S+1) - 3)\left(3\tau_v + \frac{5\tau_v}{1+\omega_S^2\tau_v^2} + \frac{2\tau_v}{1+\omega_S^2\tau_v^2}\right) \qquad (15)$$

with Δ^2 being the mean squared fluctuation of the zero field splitting (s^{-2}) and τ_v the correlation time for instantaneous distortions of the coordination polyhedron.

Considering that r_{IS} does not change with time, the time dependence of the SI interaction is entirely due to the rotation of the molecule characterized by the rotational correlation time $\tau_R^{(2)}$ or, in a more formal way, for isotropic rotation of the molecule (not taking into account electronic relaxation due to zero-field splitting):

$$\tau_R^{(2)} = \frac{1}{6D_R} \qquad (16)$$

where D_R is the rotational diffusion constant $D_R = \frac{k_B T}{f_r}$, and in the case of a sphere:

$$f_{r,sphere} = 8\pi\eta R^3 \qquad (17)$$

with η being the dynamic viscosity ($N.s/m^2$), R the molecule radius, K_B the Boltzmann constant and T the absolute temperature. The value of τ_R has also a monoexponential temperature dependence with an activation energy E_R:

$$\tau_R = \tau_R^{298} exp\left[\frac{E_R}{R}\left(\frac{1}{T} - \frac{1}{298.15}\right)\right] \qquad (18)$$

Assuming that the water residence time follows the Eyring equation:

$$\frac{1}{\tau_M} = \frac{k_B T}{h} exp\left(\frac{\Delta S^{\ddagger}}{R} - \frac{\Delta H^{\ddagger}}{RT}\right) = \frac{k_{ex}^{298} T}{298.15} exp\left(\frac{\Delta H^{\ddagger}}{R}\left(\frac{1}{298.15} - \frac{1}{T}\right)\right) \qquad (19)$$

where $\Delta S^{\ddagger}$ and $\Delta H^{\ddagger}$ are the activation entropy and enthalpy of the water exchange process, respectively.

The equations describing the second-sphere contribution r_i^{OS} will not be presented here since there is no clear formal description of the occurring processes.[20] However, the main parameters involved in the outer-sphere contribution are the correlation time of electronic spin relaxation τ_S; the minimum distance between solute ion and bulk solvent molecules (a) and; the relative diffusion constant solute-solvent (D) (Fig. 1. 7).[22]

The choice of the Gd^{III} as an ideal candidate for MRI applications, among other lanthanide and transition metal ions, is due to its high effective magnetic moment μ_{eff} (7.94 μB) and slow relaxation rates of the unpaired electrons (10^{-8}-10^{-9} s) as a result of the seven unpaired

electrons ([Xe] $4f^7 5d^1 6s^2$) and to the symmetric S-state. These physical properties are in close tune with the spatiotemporal events occurring during the transfer of the paramagnetic effect to water protons.

In conclusion, several parameters are involved in the efficiency of solute metal ions in increasing the relaxation rates of solvent water protons. Due to safety reasons, the Gd(III) ions has to be bound to organic chelates, affecting some of these parameters: decrease of q value, increase of τ_M, r_{IS}, τ_R, a and D. It is possible to further manipulate these parameters by choosing the appropriate ligands. Generally speaking, by increasing the volume of the molecule (therefore increasing R) the value of τ_R will also increase, leading to higher relaxivity values (↑R; ↑τ_R; ↑r_i). Also, since τ_M of Gd(III) complexes is up to two orders of magnitude higher than in Gd^{III} aqua-ion (1.2 ns), systems with lowest possible value of τ_M are also preferable (↓τ_M; ↑r_1^{is}; ↑r_i). The same applies for the highest possible value of q (↑q; ↑r_1^{is}; ↑r_i). The structural parameters affecting these properties will be discussed below, with some considerations about the design of new ligand molecules.

III) Structural parameters of Ln^{III} complexes based on DOTA and DOTA analogues

The DOTA ligand (1,4,7,10-tetraazacyclododecane-1,4,7,10-tetraacetic acid)consists of a cyclen macrocycle with four acetate pendant arms bound to the four ring nitrogen atoms.[23-26] The high thermodynamic stability and kinetic inertness presented by this compound are the result of a good match between the size of the metal Ln^{III} ions and the macrocycle cavity. The eight coordination sites of the central ion are occupied by four nitrogen atoms from the macrocycle and four oxygen atoms from the pendant arms. One coordination site is left for water molecule coordination. These two sets of coordination atoms form two planar and parallel planes, N_4 and O_4, with the central metal ion between the two. The result is a squared antiprimstatic geometry. The gauche conformations of the macrocycle ethylene groups form a five-membered metallacycle with two possible configurations, δ or λ, leading to two possible square [3,3,3,3] conformations of the macrocycle, δδδδ (g^+) and λλλλ (g^-).[16,24] Also, the acetate pendant arms may occupy two orientations in relation to the macrocycle, Δ (clockwise) or Λ (counterclockwise). The interconversion of both ring (δ↔λ) and acetate pendant arm (Δ↔Λ) originates four stereoisomers or two pairs of diastereoisomers: Δδδδδ/Λλλλλ and Δλλλλ/Λδδδδ. Theoretical calculations have indicated that the arm rotation pathway is a one-step process with simultaneous rotation of the four acetate arms.[27]

There are differences in the structural parameters of both diastereoisomers (Fig. 1. 8). One of them is the rotation angle ω formed between the N_4 and O_4 planes. In the Δλλλλ/Λδδδδ

isomer, this angle is ~40°, being close to an ideal 45° of a perfect antiprism, therefore being denoted Square Antiprismatic (SAP) isomer. In the case of the ΛλλλλΛ/ΔδδδδΔ isomer, the angle is ~24° leading to a distorted geometry and therefore being denoted Twisted Square Antiprismatic (TSAP) isomer. In Ln^{III}-DOTA complexes they are present in different abundances due to their different stabilities. The SAP isomer is present in higher abundance than the TSAP isomer and for this reason they are also denoted **M** (from Major) or **m** (from minor) isomers, respectively.[25] However, in Ln^{III} complexes of DOTA-like derivatives the SAP/TSAP ratio can vary. The reasons for this are the shape of ligand cavity and the size of the Ln^{III} ion, as it has been shown in several studies. [26,28,29]

Ligand cavity size is mostly dependent on the degree of rotation of the pendant arms, since the distance between the N_4 and O_4 planes are dependent on their orientation. For larger Ln^{III} ions, such as La^{III} or Ce^{III}, the cavity is expanded by elongation of the distance between planes (*d*) and the TSAP arrangement is preferred. As the ionic radius decreases along the Lanthanide series, the distance between planes decreases and the SAP arrangement becomes predominant.[16]

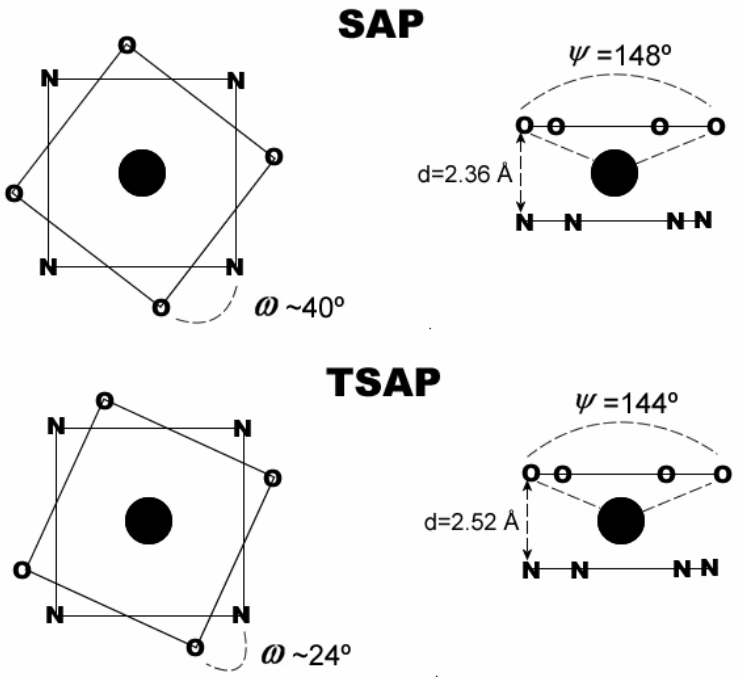

Fig. 1. 8: Structural parameters in SAP (top) and TSAP (bottom) isomers. Left – top view; Right – side view

Another important structural parameter is the opening angle ψ (O-Ln-O angle between transannular oxygen atoms), which is dependent on the distance between N_4 and O_4 planes and the central ion radius (and consequently in the type of isomer). A relationship between the ψ angle and the number of bound water molecules has been shown: If the angle is smaller

than 135° no water molecule is coordinated to the central ion; if it is bigger than 145° the water molecule can be substituted for another group, such as a carboxylate group.[30] The effect of ion size in the ψ angle can be seen in the case of DOTA complexes of Pr^{III} (SAP isomer) and Ce^{III} (TSAP isomer), where the ψ angle is found smaller for the latter complex (ψ = 148°→ 144°).[26] The importance of the ψ angle is also demonstrated in the case of DOTP and $DOTP^{R}$ derivatives, where all carboxylic functions of DOTA are replaced by phosphonic or phosphinic acid groups, respectively.[31,32] The bulky phosphorous acid pendants together with the tetrahedral geometry of the phosphorous atom are most likely the reasons for the exclusive TSAP isomerism presented by the respective complexes, leading to a decrease of the ψ angle and an increase in the distance between N_4 and O_4 planes. This leads to the expulsion of water molecules from the inner sphere of coordination, except for some La^{III} and Ce^{III} complexes.[33,34]

In sum, three structural parameters are crucial for the understanding of the physicochemical properties of Ln^{III} complexes concerning their efficiency as CAs, namely the rotation angle ω, the distance between the N_4 and O_4 planes (d) and the O-Ln-O angle ψ. Together they can provide information about the steric crowding around the capped position of the central Ln^{III} ion. Since these three parameters are dependent on ligand type and central Ln^{III} ion, by manipulating the structure of the ligands it is possible to optimize the physicochemical properties of new Gd^{III} complexes.

IV) Thermodynamic and kinetic stabilities of Gd^{III}- DOTA and DOTA-like complexes

The thermodynamic stability of Gd^{III}-DOTA is high, with log K_{GdL} values ~24 (being the highest among commercially-available CAs). Through modifications of parent DOTA backbone this values can vary. Substitution of the acetate pendant arms by amide functions leads to a significant decrease of log K_{GdL} to ~13-15.[35] This is also observed with the replacement of the acetate pendant arms with methylphosphinic functions.[30] However, the same kind of replacement but with methylphosphonate functions leads to an increase of complex stability.[32] This is due to a variation in nitrogen basicity, where in the earlier cases nitrogen basicity decreases, in the former it increases. This effect, however, is dependent on the number of pendant arm substitutions since it has been observed that a replacement of only one (or two) acetate pendant arms with a phosphorous-containing or alcohol functions does not lead to such a dramatic decrease in complex stability.[36,37] Other type of modifications that have minimal effects on nitrogen protonation constants can be observed in the case of DOTASA, where one of the pendant Cα atom is functionalized with a carboxymethyl substituent, with its Ln^{III} complexes showing similar thermodynamic stabilities with parent DOTA complexes.[38]

Another structural feature involved in thermodynamic stability is the increase of chelate ring size. This can be done by elongation of the polyaza ring or of the pendant arm. In the first case, complexes of the ligand TRITA have lower thermodynamic stability than DOTA complexes.[39] As for the elongation of pendant arms, DO3ACE complexes also show lower thermodynamic stabilities.[40] The main consequence of lower thermodynamic stability of Gd^{III} complexes is a decrease in ligand specificity for Gd^{III} ions that would lead to different species distributions in the presence of other endogenous metal ions.

Kinetic stability of DOTA and DOTA-like Ln^{III} complexes is very high, as measured through proton- and metal-assisted (such as endogenous Zn^{II} and Ca^{II}) decomplexation rates. In these cases the caging of the central metal ion leads to very slow decomplexation rates, typically less than 10% over a period of 3 days for Zn^{II}-assisted decomplexation. In the case of substitution of DOTA pendant arms with amide or methylphosphinic groups the kinetic inertness increases, while remaining very similar to the one of DOTA in the case of methylphosphonate substitution. Increase of one portion of the tetraaza ring - as in TRITA complexes - leads to a small decrease in complex inertness and removal of one pendant arm - as in DO3A complexes - leads to a decrease of Ln^{III} complexes inertness.[16,41]

In sum, DOTA and DOTA-like complexes have very high thermodynamic and kinetic stabilities and thus are good models for ligand optimization. Different ligand structural modifications have an impact on the resulting complex stability, and it has been observed that although some modifications decrease thermodynamic stability, the opposite is observed with an increase in kinetic inertness. Ligand design has to take into account these facts and special emphasis has to be given to kinetic inertness over thermodynamic stability, as this physicochemical property is more relevant for clinical applications.[15]

V) Ligand Modulation

Ligand modulation is based on structural modifications of the aminocarboxylate backbone. Based on parent DOTA ligand, three types of modifications can be performed: *i)* modifications at the level of the macrocycle ring, with variations in the number of methylene groups or introduction of new functions that lead to differences in cavity size and shape; *ii)* pendant arm removal (usually only one), forming heptadentate ligands or; *iii)* modifications at the level of the pendant arms, such as functional group substitution, arm elongation, introduction of linkers, spacers, targeting moieties or reactive functions for further functionalization.[16] Special emphasis will be given to the last two types of modifications since they are the most common approaches in the rational design of new CAs. These kinds of modifications affect primarily the

structural features presented by the respective Gd^{III} complexes, as discussed above, and will be translated in the presented physicochemical properties concerning their relaxivity and stability:

Number of coordinated water molecules (q)

The number of coordinated water molecules (hydration number) in a Gd^{III} complex is dependent on the steric constraints around the O_4 plane, translated in a decrease of the opening angle ψ. In all commercially-available CAs and in most DOTA derivatives, q=1. Replacement of carboxylate functions in the pendant arms by bulky functions leads to q=0. This is the case for tetraphosphorus acid derivatives, with replacement by phosphonate (DOTP) or phosphinic ($DOTP^R$) functions. In some cases, the increase of chelate ring size also leads to q=0, as in the case of mono-amide triacetate derivatives of DOTA.[42]

An increase to q=2 is possible with heptadentate or hexadentate ligands.[43] The decrease of the number of pendants would lead to an additional free position for water coordination. However, formation of ternary complexes, either with small bidentate ligands (*e.g.* acetate, lactate, citrate, etc) or lateral chain protein residues (*e.g.* HSA) leads to the expulsion of bound water molecules from the inner sphere. This is related to the *cis* coordination geometry of water molecules in these systems. A way to avoid this drawback in kinetic stability is to design heptadentate or hexadentate ligands that would only allow the coordination of water molecules in *trans* positions, as demonstrated for HOPO and DTTA derivative complexes.[44,45]

Residence time of coordinated water molecules (τ_M)

The value of τ_M, or k_{ex} ($k_{ex} = 1/\tau_M$), is extensively dependent on complex structure, as it is influenced by various factors: *i)* overall charge of the complex; *ii)* solvent accessibility; *iii)* steric crowding around the coordination site; *iv)* kind of isomerism; *v)* flexibility of the coordination cage and; *vi)* water exchange mechanism. By taking into account the τ_M values found for parent Gd^{III}-DOTA complexes (τ_M = 244 ns), it is possible to analyze the effects of structural modifications in each of the above mentioned parameters.

In terms of complex charge, τ_M can vary up to three orders of magnitude between negatively (*e.g.* Gd^{III}-DO3AP, τ_M = 14 ns), neutral (*e.g.* Gd^{III}-DO3A, τ_M = 160 ns) and positively charged species (*e.g.* Gd^{III}-DOTAM, τ_M ~ 3.06 ms).[16] It is thought that the water accessibility surface can also be influenced by hydrophobic/hydrophilic interactions between substituent groups of amide of phosphinic derivatives of DOTA, leading to changes in k_{ex}.[16]

The steric crowding around the coordination site plays a key role in the value of τ_M, and its modulation can be achieved by increasing chelate ring size, either on the tetraaza ring (TRITA)

or pendant arm (DO3A-py^{NO}), or by replacement of one acetate pendant arm with a bulky substituent.[39,41] The increase of electronic density near the coordination site leads to a controlled destabilization of the Ln-OH_2 bond thus favoring the expulsion of the bound water molecule. Another factor to be taken into account is the kind of isomerism presented by the complex. In TSAP isomers the value of τ_M is up to two orders of magnitude smaller than in SAP isomers.[46] This can be explained by an increased steric crowding around the O_4 plane. However another parameter may be at play, namely the flexibility of the coordination cage. While in some cases TSAP isomers (with increased flexibility over SAP isomers) show very small values of τ_M, the opposite has been observed for Gd^{III}-DO3A-py^{NO} complexes showing an exclusive SAP isomerism (this will be further discussed in Chapter 4).

Concerning the mechanism of exchange of bound water molecules, the associative type leads to a significant decrease of τ_M over the dissociative type. This is due to the rate-determining step in each case. In the associative type there is the formation of an intermediary with q=2, while the dissociative type involves the dissociation of the bound water molecule. One good example is the case for Gd^{III}-DO3A (τ_M= 160 ns) with an associative mechanism over Gd^{III}-DOTA (τ_M = 244 ns) with a dissociative, despite the additional water molecule present in former case. [16]

Second-sphere contribution (q_{ss} and τ_{Mss})

The contribution of second-sphere water molecules also plays a significant role in the overall efficiency of CAs (5-15% increase in relaxivity).[31] This effect originates from the proximity between the metallic centre and water molecules that are bound to the complex by hydrogen bonds. This is the case for phosphorus acid derivates of DOTA, such as DOTP or DOTP^{R}, and it can also be the case for DOTA tetraamides.[27,31,47] Ligand modulation can also point in the direction of favoring this kind of interaction, as in the case of DOTA-Glu_{12}, where a large number of –OH groups were introduced in a DOTA-like structure, increasing the efficiency of the respective Gd^{III} complex by ~6 fold.[48]

Rotation correlation time (τ_R)

One straightforward approach to decrease the reorientational motion (concomitant with the increase of the rotation correlation time τ_R) of Gd^{III}-complexes is to increase their effective molecular volume. This can be done by an increase of the effective molecular weight and the placement of the Gd^{III} ion in the barycenter of the molecule through modifications in the pendant arms in order to attach new moieties. One typical example is the case of DOTA-Glu_{12} where the pendant arms of TCED are derivatized in order to bind trissacharide wedges.[49]

Another approach is to favor non-covalent and covalent interactions between Gd^{III} complexes and macromolecules. For non-covalent interactions, the most common examples are interactions with human serum albumin (HSA), Ciclodextrins and supramolecular aggregates such as lipoparticles.[50] Covalent interactions are made by conjugation of macromolecules with appropriate bifunctional ligands that possess reactive groups (-N=C=S; -NH_2; -CO_2H; -SH) or via amide bonds between the carboxylic functions of the pendant arms and the macromolecule. The number of tested macromolecules is large and ever-growing but in general terms is based on: *i*) polylysines, dextran, polyethylene glycol and polyamines; *ii)* antibodies, avidine/biotine, peptides and polyssacharides. [51]

One problem that is encountered in the above mentioned strategies is the fact that the global mobility of the macromolecules is not translated in the local mobility of the attached Gd^{III} complexes. This is due to the flexibility of the linkages and by the use of one-point attachments. The use of more rigid linkages and more rigid structures is therefore preferable and it is an important factor to be taken into account, as it has been extensively described in a case study of PAMAM dendrimers attached with Gd^{III}-DO3A-py^{NO}, reported by Polášek *et al.*[52] The design of ligands that allow a two-point attachment as well as the ability to form multinuclear complexes is also a promising strategy to increase the rotational correlational times of Gd^{III} complexes.

VI) General considerations

Ligand design is a very challenging task since it has to take into account several physicochemical parameters of the respective Ln^{III} complexes, assure their high thermodynamic stability, kinetic inertness and suitability for available imaging fields. An ideal candidate would be one with a highest possible value of q and fine-tuned water residence time and rotational correlation times. For higher field applications, τ_M should be as low as possible (< 10 ns) and τ_R should have intermediate values (~1 ns).

It should also be mentioned that there are other classes of CAs available for biomedical research and clinical applications besides mononuclear paramagnetic chelates such as the Gd^{III} complexes described above. T_1 agents based on metallofullerene nanoplatforms (f-Gd_3N@C8) have also showed to be promising candidates for dual imaging and diagnostic porposes.[53] T_2-CAs are based on paramagnetic or superparamagnetic particles (*e.g.* Iron Oxides, Gd^{III}-Labeled zeolites) and act mainly on the transversal relaxation rates of water protons. Polymeric (Gadovist 17) or macromolecular carriers (MS-325) and particulate CA (paramagnetic micelles and liposomes) are also very promising compounds, since they can combine the properties of

both T_1/T_2 CAs and also be used in drug delivery applications.[50] Furthermore, targeting vectors can be easily incorporated in these nanosystems, thus giving them organ/tissue specificity. Responsive CAs are also of great potential, consisting mainly on T_1-CA in which the relaxometric properties are dependent on the chemical environment (*e.g.* pH, pO_2) or the presence of metal ions and biomolecules (β-galactosidase).[54] In these cases a bifunctional ligand is able of metal coordination and is also endowed with an additional linker/spacer moiety that allows the conjugation with responsive units. An alternative to conventional Gd^{III} complexes as T_1-CAs are Mn^{II} complexes that also possess suitable magnetic properties.

An emerging class of CAs is CEST Agents. Here, Ln^{III} ions other than Gd^{III} induce a paramagnetic shift on the complex protons that are in a slow-to-intermediate exchange with bulk water molecules. By selectively saturating these protons the magnetic saturation is then transferred to the water resonance and the signal intensity is decreased.

CAs that are not based on ^{1}H detection have become increasingly explored. These consist on the direct detection of other NMR active nuclei, such as ^{19}F or hyperpolarized ^{13}C-containing molecules.[50]

It should also be considered the potential of CAs agents based on Proteins. Various proof-of-concept have been reported recently, such as genetically encoded contrast-agents based on ferritin overexpression, CEST proteins with a large number or slow-exchangeable protons and proteins responsive to dopamine and other neurotransmitters.[55-61]

The possibilities of designing new MRI CAs are an expanding field of research, especially if the combination of MRI with other imaging modalities is considered. In the next section, special attention will be given to the creation of MRI/Optical imaging probes.

1.3 - Bimodal MRI/NIR probes

In biomedical research several *in vivo* imaging modalities are available, such as MRI, Single photon emission computed tomography (SPECT), positron emission tomography (PET), ultrasounds and Optical Imaging (OI). Each of these modalities has inherent advantages and drawbacks in terms of spatial and temporal resolution and sensitivity of signal detection. One way to overcome these difficulties is the combination of two or more of these modalities and complementary improvement of the respective imaging probes. This has led to a great effort

to create new imaging probes and hardware capable of bimodal signal detection that would allow for colocalization of biochemical phenomena and validation of *in vivo* experiments.[62]

I) Optical Probes

In the case of MRI (where millimolar concentrations of CA are required for signal detection), its superior resolution can be combined with nuclear or optical modalities that possess high sensitivity (only picomolar to micromolar concentrations are required). Considering OI, two modalities are of particular interest, fluorescence imaging and luminescence imaging. In fluorescence imaging, signal generation occurs after excitation with proper wavelengths followed by emission typically at longer wavelengths. In the case of bioluminescent or chemiluminescence the signal is generated in consequence of a chemical reaction. In both cases contrast can be generated by administration of suitable probes and detection of their generated signal upon excitation. The most common type of bimodal MRI/OI probes is a combination of Gd^{III} complexes or iron oxide nanoparticles (MRI) with organic dyes or Quantum Dots (Optical). [63]

In the above mentioned systems, bimodality of the compounds is achieved through combination of two different molecules with distinct physical and chemical properties. A promising alternative to this is the utilization of Ln^{III} complexes since they have distinct physical (luminescent and magnetic) properties along the series while retaining very similar chemical properties. Luminescent properties of lanthanide ions derive from their characteristic $[Xe]4f^n$ (n = 0-14) electronic configuration, which is responsible for a great number of electronic levels [14!/n!(14-n)!].[64-66] These are characterized by three quantum numbers (S, L and J) with well defined energy levels and little sensibility to chemical environment due to shielding of the 4f orbitals by the filled $5s^2sp^6$ subshells. The resulting parity forbidden 4f-4f transitions are sharp and characteristic of each Ln^{III} ion, allowing for better discrimination from background fluorescence and realization of time-resolved experiments due to long life-times of the excited states. Therefore, the emissive properties of these compounds can be modified by simple Ln^{III} ion substitution, spanning from Gd^{III} (UV) to Eu^{III} and Tb^{III} (UV-Vis) and to Nd^{III} and Yb^{III} (Near-Infrared Region - NIR), thus allowing for multiplex assays (Fig. 1. 9).[67] An additional advantage of lanthanide complexes in relation to organic dyes is their resistance to photobleaching. However, the major drawback of Ln^{III} luminescence is their very low Intrinsic Quantum Yields.

The Intrinsic Quantum Yield corresponds to the ratio between the number of emitted photons and the number of absorbed photons by a Ln^{III} ion and can be calculated by taking

into account the life-time of the excited state τ_{obs}, the corresponding rate of de-population of the excited state k_{obs} (s^{-1}) (τ_{obs}= 1/ k_{obs}) and the radiative rate constant k^{rad}:[64]

$$Q_{Ln}^{Ln} = \frac{k^{rad}}{k_{obs}} \qquad (20)$$

It is possible to overcome the weak emissive properties of Ln^{III} ions by conjugation with proper organic molecules, as in the case of some Ln^{III} complexes where excitation in the ligand region leads to a metal-centered luminescence. This happens when part of the energy absorbed by the organic ligand is transferred to Ln^{III} excited states giving origin to sharp bands that correspond to internal conversion to the emitting level. This effect is termed "Antenna Effect" or Sensitization (of metal-centered) Luminescence. Several energy migration paths have been proposed, such as exchange or superexchange mechanisms (Dexter type) or dipole-dipole (or dipole-multipole) mechanisms (Förster type) involving singlet, triplet or intraligand charge transfer states.[64] The most common migration path is through ligand-centered Laporte- and spin-allowed absorptions ($^1S^* \rightarrow {}^3T^*$, k_{ISC}) with consequent intersystem crossing ($^3T^* \rightarrow Ln^*$, k^{et}) and metal centered emission. However, other mechanisms may be involved and no simple scenario is at play, such as Ligand-to-Metal Charge Transfer (LMCT), 4f-5d transitions or d-Metal-to-Ligand Charge Transfer (^{3}MLCT). In the case of lanthanides, LMCT, 4f-5d and 4f-4f transitions occur. Of particular interest are 4f-4f transitions, involving parity allowed magnetic dipole transitions (MD) and parity forbidden electric dipole transitions (ED). ED transitions become partly allowed when mixing of electronic states of opposite parity occur. This is due to non-centrosymmetric interactions caused by placement of Ln^{III} ions in a chemical environment, with the resulting bands being named "hypersensitive transitions". Electric quadropole (EQ) transitions are also involved, although they are not usually indentified experimentally. A simplified Jablonski diagram describes the process of energy transfer (Fig. 1. 10).

The *Overall Quantum Yields* Q_{Ln}^{L} corresponds to the obtained Quantum Yields in the presence of an energy donor, such as in the case of antenna-like ligands mentioned above. In these cases the efficacy with which the energy is transferred from the ligand to the metal ion excited states is termed *sensitization efficiency*, η_{sens}:

$$Q_{Ln}^{L} = \eta_{sens} Q_{Ln}^{Ln} = \eta_{pop}^{D} \eta_{et} Q_{Ln}^{Ln} \qquad (21)$$

where η_{pop}^{D} is the efficiency with which the feeding level is populated and η_{et} the efficiency of energy transfer from the donor state to the accepting level. The design of new lanthanide

complexes with high emissive rates has to take into account these two parameters. Energy transfer must be maximized whereas non-radiative processes have to be minimized. Although a complete description of the mechanisms involved in energy transfer are still unknown, a simplified strategy in the design of new ligands can be employed by considering that the energy transfer path $^{1}S^{*} \rightarrow {}^{3}T^{*} \rightarrow Ln^{*}$ is the only (or at least the main) operative one. Therefore, special considerations are given to the energy difference between the $^{3}T^{*}$ and the Ln^{III} emitting level, taking into consideration that the energy gap between the receiving excited state and the emitting state of the Ln^{III} ion should be large enough to minimize back transfer of energy.[65]

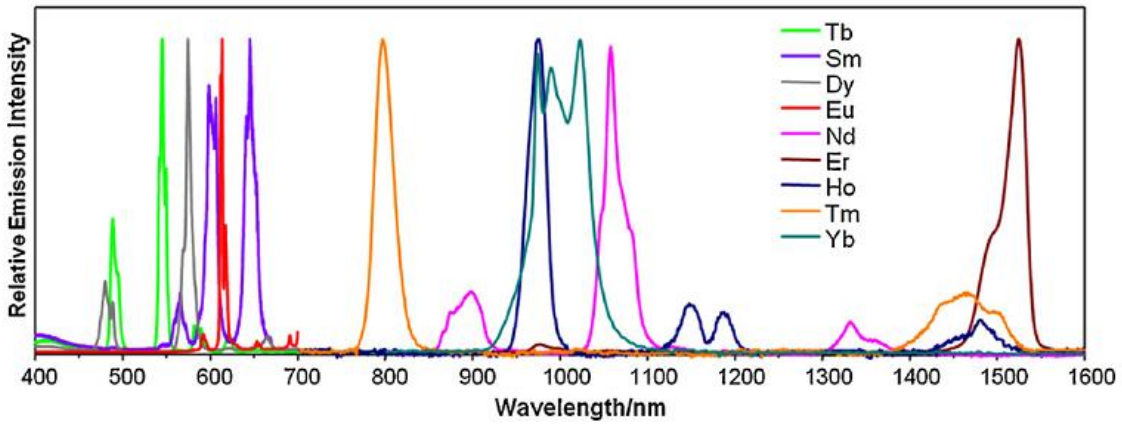

Fig. 1. 9: Normalized emission spectra of luminescent lanthanide complexes in solution, illustrating the sharp emission bands and minimal overlap of lanthanide luminescence (adapted).[66]

The use of organic ligands is severely limited due to the presence of strong C=C and C-H vibrators. One of the most common types of chromophores is 8-hydroxyquinolinate and its derivatives with bromide atoms, where the removal of C-H bonds from the ligand core and the contribution from "heavy-atom effect" leads to an effective increase of the Overall Quantum Yields. However, some of these complexes have low solubility and in most cases the highest values of overall quantum yields are obtained in solid-state. In order to overcome this problem these ligands are usually incorporated in larger tripodal ligands, forming new complexes with increased water solubility and efficiency. In fact, the design of MRI/Optical probes based on Ln^{III} complexes is a demanding task since the presence of O-H vibrators strongly quenches metal-centered luminescence. For this reason it is difficult to reach a good compromise between a suitable number of coordinated water molecules for MRI applications and minimal luminescence quenching.

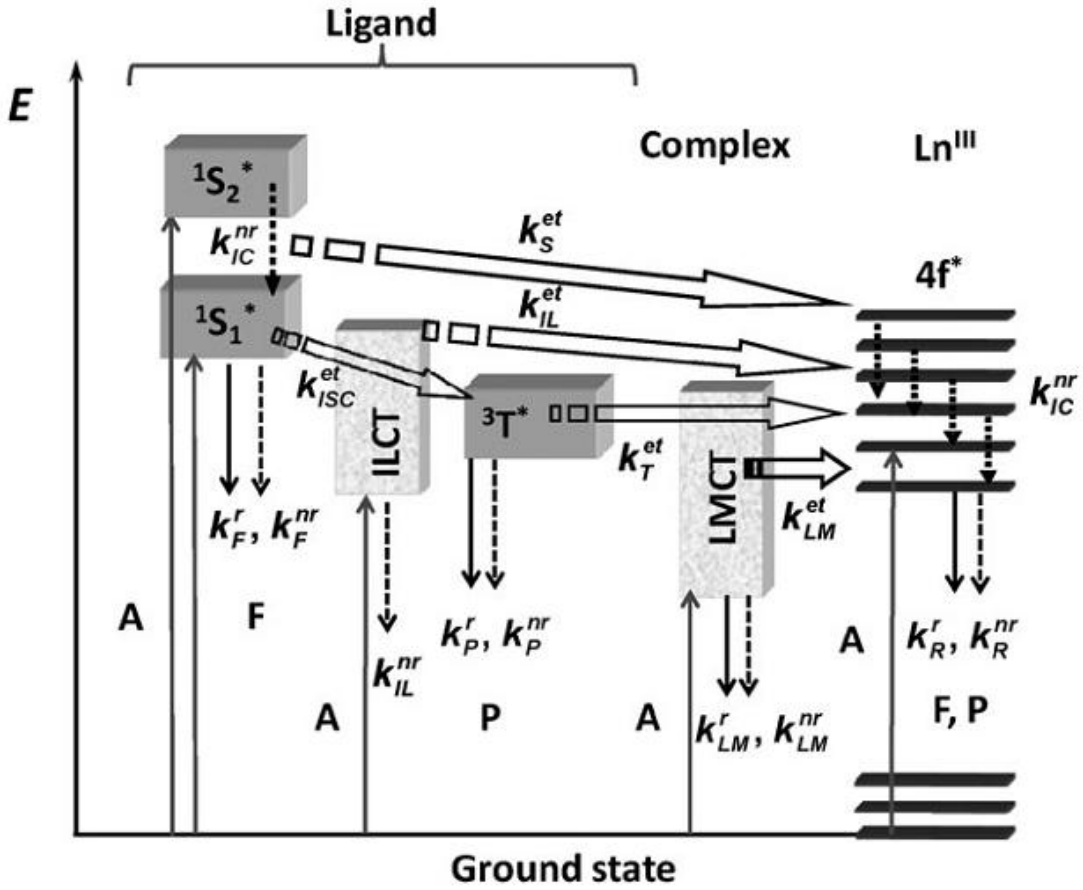

Fig. 1. 10: Schematic representation of energy absorption, migration, emission (plain arrows) and dissipation (dotted arrows) processes in a Ln^{III} complex. 1S* or S = singlet state, 3T* or T = triplet state, A = absorption, F = fluorescence, P = phosphorescence, k = rate constant, r = radiative, nr = non-radiative, IC = internal conversion, ISC = intersystem crossing, ILCT (indices IL) = intra-ligand charge transfer, LMCT (indices LM) = ligand-to-metal charge transfer. (adapted).[65]

II) NIR Imaging

Conventional *in vivo* microscopy uses radiation in the visible region. However, for deeper tissue examination NIR imaging, where NIR radiation ranges from 650 to 1500 nm, has been the prevailing strategy. This is because of the low absorption coefficients of hemoglobin (main absorber of visible radiation), water and lipids (main absorbers in the infrared region) in the 650-990 nm range.[68] Also, NIR signal detection takes advantage of minimal tissue autofluorescence thus increasing the signal-to-noise ratio. Other important factors are the possibility of obtaining higher resolution - due to the lower diffraction of NIR radiation in relation to visible radiation - and also the possibility of excitation of NIR probes at longer wavelengths, thus being more suitable for biological tissue examination.[67,68] The development of NIR imaging probes has great potential for biomedical research and there has been a constant improvement in this field of research with the report of new organic or inorganic

compounds. However, one of the main drawbacks of NIR imaging probes is their typical lower Overall Quantum Yields in relation to visible and UV probes. A considerable improvement is the creation of bimodal MRI/NIR probes with reasonable efficiency both in terms of relaxometric and luminescent properties. In this regard, Lanthanide complexes have great potential in fulfilling these demands.

CHAPTER 2

Methods

2.1 - Theory

Longitudinal Relaxation Times

The relaxation of ^{1}H nuclei can be described in succinct terms under the principles of NMR spectroscopy. For a sample containing NMR active nuclei placed in an effective magnetic field B_0 oriented along the *zz* axis, a magnetic component M_z is created, corresponding to the overall contribution of all sample spins. An M_{xy} component (in the rotatory frame of reference) is created with the application of a perpendicular RF pulse (B_1) in relation to B_0 that evolves again to the *zz* axis. This return to the thermal equilibrium, defined by the Boltzmann equation and therefore being dependent on the applied B_0 field, is termed Relaxation. This process occurs via two different mechanisms that are characteristic for each non-equivalent spins in the sample, namely the Longitudinal (T_1) and Transversal (T_2) Relaxation. The former being described in terms of a spin-lattice relaxation mechanism and the former in terms of a spin-spin relaxation mechanism. In relaxometric studies water protons originate the observed signal.[3]

Determination of longitudinal relaxation times is done with the inversion-recovery experiment (Fig. 2. 1).

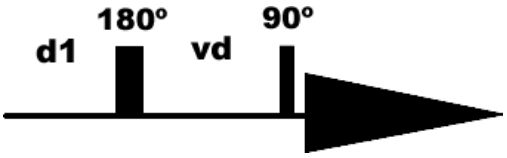

Fig. 2. 1: Schematic representation of the inversion-recovery pulse sequence.

where **180°** represents a 180° RF pulse, after a delay period **d1**, that leads to an inversion of spin populations, **vd** represents the variable delay time that corresponds to M_z evolution and **90°** represents a 90° RF pulse that allows the acquisition of a M_{xy} component corresponding to M_z. The T_1 values and evolution of the magnetization vectors are described by the Bloch equations.[3]

Bulk Magnetic Susceptibility

The Bulk Magnetic Susceptibility (BMS), or Evans method, is a simple method to measure the concentration of a paramagnetic species in solution.[69] It is based on the bulk magnetic susceptibility shift (Δχ) of a NMR resonance of an inert compound, *e.g. t*-butanol, in the presence of a paramagnetic solute. This results from the partial alignment of the magnetic

moments of the paramagnetic species in relation to the external magnetic field, therefore affecting the bulk magnetic susceptibility. Δχ is expressed by:

$$\Delta_\chi = \frac{4\pi cs}{T}\left(\frac{\mu_{eff}}{2.84}\right)^2 \times 10^3 \qquad (22)$$

where c is the concentration of the paramagnetic species (mol^{-1}), s is a parameter dependent on the shape of the sample and its relative position to the magnetic field (s = 1/3 for used tubes), T is the absolute temperature and μ_{eff} is the effective magnetic moment of the lanthanide ion (for Gd^{III}, μ_{eff} =7.94 μB)

In this technique a sample containing the paramagnetic compound (in this work a Gd^{III} complex) and 10% *t*-butanol solution is placed in a NMR tube and the frequency shift of *t*-butanol is determined by comparison with a diamagnetic solution containing the same solvent and percentage of *t*-butanol.

<u>^{1}H Nuclear Magnetic Resonance Dispersion and ^{17}O NMR Spectroscopy</u>

The equations describing the theory of ^{1}H Nuclear Magnetic Dispersion (NMRD) profiles have been given in Chapter 1.

^{17}O NMR spectroscopic studies are used to evaluate the number of water molecules in the inner coordination sphere (q) of Gd^{III} complexes, since the water ^{17}O chemical shifts are dependent on the Gd^{III}-induced contact shift.[19]

From the measured ^{17}O NMR relaxation rates and angular frequencies of the paramagnetic solutions - $1/T_1$, $1/T_2$ and ω - and of the acidified water reference - $1/T_{1A}$, $1/T_{2A}$ and ω_A - one can calculate the reduced relaxation rates and chemical shifts – $1/T_{1r}$, $1/T_{2r}$ and $\Delta\omega_r$ - which may be written as:

$$\frac{1}{T_{1r}} = \frac{1}{P_m}\left[\frac{1}{T_1} - \frac{1}{T_{1A}}\right] = \frac{1}{T_{1m}+\tau_m} + \frac{1}{T_{1os}} \qquad (23)$$

$$\frac{1}{T_{2r}} = \frac{1}{P_m}\left[\frac{1}{T_2} - \frac{1}{T_{2A}}\right] = \frac{1}{\tau_m}\frac{T_{2m}^{-2}+\tau_m^{-1}T_{2m}^{-1}+\Delta\omega_m^2}{\left(\tau_m^{-1}+T_{2m}^{-1}\right)^2+\Delta\omega_m^2} + \frac{1}{T_{2os}} \qquad (24)$$

$$\Delta\omega_r = \frac{1}{P_m}(\omega - \omega_A) = \frac{\Delta\omega_m}{\left(1+\tau_m T_{2m}^{-1}\right)^2+\tau_m^2\Delta\omega_m^2} + \Delta\omega_{os} \qquad (25)$$

where $1/T_{1m}$ and $1/T_{2m}$ are the relaxation rates of the bound water and $\Delta\omega_m$ is the chemical shift difference between bound and bulk water, τ_m is the mean residence time or the inverse of the water exchange rate k_{ex} and P_m is the mole fraction of the bound water. Previous studies have shown that outer sphere contributions to the ^{17}O relaxation rates are negligible. The

chemical shift of the bound water molecule, $\Delta\omega_m$, depends on the hyperfine interaction between the Gd^{III} electron spin and the ^{17}O nucleus and is directly proportional to the scalar coupling constant, $A/\hbar$, expressed as:

$$\Delta\omega_m = \frac{g_L \mu_B S(S+1)}{3k_B T}\frac{A}{\hbar} \quad (26)$$

where the isotopic Landé g factor is equal to 2.0 for the Gd^{III}, B represents the magnetic field, and k_B is the Boltzmann constant.

The outer-sphere contribution to the chemical shift is assumed to be linearly related to $\Delta\omega_m$ by a constant C_{os}:

$$\Delta\omega_{os} = C_{os}\Delta\omega_m \quad (27)$$

The longitudinal relaxation of ^{17}O is given by:

$$\frac{1}{T_{1m}} = \left[\frac{1}{15}\left(\frac{\mu_0}{4\pi}\right)^2 \frac{\hbar^2\gamma_I^2\gamma_S^2}{r_{GdO}^6} S(S+1)\right] \times \left[6\tau_{d1} + 14\frac{\tau_{d2}}{1+\omega_S^2\tau_{d2}^2}\right] + \frac{3\pi^2}{10}\frac{2I+3}{I^2(2I-1)}\chi^2\left(1+\frac{\eta^2}{3}\right)\tau_{RO} \quad (28)$$

Having,

$$\frac{1}{\tau_{di}} = \frac{1}{\tau_m} + \frac{1}{\tau_{RO}} + \frac{1}{T_{ie}} \quad (29)$$

where γ_S is the electronic gyromagnetic ratio and γ_I is the nuclear gyromagnetic ratio, r_{GdO} is the effective distance between the electronic charge and the ^{17}O nucleus, I is nuclear spin (5/2 for ^{17}O), χ is the quadrupolar coupling constant and η is a symmetry parameter.

In the transverse relaxation, the scalar contribution, $1/T_{2sc}$, is the most important parameter:

$$\frac{1}{T_{2m}} \cong \frac{1}{T_{2sc}} = \tau_{s1}\frac{S(S+1)}{3}\left(\frac{A}{\hbar}\right)^2 \quad (30)$$

where $1/\tau_{s1}$ is the sum of the exchange rate constant and the electron spin relaxation $1/T_{1e}$ rate:

$$\frac{1}{T_{s1}} = \frac{1}{\tau_m} + \frac{1}{T_{1e}} \quad (31)$$

where the exchange rate is supposed to obey the Eyring equation.

Photophysics and Quantum Yield Determination

The UV-Vis absorption spectrum allows for the determination of the region of maximum absorption of an organic ligand. When an energy-transfer process occurs, lanthanide luminescence can be obtained at room-temperature (RT) by excitation in the ligand-centered region. Otherwise, since the forbidden 4f-4f transitions are Laporte- and spin-forbidden, lanthanide luminescence is usually not observed at RT and in water solutions. The obtained Quantum Yields are dependent on the type of solvent and physical state of the sample as well as on sample shape. One way to calculate the quantum yield of a sample is to compare it to a reported value of another compound in which the experimental conditions resemble as much as possible the current ones, although some considerations should be taken into account.[65] In this study the reference compound was a Tropolonate ligand in DMSO, and the quantum yields were calculated using the equation:

$$\frac{F_x}{F_r} = \left[\frac{A_r ?_r}{A_x ?_x}\right]\left[\frac{I(\eta_r)}{I(\eta_x)}\right]\left[\frac{\eta_x^2}{\eta_r^2}\right]\left[\frac{D_x}{D_r}\right] \quad (32)$$

where subscript *r* stands for the used reference and *x* for the sample, A is the absorbance at the excitation wavelength, I is the intensity of the excitation light at the same wavelength, η is the refractive index (η = 1.479 in DMSO and η = 1.333 in water), and D is the measured integrated luminescence intensity.[67] One advantage of these systems is that, since the absorption is made by the chromophore and emission by the lanthanide ion, there is an energy gap between the absorption and emission bands of the lanthanide complexes, therefore minimizing luminescence reabsorption and corresponding quantification artifacts.[66]

Lanthanide Induced Shifts

The binding of a ligand to a paramagnetic Ln^{III} ion such as Yb^{III} results in large NMR frequency shifts at the ligand nuclei, with magnitudes and signs depending on both the nature of the lanthanide ion and the location of the nucleus relative to the metal center.[70] For a given nucleus *i*, the isotropic paramagnetic shift induced by a lanthanide ion *j* (δ_{ij}^{para}) is generally a combination of the Fermi contact (δ_{ij}^{con}) and dipolar (δ_{ij}^{dip}) contributions:

$$\delta_{ij}^{para} = \delta_{ij}^{exp} - \delta_i^{dia} = \delta_{ij}^{con} - \delta_{ij}^{dip} \qquad (33)$$

where the diamagnetic contribution δ_i^{dia} is obtained by measuring the chemical shifts for analogous diamagnetic complexes. The hyperfine ^{1}H NMR shifts in Yb^{III} complexes are considered to be largely pseudocontact in origin and therefore the analysis of the paramagnetic shifts observed in the ^{1}H NMR spectrum of the Yb^{III} complex is made under the assumption that they are dominated by dipolar contributions, which can be written as linear combinations of the five components of the susceptibility tensor χ as given by the following equation:[71]

$$\delta_{ij}^{dip} = \left(\chi_{zz} - \frac{1}{3}Tr\chi\right)\left(\frac{3z^2-r^2}{r^5}\right) + \left(\chi_{xx} - \chi_{yy}\right)\left(\frac{x^2-y^2}{r^5}\right) + \chi_{xy}\left(\frac{4xy}{r^5}\right) + \chi_{xz}\left(\frac{4xz}{r^5}\right) + \chi_{yz}\left(\frac{4yz}{r^5}\right) \qquad (34)$$

with $r = \sqrt{x^2 + y^2 + z^2}$ (35)

Here, the Cartesian coordinates of atom i relative to the location of a paramagnetic ion are used in place of the more usual spherical coordinates. In the principal magnetic axis system $\chi xy = \chi xy$ = and $\chi xy = 0$, and for axial symmetry $\chi xx - \chi yy = 0$. According to the Neumann's principle, one of the principal magnetic axis of Yb^{III} complex must coincide with the symmetry axis of the molecule.[72] For the case of the studied Yb^{III}-L1 complex, it is assumed that the z axis of the principal axis of the magnetic susceptibility tensor coincides with the C2 axis of the molecule. As a consequence, it was considered only three (rather than five) parameters, namely the axial [χzz – 1/3(χxx + χyy + χzz)] and rhombic (χxx - χyy) anisotropies of the magnetic susceptibility tensorχ, and the orientation of the magnetic axis in the xy plane with respect to the Cartesian axis, as given by an angle α.[73]

2.2 - Experimental

Materials and reagents

Ln^{III} salts were obtained from Sigma-Aldrich and used with no further purification. Solvents (MilliQ water and D_2O) were used with no further purification. The ligand DO2A-*trans*-$(py^{NO})_2$

(4,10-di[(1-oxidopyridin-2-yl)methyl]-1,4,7,10-tetraazacyclododecane-1,7-diacetic acid = **L1**) was synthesized and purified in the Department of Inorganic Chemistry, Universita Karlova and supplied by João Teixeira. The Ln^{III} (Ln^{III} = La^{III}, Lu^{III}, Eu^{III}, Yb^{III}) complexes of DO3P (1,4,7,10-tetraazacyclododecane-1,4,7-triyl)tris(methylene)-triphosphonic acid = $[Ln(DO3P]^{3-}$), DO3P1Pr (3-(4,7,10-tris(phosphonomethyl)-1,4,7,10-tetraazacyclo-dodecan-1-yl)propanoic acid = $[Ln(DO3P1Pr]^{4-}$) and DO3P1ol (10-(3-hydroxypropyl)-1,4,7,10-tetraazacyclododecane-1,4,7-triyl)tris(methylene)triphosphonic acid = $[Ln(DO3P1ol]^{3-}$) were supplied by Dra. Rita Delgado from Instituto de Tecnologia Química e Biológica, Universidade Nova de Lisboa. ^{17}O- enriched water (^{17}O: 11.4%) was added to the solution used in ^{17}O NMR measurements to improve sensitivity.

Sample preparation

Free ligand solution ([L1] = 10 mM, pH 6.9) was prepared from a stock solution of L1 and dissolved with MilliQ water, pH was adjusted with KOH and HCl stock solutions. The complexation procedure was optimized for this kind of systems, taking into account the complexation kinetics of lanthanide ions by macrocyclic ligands. For Ln^{III}-L1 (Ln^{III} = Lu^{III}, Yb^{III}, Eu^{III}) complexes ($[Ln(L1)]^{+}$), the corresponding chloride salts were added to free ligand solutions in amounts corresponding to 1:1.05 molar proportions and the resulting solution was heated at 338K under stirring for at least 12h. The value of pH was kept close to 7 by addition of stock HCl and NaOH solutions. The sample was heated at 338K for at least 12h under stirring and the presence of free Ln^{III} ions in solution was checked with the Xylenol Orange Test.[74] The resulting solutions used for ^{1}H NMR studies were evaporated under reduced pressure, re-dissolved in 1 mL of 99.9% D_2O and pH values were measured again (considering pH = pD – 0.4).[75] In the case of Gd^{III}-L1 complexes, the corresponding $GdCL_3$ salt was added to a 3 mM L1 solution in the amount corresponding to a 1:1.10 molar proportion following the same complexation procedures described above. A 5 mM Gd^{III}-L1 solution for ^{1}H NMRD studies was prepared following the same complexation procedure with an additional filtration step. However, concentration determination with the BMS method indicated that real sample concentration was 3.7 mM. Presence of free Gd^{III} ion in solution was verified with Xylenol Orange Test. For luminescence studies, Ln^{III}-L1 complexes (Ln^{III} = Ho^{III}, Pr^{III}, Nd^{III}, Tb^{III} and Eu^{III}) were prepared from a 0.2 mM L1 solution by adding equimolar amounts of the corresponding chloride salts following again the same complexation procedure. Some of the resulting samples were further diluted with distilled water in order to obtain optimal photon count. Concentration and pH values for the aforementioned Ln^{III} complexes are present in Tab. 2. 1.

Studies involving DO3P, DO3P1Pr and DO3P1ol Ln^{III} complexes involved no additional preparation or purification steps.

Tab. 2. 1: Solutions of Ln^{III}-L1 complexes prepared in this work

Ln-L1	Ce^{III}	Eu^{III}	Gd^{III}	Tb^{III}	Ho^{III}	Pr^{III}	Nd^{III}	Yb^{III}	Lu^{III}
[ ] (mM)	10	10; 0.05[a]	5 (3.7)[b]	0.05[a]	0.2[a]	0.2[a]	0.05[a]	10; 0.05[a]	10
pH		7.5	7.0	≈7	≈7	≈7	≈7	6.9	6.9

a – samples used in Luminescence studies

b – As determined by BMS

^{1}H NMR and ^{31}P NMR

1D and 2D COSY ^{1}H NMR spectra were obtained at 298 and 333K for ligand L1 and its Ln^{III} complexes in a Varian VNMRS 600 MHz operating at 599.72 MHz (^{1}H) with a 3-mm PFG triple resonance I.D. probe. ^{1}H and ^{31}P NMR spectra were obtained at 298, 333 and 353K for DO3P, DO3P1Pr and DO3P1ol and their respective Ln^{III} complexes in a Varian Unity 500 spectrometer operating at 499.83 (^{1}H) and 202.33 Mhz (^{31}P) with a 5-mm PFG Broadband probe and additional ^{31}P NMR spectra were obtained in a Bruker Avance III 400 spectrometer operating at 162 MHz (^{31}P). 2D COSY and DQF-COSY ^{1}H NMR spectra were also obtained in a Varian VNMRS 600 spectrometer operating at 599.72 MHz (^{1}H). For ^{1}H NMR experiments, solvent (D_2O) signal was used as an internal reference (^{1}H, δ 4.65 ppm) and for ^{31}P NMR experiments an 85% H_3PO_2 water solution with a few drops of D_2O was used as an external reference signal (^{31}P, δ 0.0 ppm). Spectra analysis and processing were performed with MestreNova (v6.0. 2-5475, 2009 Mestrelab Research S.L.) software for both types of systems.

^{17}O NMR and BMS

Variable-temperature ^{17}O NMR measurements were performed on a Bruker Avance-500 (11.7 T) (from the NMR facility of the Centre de Biophysique Moléculaire, CNRS, Orléans, France) spectrometer and a BVT-3000 temperature control unit was used to stabilize the temperature, measured by a substitution technique. The sample (Gd^{III}-DO3P1ol) was sealed in a glass sphere that fitted into a 10 mm o.d. NMR tube, to eliminate susceptibility corrections to the chemical shifts. Longitudinal relaxation rates 1/T1 were obtained by the inversion recovery method and transverse relaxation rates 1/T2 by the Carr-Purcell-Meiboom-Gill spin-echo technique. As an external reference, acidified water of pH 3.4 was used. The final solution concentration was 26.86 mmol/kg. For the BMS test, a co-axial 5 mm tube containing a 10% *t*-

butanol solution inside the reference tube and a complex solution (Gd^{III}-L1 or Gd^{III}-DO3P1ol) containing 10% *t*-butanol in the outer tube were used.

^{1}H NMRD

The measurements were performed by using a Stelar Spinmaster FFC NMR relaxometer (0.01-20 MHz) equipped with a VTC90 temperature control unit (from the NMR facility of the Centre de Biophysique Moléculaire, CNRS, Orléans, France). At higher fields, the ^{1}H relaxivity measurements were performed on a Bruker Electromagnet at the frequencies of 20MHz, 40MHz, 60MHz and 80MHz. A 5 mM Gd^{III}-L1 solution was used in each case and the temperature was measured by a substitution technique. Variable temperature measurements were performed at 298 and 310K.

Photophysical Studies and Quantum Yield measurements

Absorbance UV spectra were performed on an Uvikon spectrophotometer. Emission and Excitation (lanthanide luminescence) spectra were measured using modified Jobin-Yvon Horiba Fluorolog-322 spectrofluorimeter equipped with a Hamamatsu R928 detector (for the visible domain) and a DSS-IGA020L (Electro-Optical Systems, Inc.) detector (for the NIR domain). All these experiments were performed in the Centre de Biophysisque Moléculaire, CNRS, Orléans, France. Luminescence and excitation Spectra were corrected for variations in lamp output, non-linear response of the detector and the use of neutral density filters (where applicable). Luminescence quantum yields were obtained in the same spectrophotometer fitted with an integration sphere developed by Frédéric Gumy and Prof. Jean-Claude G. Bünzli (Laboratory of Lanthanide Supramolecular Chemistry, École Polytechnique Féderale de Lausanne (EPFL), BCH 1402, CH- 1015 Lausanne, Switzerland) as an accessory to the Fluorolog-322 spectrometer (Patent pending), using a quartz tube sample holder. Ln^{III} (Ln^{III} = Eu^{III}, Tb^{III}, Yb^{III}, Nd^{III}, Er^{III}, Ho^{III} and Pr^{III}) luminescence quantum yields were measured by using the Yb^{III}-Tropolonate as a reference compound.[67] The calculated values were determined by integrating the emission profiles, averaged from four separate trials, and substitution into the ratio of emitted photons over absorbed photons.

Computational methods

The computational methods, namely the DFT calculations and the least squares fit between calculated and experimental Yb^{III}-induced paramagnetic shifts, were made by the research group of Dr Carlos Platas-Iglesias in the Departamento de Química Fundamental, Universidade da Coruña, Spain.

All calculations were performed employing DFT within the meta generalized gradient approximation (meta-GGA), with the mPWB95 exchange-correlation functional,[76,77] and the Gaussian 09 package (Revision A.02).[78] Full geometry optimizations of the Yb^{III}-L1 system were performed in water solution by using the effective core potential (ECP) of Dolg *et al.*, the related [5s4p3d]-GTO valence basis set for the lanthanides[79] and the 6-31G(d) basis set for C, H, N and O atoms. No symmetry constraints have been imposed during the optimizations. The default values for the integration grid ("fine") and the SCF energy convergence criteria (10^{-6}) were used. The stationary points found on the potential energy surfaces as a result of the geometry optimizations have been tested to represent energy minima rather than saddle points via frequency analysis. Solvent effects were evaluated by using the polarizable continuum model (PCM), in which the solute cavity is built as an envelope of spheres centered on atoms or atomic groups with appropriate radii. In particular, the integral equation formalism (IEFPCM) variant was used as implemented in gaussian 09.[80] In aqueous solution relative free energies of the different isomers include non-potential-energy contributions (zero point energies and thermal terms) obtained through frequency analysis.

The Kemple procedure for the determination of solution structures of Ln^{III} complexes from experimental pseudo-contact shifts consists on the calculation of geometric factors in the molecular coordinate system followed by a three-parameter (defined above) linear least-square search for minimization of the difference between the calculated and measured pseudo contact shifts δ_{pc} values. This is done according to an agreement factor defined by:

$$R = \left[\frac{\sum_i (\delta_{calc} - \delta_{obs})^2}{\sum_i \delta_{obsi}{}^2}\right]^{1/2} \qquad (36)$$

Since the δ_{pc} depends only on the anisotropy (traceless part of χ') of the susceptibility tensor χ, the determination of these three fitting parameters is sufficient to determine the principal values of χ'. The principal directions of χ'(and χ) are then determined by diagonalization of χ'.[71]

Relaxometric studies

Longitudinal relaxation studies were performed on a Bruker Minispec mq20 (20 MHz, B_0 = 0.47 T) relaxometer with a Haake DC10 (Thermo Electron Corporation) temperature controller, using the inversion-recuperation method (20 measurements, 4 scans). For determination of the longitudinal relaxivity (r_1) of Gd^{III}-L1, R_{1p} values of 0-3 mM samples prepared from an initial 3 mM Gd^{III}-L1 solution were determined at 298 and 310K. The diamagnetic contribution R_{1d}

was obtained by measuring the R_{1obs} value of distilled water. Temperature-dependence studies were performed with a 1 mM, pH 7.0 Gd^{III}-L1 solution in the 275-350K range. The dependence of R_{1obs} with pH was also studied in a 1 mM Gd^{III}-L1 solution with pH values ranging from 2.41 to 12.20.

Transmetallation studies

The transmetallation process of Gd^{III}-L1 with Zn^{II} ions was studied by measuring the time-dependent decrease of R_{1obs} with a Bruker Minispec mq20 (20 MHz, B_0 = 0.47 T) relaxometer in a 40 mM pH 7.0 PBS solution containing 1 mM of Gd^{III}-L1 with further addition of equimolar amounts of $ZnCl_2$ at 298K.

The reaction processes are equated below:[81]

$$\mathrm{Gd\text{-}L^{(n)-} \leftrightarrow L^{(n+3)-} + Gd^{3+}}$$
$$\mathrm{L^{(n+3)-} + Zn^{2+} \leftrightarrow Zn\text{-}L^{(n+1)-}}$$
$$\mathrm{Gd^{3+} + PO_4^{3-} \rightarrow Gd(PO_4)_{ins}}$$

Data analysis

Data obtained in ^{17}O NMR, ^{1}H NMRD, Luminescence and Quantum Yield measurement studies were processed in OriginLab Pro 8 SRO. Data from relaxometric and transmetallation studies were processed with Microsoft Office Excel 2007.

CHAPTER 3

Cyclen derivatives with three methylphosphonate pendant arms: synthesis and study of the effect of an additional pendant arm on metal complexation

3.1 - Introduction

One common approach in the design of new cyclen-based ligands is the attachment of a different number of pendant arms containing carboxylic, amides, phosphinates or phosphonates moieties. In this regard, DOTA and DOTP ligands and their metallic complexes are by far the most characterized in terms of both physicochemical and structural properties. [25,32]Recently, combinations of pendant arms based on both carboxylic and phosphonate were also attempted (Fig. 3. 1). This is the case of a DOTA analogue where one acetate pendant was replaced by a methylphosphonate one, DO3A1P, with its respective Ln^{III} complexes showing reasonable thermodynamic stability and kinetic inertness as well as suitable relaxometric properties.[28,82,83] Further acetate substitution of acetate pendants was also reported, such as the case of Ln^{III} complexes of DO2A2P and DO3P1A, the former presenting high stability and reasonable kinetic inertness for its Ln^{III} complexes and the latter showing reasonable stability *in vivo* and bone-targeting predisposition.[27,36,84-86]

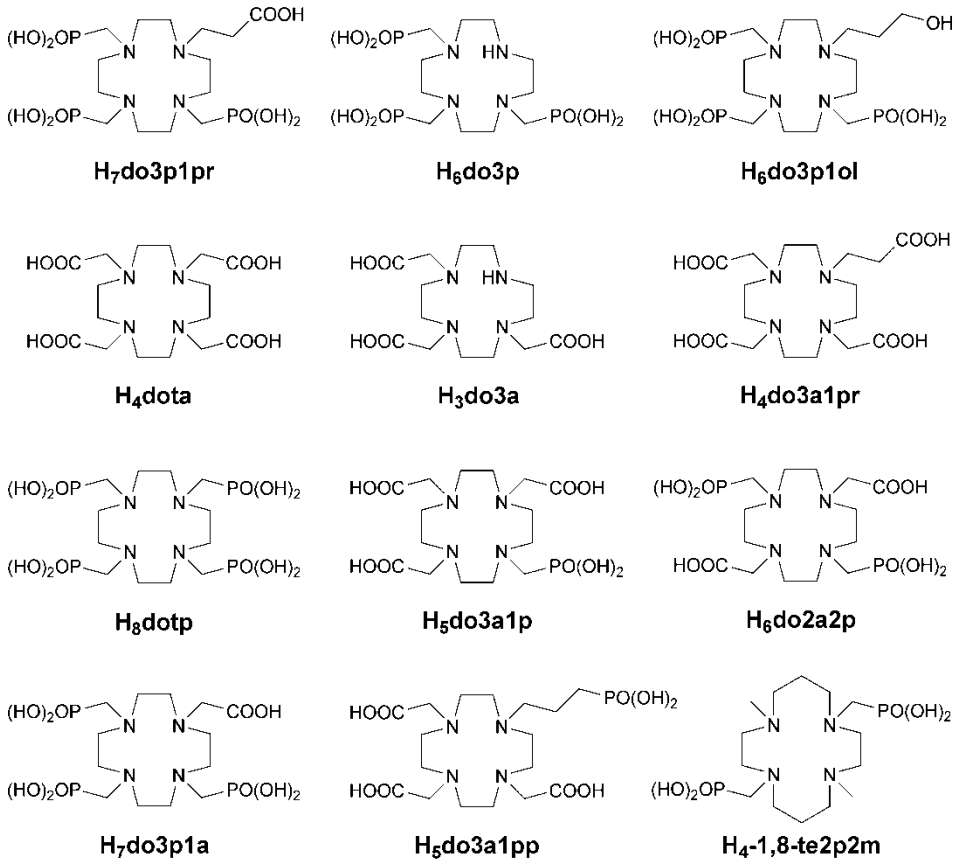

Fig. 3. 1: Ligands discussed in this work

Another type of DOTA analogue was reported recently, DO3A1Pr, where an acetate pendant was replaced by a propionate moiety, resulting in improved complexation kinetics of its Ln^{III} complexes.[87,88] Considering this feature and the suitable characteristics of DOTP and its analogues, a combination of both was thought in the design of new cyclen-based chelators by starting from DOTP and replacing one of its methylphosphonate pendant arms by another capable of forming a six-membered chelate ring (instead of the usual five-membered ones). Two donor groups were chosen, a carboxylate for its ability to bind a wide variety of metal ions and also an alcohol for its higher lipophilicity and neutral charge. These ligands are DO3P1Pr and DO3P1ol, respectively. An additional ligand was also considered, DO3P, a DOTP analogue with only three pendant arms. This work is part of a project where the physicochemical and structural properties of these ligands and their respective complexes are studied.[89] It is focused mainly in the structural features presented in solution but in the case of DO3P1ol it also addresses some physicochemical aspects concerning its suitability as a CA.

3.2 - Results and Discussion

Determination of the acid-base behavior and thermodynamic stability of DO3P, DO3P1Pr and DO3P1ol and their metal complexes led to the conclusion that they present a very high overall basicity, which increases from DO3P1ol to DO3P and then to DO3P1Pr, and also that their pM values are lower for those of model DOTA and DOTP Ln^{III} complexes, with DO3P1Pr showing the highest values between them (Tab. 3. 1). However, the role of the additional propionate and propanol arms in metal ion coordination after encapsulation in the macrocyclic framework was still left to be elucidated. By considering only the pM values it is not possible to make any inference, since in the case of DO3P1Pr the highest pM values could simply be a result of its increased basicity. However, by studying the solution structures of these complexes it is possible to take some conclusive insights. Variable-temperature ^{1}H and ^{31}P NMR spectroscopy are widely used to study the structural dynamics of macrocycle-based ligands and metal complexes. For this reason, ^{1}H and ^{31}P NMR spectra of all three ligands and their Ln^{III} complexes in D_2O were studied (Ln^{III} = Lu^{III}, Eu^{III}, Yb^{III}) at pH 8.5-9.0, corresponding to the fully deprotonated ML species.

Tab. 3. 1: Values of pM calculated for Ln^{III} complexes of the discussed ligands at pH 7.4 obtained in the accompanying work (Annex I) or taken from the literature.[a,b]

Ln^{III}	DO3P1Pr	DO3P	DO3P1ol	DOTA	DOTP
La^{III}	10.52	10.22	10.10	–	–
Sm^{III}	11.98	11.56	11.70	16.25[c]	14.76[c]
Gd^{III}	12.26	12.05	11.91	–	–
Ho^{III}	12.60	12.26	12.11	17.75[c]	16.49[c]
Lu^{III}	13.53	13.12	13.15	–	–

[a] Values calculated for 100% excess of ligand concentration at $c_M = 1.00\times10^{-5}$ mol dm^{-3}; [b] adapted[89]; [c] Adapted.[90]

Solution structures of free DO3P, DO3P1Pr and DO3P1ol ligands

In the case of DO3P, at 298K the resonances are broad except for the methylphosphonate protons with a well defined doublet at 3.38 ppm and two partially-overlapped doublets at 2.76 ppm (Fig. 3. 2 A). By increasing the temperature to 333K, polyaza resonances are re-distributed and merged, with the respective ethylene triplets and doublets becoming more defined. Peak assignment was based on bi-dimensional DQF-COSY spectra at 600 MHz (not shown) and comparison with ^{1}H NMR spectra obtained for similar structures.[25,32,84] Further temperature increase to 353K leads to no significant changes in the resonance profile thus indicating that the ligand has essentially the same structural dynamics at both temperatures. The large number of resonances is due to the C1-simmetry of the molecule as a result of pendant arm removal.

As for DO3P1Pr, all recorded spectra are similar to the one of DO3P with the exception of two additional triplets at 2.45 and 3.81 ppm corresponding to the ethylenic protons of the propionate pendant arm (Fig. 3. 2 B). The temperature dependence of the resonance profile also indicates that the same structural dynamics is at play.

Regarding DO3P1ol, at 333K the two triplets are found at 2.25 and 3.7 ppm and the quintet is at 1.93 ppm, corresponding to the propanol moiety (Fig. 3. 2 C). However, by taking into account the resonance profile in this ligand, the structural dynamics is relatively different from the other two compounds. In both DO3P1Pr and DO3P1ol the geminal methylene protons of the pendant arms present sharp multiplets as expected from freely rotating unbound groups.

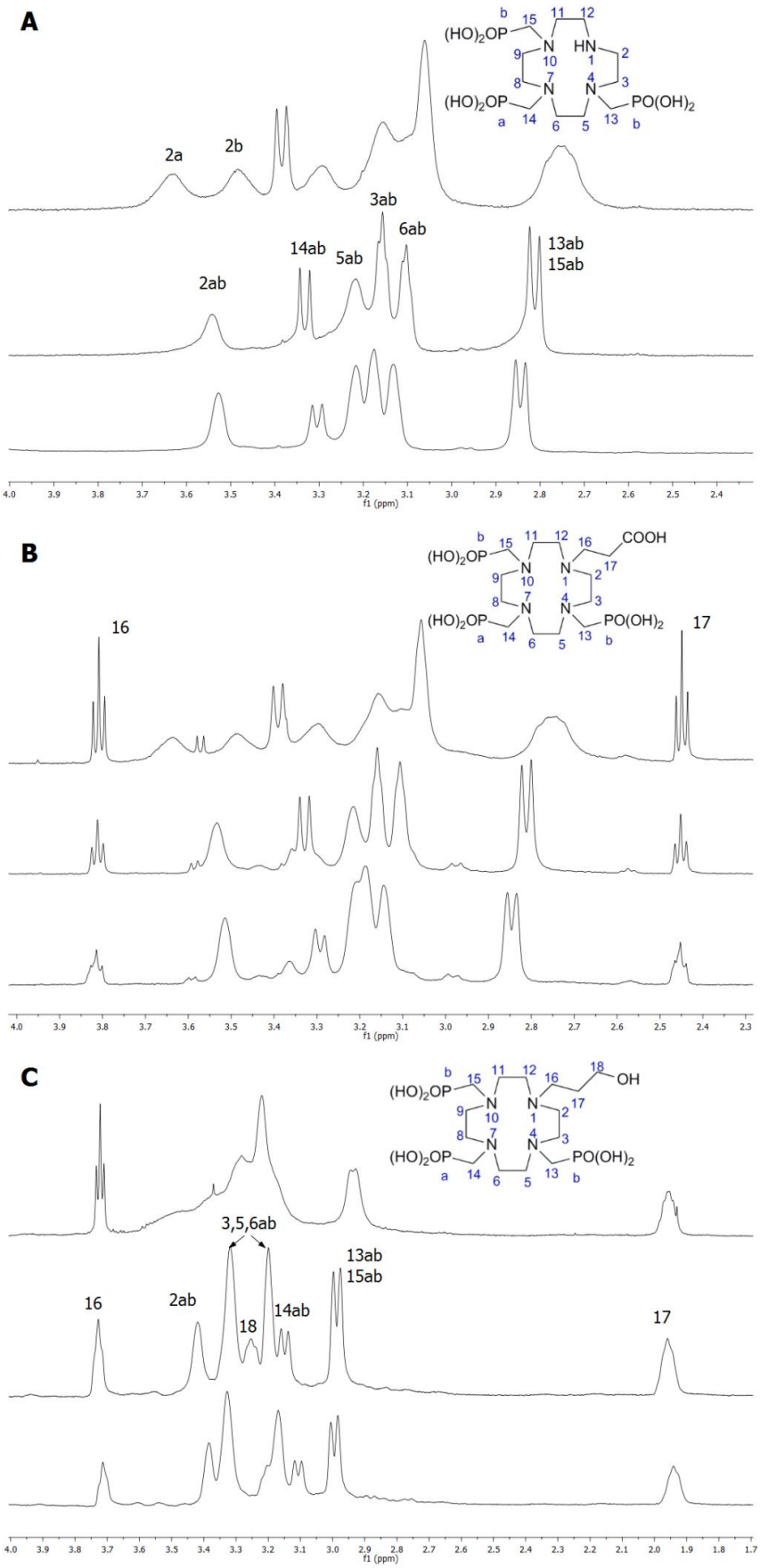

Fig. 3. 2: ^{1}H NMR spectra in 10 mM D_2O solution at variable temperature (298 K at the top, 333 K at the middle and 353 K at the bottom) of: A) DO3P, B) DO3P1Pr, C) DO3P1ol at pH ≈ 8.0.

Solution structures of Ln^{III} complexes

The ^{1}H NMR spectra of all three Lu^{III} complexes show some similarities with those described for Lu^{III}-DO2A2P complexes, thus indicating that the metal ion in these complexes is coordinated through the four macrocyclic nitrogen atoms and an oxygen atom of each of the three phosphonate groups (Fig. 3. 3). The same spectra also show that the propionate and propanol pendant arms are not bound to the Lu^{III} ion since the corresponding geminal methylene protons maintain their sharp multiplets presented in the free ligand spectra. If they were bound to the Lu^{III} ion, they would originate detectable AB or AX multiplet patterns. [36,84]

The coordination geometries of these complexes can also be addressed by examining the temperature dependence of the resonance profiles. Considering the resonances of the ethylenic protons, they are quite broad at 298K and show a significant sharpening at 333K and above. This is an indicator of the isomerization process occurring between the SAP and TSAP structures, which becomes fast in the NMR time scale above 333K. This temperature-dependency is also observable in other Lu^{III} complexes with carboxylate/phosphonate pendant arms, but is absent in those which occur in exclusive TSAP geometry. [36,84]

Tab. 3. 2: ^{31}P NMR chemical shifts (δ/ppm) in 10 mM D_2O solution of the P_a (a) and P_b (b) atoms of the DO3P, DO3P1Pr and DO3P1ol at 162 MHz and some of their Ln^{III} complexes at 202 MHz, in D_2O.

Compound	pH	Temp. (K)	δ (ppm)
DO3P	8.0	298	18.30 (**b**), 9.54 (**a**)
		333	18.30 (**b**), 9.54 (**a**)
Lu^{III}-DO3P	8.56	333	19.20 (**b**), 18.08 (**a**)
Yb^{III}-DO3P	8.50	333	-22.45 (**b**), -33.70 (**a**)
DO3P1Pr	8.0	298	17.69 (**b**), 9.14 (**a**)
		333	18.03 (**b**), 9.65 (**a**)
Lu^{III}-DO3P1Pr	8.69	298	19.84 (**b**), 18.81 (**a**)
		333	19.53 (**b**), 18.40 (**a**)
Yb^{III}-DO3P1Pr	8.62	298	-43.73 (**b**), -58.99 (**a**)
DO3P1ol	8.0	333	16.14 (**b**), 7.89 (**a**)
Lu^{III}-DO3P1ol	8.96	298	18.42 (**a**,**b**)
		333	18.13 (**a**,**b**)
Yb^{III}-DO3P1ol	?	298	-11.85 (**a**,**b**)
		333	-5.38 (**a**,**b**)

The ^{31}P NMR spectra of the three ligands show two resonances with 1:2 relative intensities that correspond to the P_a and P_b phosphates (Tab. 3. 1). After coordination to Lu^{III} and Yb^{III} ions there is a shift in the P_a and P_b resonances. In the case of Lu^{III} complexes the shifts are very similar, thus reflecting the equivalent binding of the three phosphate atoms. The large ^{31}P shifts caused by the paramagnetic Yb^{III} ion give further evidence of coordination of the phosphate atoms to the central metal ion.

The ^{1}H NMR spectra of the paramagnetic Yb^{III} and Eu^{III} complexes of DO3P and DO3P1Pr show a clear temperature dependence, with the paramagnetic shifts being very broad and most of them not being observable at 298K (Fig. 3. 4, Fig. 3. 5). Only at 333K and 353K is possible to observe them as they become sharper and the number of resonances shifted to the upfield region correspond to axial macrocyclic ring protons of the TSAP arrangement. The opposite is observed for the Eu^{III}-DO3P1ol complex, where the paramagnetically shifted resonances are sharp at 298K and with increased temperature become increasingly broader. This temperature dependence indicates a dynamic equilibrium between the two SAP and TSAP isomers since the number of resonances shifted upfield correspond to the axial ring protons with 1:1:2 relative intensities for each isomer. Based on the comparison with other ^{1}H NMR spectra obtained for Ln^{III} complexes of DOTA, DOTP, DO2A2P and other ligands with mixed pendant arms, the three low-field resonances found for Yb^{III}-DO3P, Eu^{III}-DO3P and Yb^{III}-DO3P1Pr at 353K are characteristic of axial ring protons in TSAP isomers. However, for the Eu^{III}-DO3P1ol complex at 298K two sets of axial ring proton are present in approximately 1:1 ratio, thus indicating the presence of both SAP and TSAP isomers. The relatively small paramagnetic shifts of the propionate and propanol pendant arms indicate that they are not bound to the paramagnetic center.

^{17}O NMR and ^{1}H NMRD profiles

The relaxometric properties of Gd^{III}-DO3P1ol were studied at 298K, namely its ^{1}H NMRD profile and the temperature dependence of the water ^{17}O NMR longitudinal and transversal relaxation rates and chemical shifts. The simultaneous fitting of the obtained curves was not possible; therefore no quantitative analysis of the parameters describing the water exchange, rotation, electronic relaxation and proton relaxivity could be performed. However, some qualitative conclusions can be drawn. The ^{17}O NMR data show that the q value is between 0-1, since the reduced ^{17}O chemical shifts of water are close to zero (<200 Hz) instead of around 8-10x10^5 Hz expected for Gd^{III} complexes with q=1. Furthermore, the reduced transverse relaxation rates are much lower than those found in q=1 complexes (Fig. 3. 6).[25]

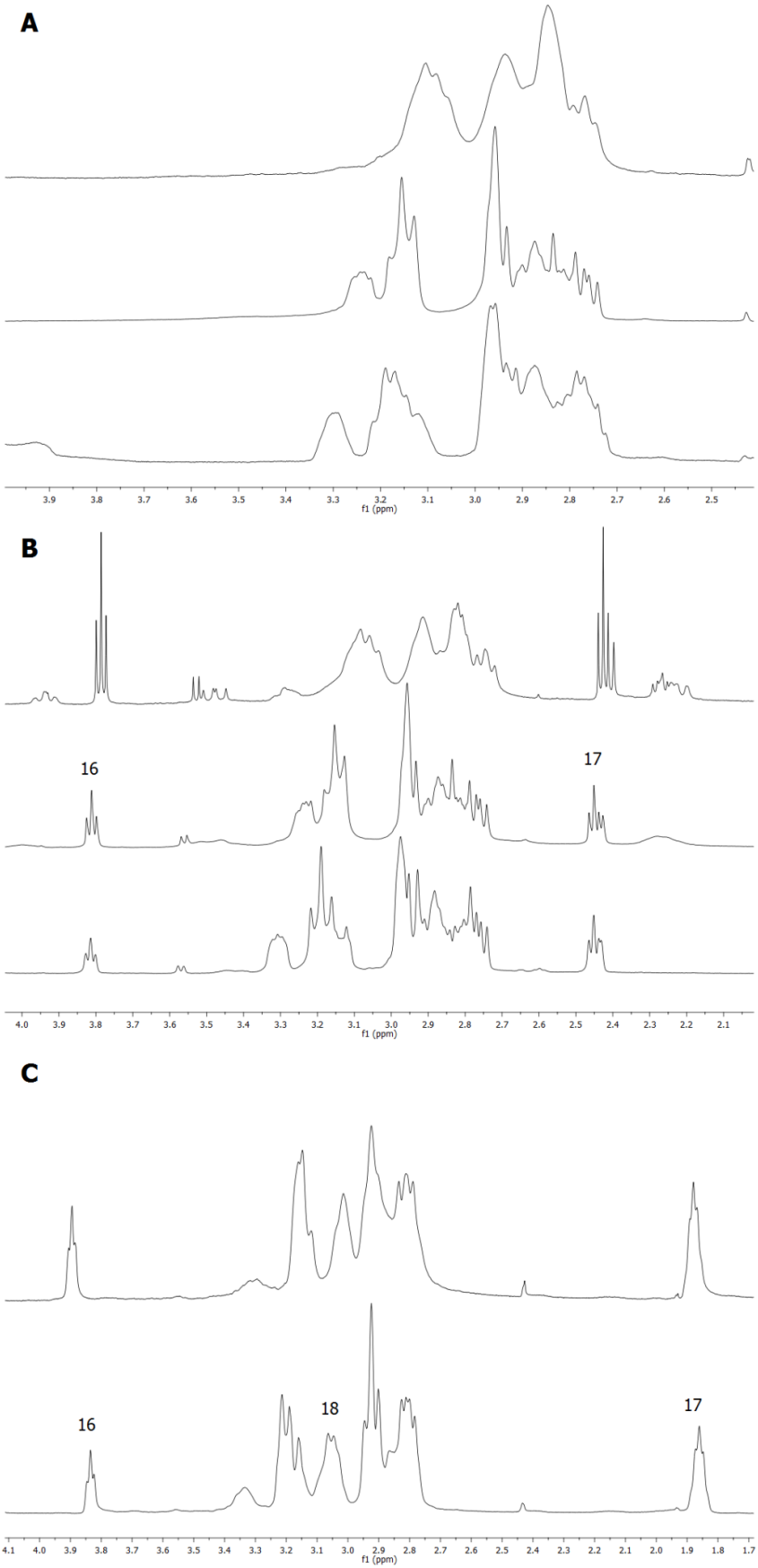

Fig. 3. 3: ^{1}H NMR spectra in 10 mM D_2O solution at variable temperature of the complexes: A) Lu^{III}-DO3P (pH = 8.56, 298 K at the top, 333 K at the middle and 353 K at the bottom), B) Lu^{III}-DO3P1Pr (pH = 8.69, same temperatures as for A), C) Lu^{III}-DO3P1ol (pH = 8.96, 333 K at the top and 353 K at the bottom).

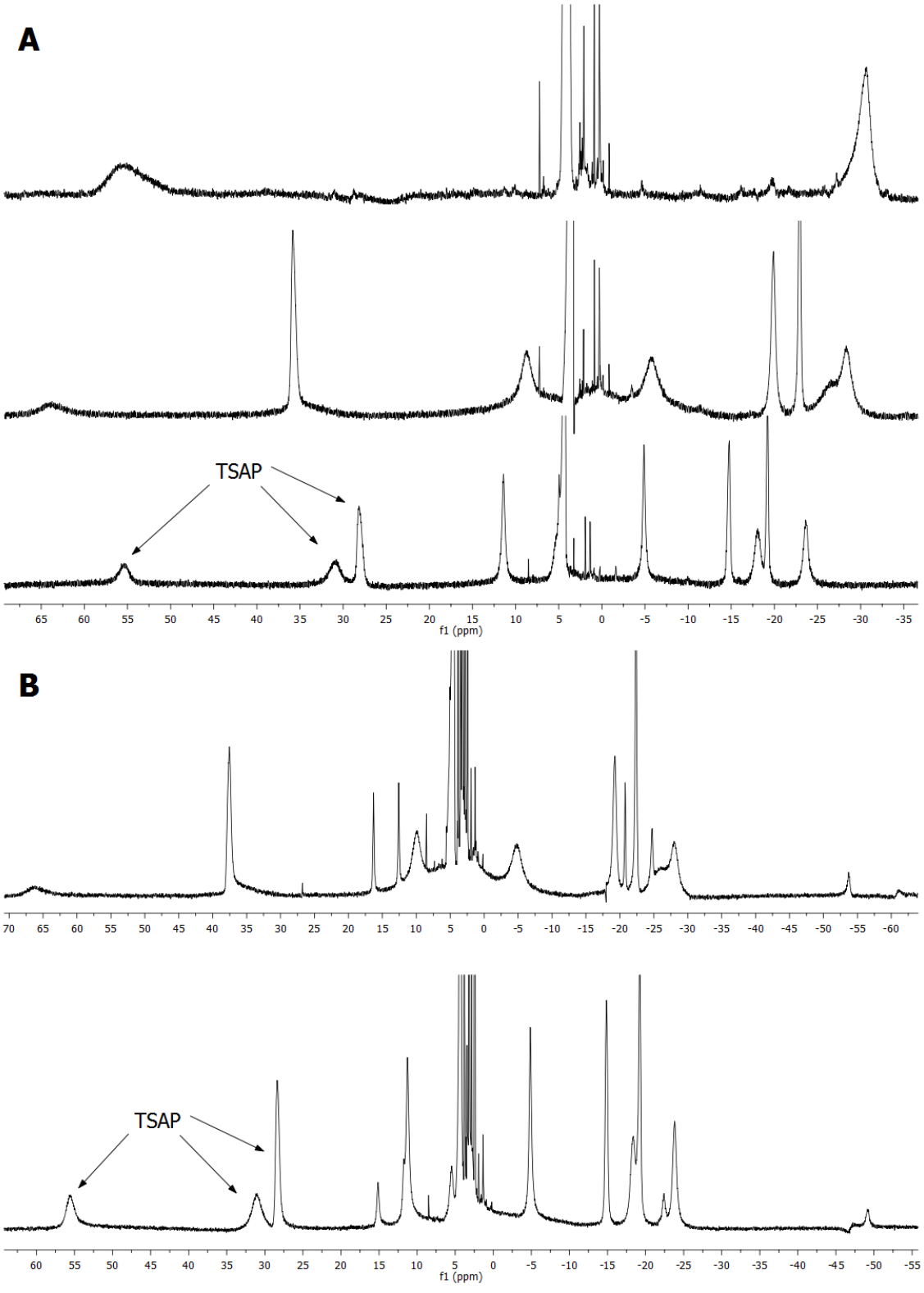

Fig. 3. 4: ^{1}H NMR spectra in 10 mM D_2O solution at variable temperature of the complexes: A) Yb^{III}-DO3P (pH = 8.50, 298 K at the top, 333 K at the middle and 353 K at the bottom), B) Yb^{III}-DO3P1Pr (pH = 8.62, 333 K at the top and 353 K at the bottom).

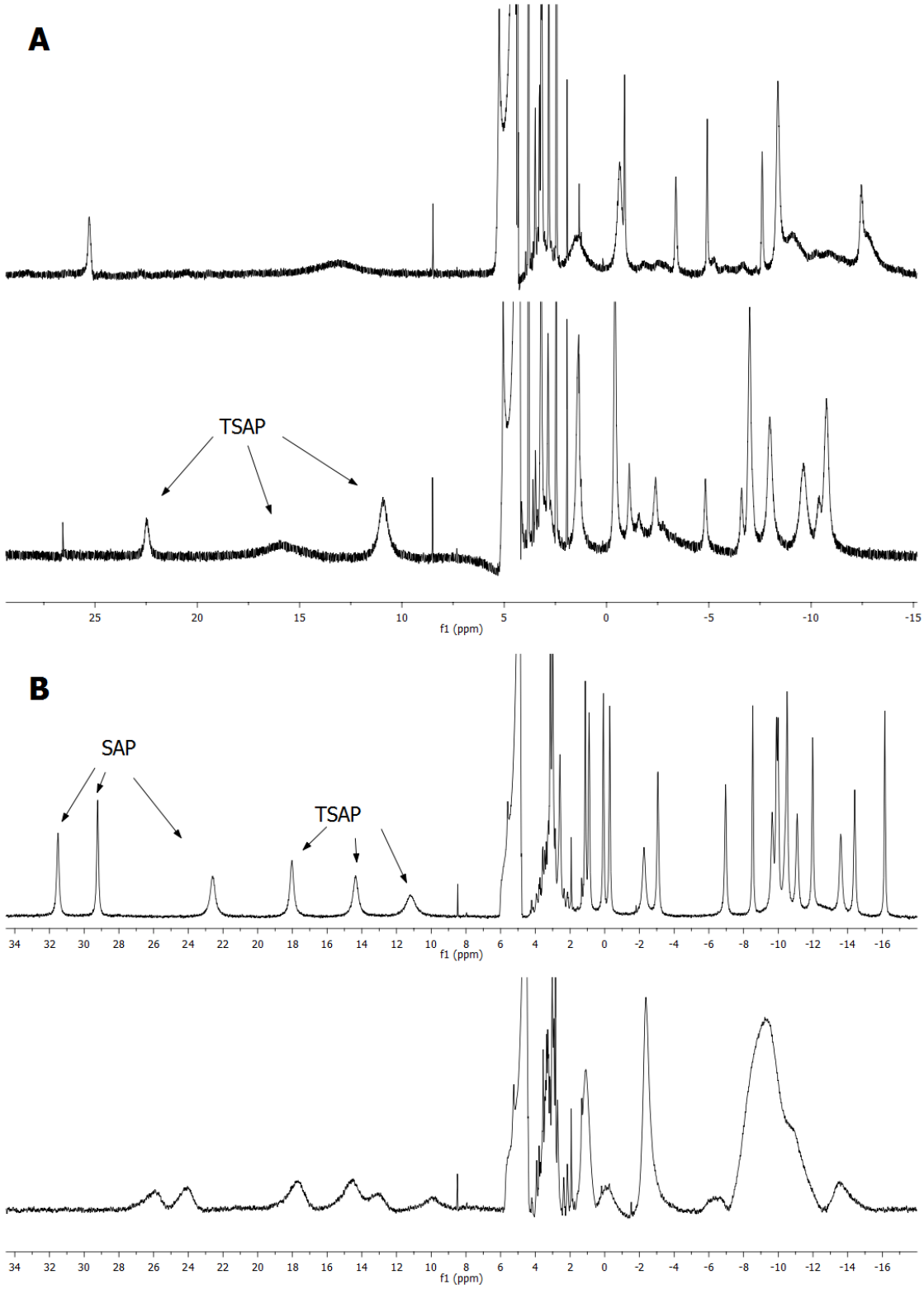

Fig. 3. 5: ^{1}H NMR spectra in 10 mM D_2O solution at variable temperature of the complexes: A) Eu^{III}-DO3P1Pr (pH = 8.92, 333 K at the top and 353 K at the bottom), B) Eu^{III}-DO3P1ol (pH = 8.63, 298 K at the top and 353 K at the bottom).

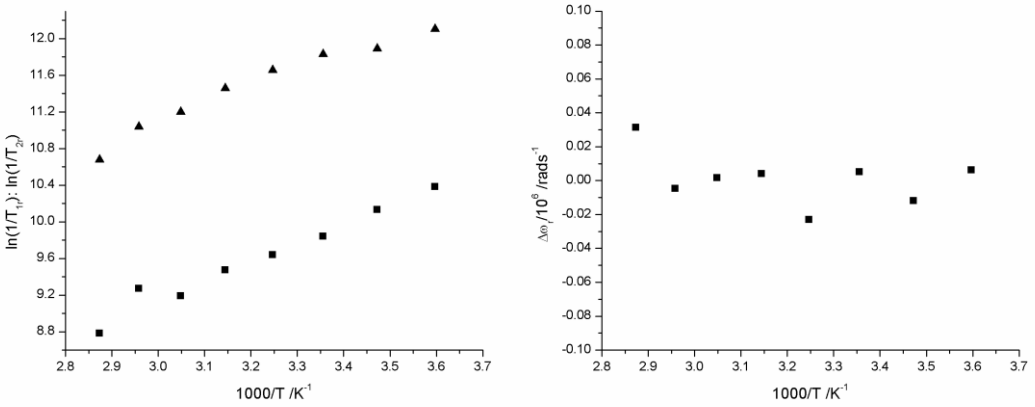

Fig. 3. 6: Temperature dependence of the logarithms of the ^{17}O reduced relaxation rates (longitudinal (■) and transverse (▲) (left) and reduced chemical shifts (right) of Gd^{III}-Do3P1ol in aqueous solution (B = 11.7 T, c = 26.86 mM, pH= 7.45).

The NMRD profile show low values of r_1 at low magnetic fields with a peak at higher fields (60 MHz) thus indicating that there is self-aggregation for this complex in experimental conditions tested (Fig. 3. 7). This has been observed for other Gd(III) macrocyclic phosphonate complexes.[91-93] The obtained values of r_1 are characteristic for complexes with q values between 0-1, corroborating the results obtained in the spectroscopic studies for the respective Eu^{III} complexes.[89] However, it should also be considered that these values can derive from a second-sphere contribution, as it is the case for DOTP.[94]

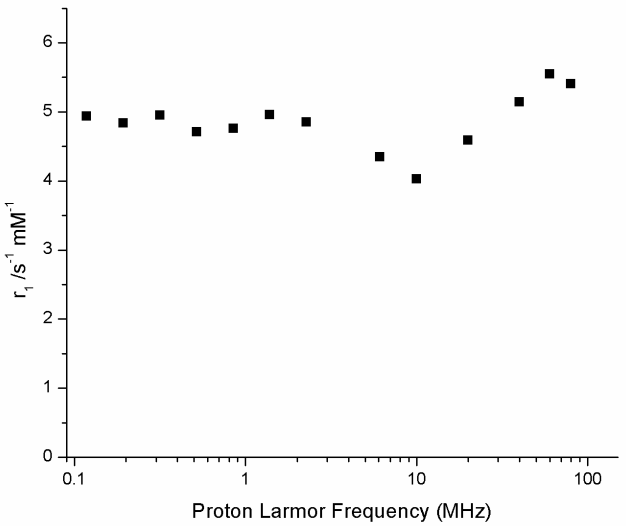

Fig. 3. 7: ^{1}H NMRD curve for Gd^{III}-DO3P1ol in aqueous solution at 298 K ([ ] = 4.56 mM, pH= 6.5).

It was not possible to obtain the NMRD profiles and ^{17}O NMR data for the Gd^{III} complexes of DO3P and DO3P1ol since that their low solubility is incompatible for these experiments.

3.3 - Conclusions

This work was intended to give structural insights on the complexation scheme presented by the Ln^{III} complexes of DO3P, DO3P1Pr and DO3P1ol and also to evaluate their relaxometric properties. The ^{1}H and ^{31}P NMR studies allowed for determination of the coordination scheme presented by the three Ln^{III} complexes. Together with the data obtained by other independent experimental techniques, it was concluded that the three phosphonate atoms of DO3P, DO3P1Pr and DO3P1ol are involved in the coordination of the Ln^{III} ions and that for both DO3P1Pr and DO3P1ol the additional pendant arm was not involved in metal coordination. The Yb^{III} and Eu^{III} complexes of DO3P and DO3P1Pr are present in a predominant TSAP conformation and the Eu^{III}-DO3P1ol complex is present in both TSAP and SAP isomers in 1:1 ratio at the observed temperatures. Variable Temperature ^{1}H NMR studies in a wider interval of temperatures (from 238 to 353K) could be used to determine the activation energy of interconversion between the two isomers and the X-ray structures could be useful in determine the orientation of the additional pendant arms in relation to the macrocycle. The ^{17}O NMR and ^{1}H NMRD studies of Gd^{III}-DO3P1ol indicated that self-aggregation occurs in the analyzed experimental conditions and that the q value is lower than one, although the role of second-sphere contribution could not be addressed. Studies performed at different values of pH and concentration, within the allowed range of these experimental techniques, could be used to obtain data that would allow the simultaneous fitting of the curves and therefore determine the physicochemical parameters describing their relaxivity under the GSBM model.

The data derived from these studies gave further understanding of the thermodynamic and kinetic properties presented by these complexes, since their lower dendicity and rigidity in comparison to DOTP complexes are responsible for low kinetic inertness and fast complexation kinetics. The results also indicate that in the design of bi-functional ligands based on cyclen with phosphonate pendant arms the targeting/linker moiety should not compromise the ability of the pendant arm to coordinate the central Ln^{III} metal ion.

CHAPTER 4

Ln^{III} complexes of Pyridine-*N*-oxide analogues of DOTA: Physicochemical and Photophysical Studies of a Potential MRI/NIR Imaging Probe

4.1 - Introduction

The design of new Gd^{III}-based CA needs to take into account the physico-chemical parameters that affect their efficacy, expressed as relaxivity (r_1). Among these, the residence time (τ_M) of the coordinated water molecules plays a significant role in the extent of magnetic information transfer from the metallic centre to the bulk water molecules. This in turn is dependent on the structure of the complex in solution, mainly the steric crowding around the water-binding site.

In DOTA-like complexes, the two diastereoisomers, TSAP and SAP, present different electronic densities around the capped position, leading to significant changes in τ_M (one to two orders of magnitude). In general terms, TSAP isomers exhibit faster water-exchanging regimes, due to higher steric crowding that favors water exchange. However, due to the fact that the distance between the bound water molecule and the metallic centre is larger for TSAP isomers, the exchange of magnetic information is less effective. Therefore, the design of new CA has been directed towards the development of systems that exhibit a predominant SAP conformation as well as a small τ_M through a fine modulation of the steric crowding around the water-biding site.

One of such examples is the system reported by Polášek *et al.* where an increase in chelate ring size led to an adoption of an exclusive isomer by the Ln^{III} complexes with one water molecule.[95-97] This was achieved by substituting one acetate pendant arm for a 2-methyl-pyridine-*N*-oxide one, the resulting ligand being named DO3A-py^{NO} (H_3do3apy^{NO} = 10-[(1-oxidopyridin-2-yl)methyl]-1,4,7,10- tetraazacyclododecane-1,4,7-triacetic acid). An additional derivative was also reported, DO3A-py^{NO-C} (H_4do3apy^{NO-C} = 10-[(4-carboxy-1-oxidopyridin-2-yl) methyl]-1,4,7,10-tetraazacyclododecane-1,4,7-triacetic acid), where the position 4 of the pyridine-*N*-oxide ring was functionalized with a carboxylic moiety (Fig. 4. 1). Both complexes showed very similar structural properties. The coordination of the pyridine-*N*-oxide oxygen atom to the central metal ion forms a six-membered chelate ring instead of the common five-membered chelate rings formed in most DOTA-like and DTPA-like complexes. This leads to a strong destabilization of the TSAP arrangement which is present only as an unstable intermediate during enantiomerization of the SA isomer. The introduction of the methylpyridine-*N*-oxide arm also originates a new kind of SAP isomerism, where the orientation of the pyridine-*N*-oxide arm in relation to the acetate pendant arms leads to *syn*-SAP or *anti*-SAP conformations. In the *syn* form the orientation of the pyridine-N-oxide function follows the direction of rotation of the acetate arms, while in the *anti* form the

aromatic ring is bent backwards. The coordination of the pyridine-*N*-oxide arm leads to an enlargement of the ligand cavity in relation to the DOTA analogues, resulting in greater flexibility of the coordination cage. The authors proposed that the increased cage flexibility in combination to higher steric hindrances were most likely the reasons for the observed fast water exchange rates (τ_M = 39 ns and 34 ns for the unsubstituted and substituted pyridine-*N*-oxide moiety, respectively), albeit the SAP conformation was strongly favored. These compounds showed favorable properties for MRI applications, such as relaxivity values and thermodynamic stability similar to those used in clinical applications and the possibility of bifunctionalization via the carboxylic moiety of the pyridine-*N*-oxide arm.

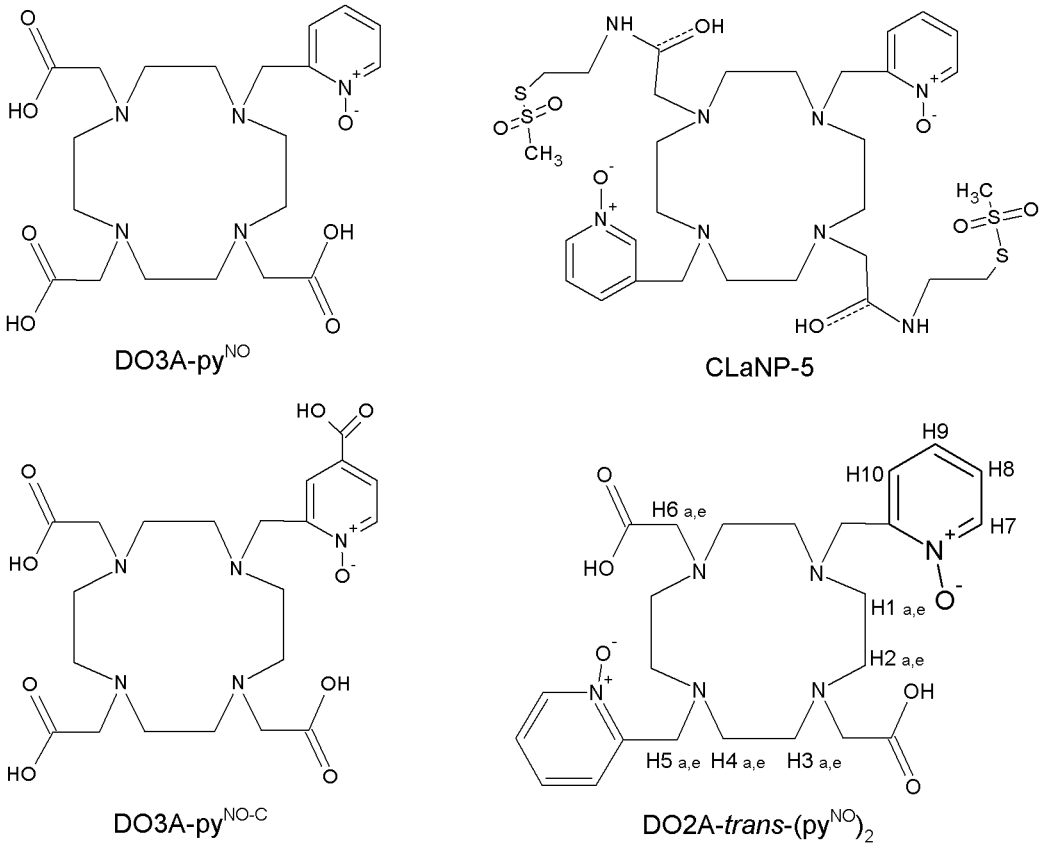

Fig. 4. 1: Ligands Discussed in this work

In another work reported by Keizers *et al.* the pyridine-*N*-oxide derivative was further modified with the objective of creating a caged lanthanide NMR probe, CLaNP-5 to be attached to proteins for NMR structural studies (Fig. 4. 1).[98] An additional pyridine-*N*-oxide arm was added in a *trans* position together with two 2-(amino- ethyl)methanethiosulfonate moieties in opposite acetate pendant arms, so that the respective Ln^{III} complexes would have a

2-fold rotational axis (C2 symmetry) with reduced ring and side chain isomerization and also with the capacity to attach to cysteine residues.

The aforementioned studies did not focus on the photophysical properties of the reported compounds. However, some luminescence studies were performed and the obtained results pointed to some interesting properties. In the case of DO3A-py^{NO} and DO3A-py^{NO-C}, the excitation spectrum in the ligand region and emission spectrum of the respective Eu^{III} complexes were performed, having shown that the ligand is able to transfer energy to the excited states of the Eu^{III} ion. Furthermore, it was also shown that the introduction of the carboxylic moiety in the position 4 of the pyridine-N-oxide does not alter the ability of the ligand to sensitize lanthanide luminescence. The excitation spectrum had a maximum at 396 nm and the emission spectrum showed a maximum at 616 nm, corresponding to the "hypersensitive" $^7F_2 \leftarrow {}^5D_0$ transition, which becomes predominant for low symmetry complexes. Luminescence lifetimes were also measured for both Eu^{III} complexes, giving monoexponential decays with τ_H = 0.624 ms for DO3A-py^{NO} and τ_H = 0.617 ms for DO3A-py^{NO-C}. Furthermore, the $^7F_0 \rightarrow {}^5D_0$ transition was also analyzed in order to determine the two types of SAP isomers present in solution.

In the case of CLaNP-5, for the Eu^{III} complex the maximum of the absorption spectrum was obtained at 250 and 210 nm (260 nm for free ligand). The excitation spectrum presented characteristic bands of the Eu^{III} ion (590, 617 and 710 nm) after excitation at 250 nm. The reported luminescence lifetimes at 617 nm were τ_H = 0.503 ms.

Lanthanide complexes are known to have great potential as optical probes. However, the number of reported cases where lanthanide sensitization is done by macrocyclic ligands such as cyclen, porphyrinate crown-ethers is relatively small in comparison to the number of reported compounds with luminescent properties based on different scaffolds such as 8-hydroxyquinolinate.[65] Considering cyclen derivatives, ligands such as fluorescein, quinoxaline and picolinate derivates were attached to a DO3A scaffold, with the resulting complexes showing lanthanide sensitization via the Antenna Effect. Another interesting case is a heterobimetallic complex where a Re^{III} chromophore is attached to a Gd^{III}-DO3A complex with consequent energy transfer through a ^{3}MLCT mechanism. Near Infrared emitting probes are also of great interest for bioimaging applications. So far, only a small number of potential bimodal MRI/NIR probes based on lanthanide complexes have been reported.[99-102] Furthermore, although Yb^{III} complexes usually have more suitable quantum yields in the NIR region for biological applications, there is also an increasing interest in other NIR emitting Ln^{III} ions, such as Ho^{III}, Nd^{III}, Pr^{III} and Er^{III}.[103] However, the possibility of creating bimodal MRI/NIR based on this kind of complexes is still relatively unexplored.

This study is focused in one of the reaction intermediates of CLaNP-5, DO2A-*trans*-$(py^{NO})_2$ (4,10-di[(1-oxidopyridin-2-yl)methyl]-1,4,7,10-tetraazacyclododecane-1,7-diacetic acid = **L1**) bearing only the two pyridine-*N*-oxide arms (Fig. 4. 1). It is intended to have more insights on the physico-chemical properties of its respective Ln^{III} complexes and also to have a better understanding of its structural dynamics. Furthermore, it is also intended to study the luminescent properties of the Ln^{III} complexes in order to assess their potential as bimodal MRI/NIR probes, given the presence of two pyridine-*N*-oxide moieties that can act as lanthanide-luminescence sensitizers.

4.2 - Results and Discussion

Relaxometric studies

The suitability of the Gd^{III} complexes for MRI applications was evaluated by relaxometric and transmetallation studies, namely the determination of its longitudinal relaxivity r_1 and evaluation of its thermodynamic and kinetic stabilities. The value of r_1 was obtained by measuring the longitudinal relaxations times of Gd^{III}-L1 solutions of increased concentrations, ranging from 0.25 mM to 3 mM at pH ~7 (Fig. 4. 2). The slope of the obtained curve corresponds to the value of r_1 and it was equivalent to 2.41 $mM^{-1}s^{-1}$ at 298K and 1.98 $mM^{-1}s^{-1}$ at 310K.

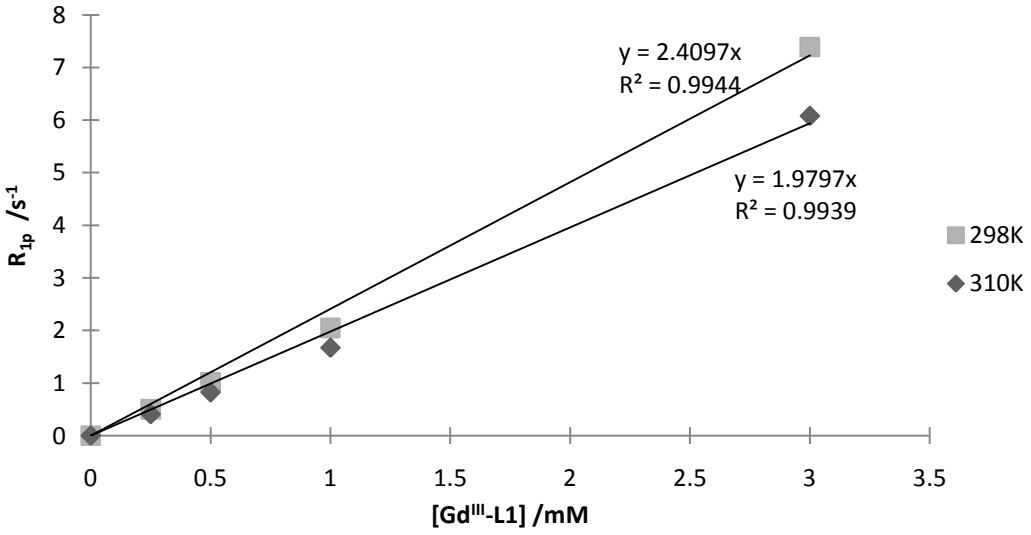

Fig. 4. 2: Paramagnetic longitudinal relaxation times (R_{1p}) as a function of increased Gd^{III}-L1 concentrations at 298K and 310K at pH ~7. The y=mx equations correspond to the obtained trend lines at both temperatures (298K – top; 310K – bottom), where r_1 = m.

The magnetic field dependency of the longitudinal relaxation rates was obtained in a NMRD study (Fig. 4. 3). The obtained profile is typical for small Gd^{III} chelates, and it closely resembles the one obtained for the analogous Gd^{III}-DO3A-py^{NO}.[95-97] However, there is some discrepancy between the values obtained for the 1 mM solution at 20 MHz in each experimental setup. This is most likely due to precipitation of the complex in solution above 3 mM, thus making the real concentration value of the 5 mM Gd^{III}-L1 solution uncertain. In order to confirm if there was in fact precipitation of the complex in solution, a 5 mM sample was prepared and filtrated and its real concentration was measured by the BMS test. The obtained value was 3.7 mM, thus indicating that complex precipitation was occurring. For this reason, the R_{1p} values obtained for solutions with concentrations below 3.7 mM are considered to be more reliable than those of 5 mM and therefore only the r_1 value obtained at 20 MHz (in Bruker Minispec) was considered.

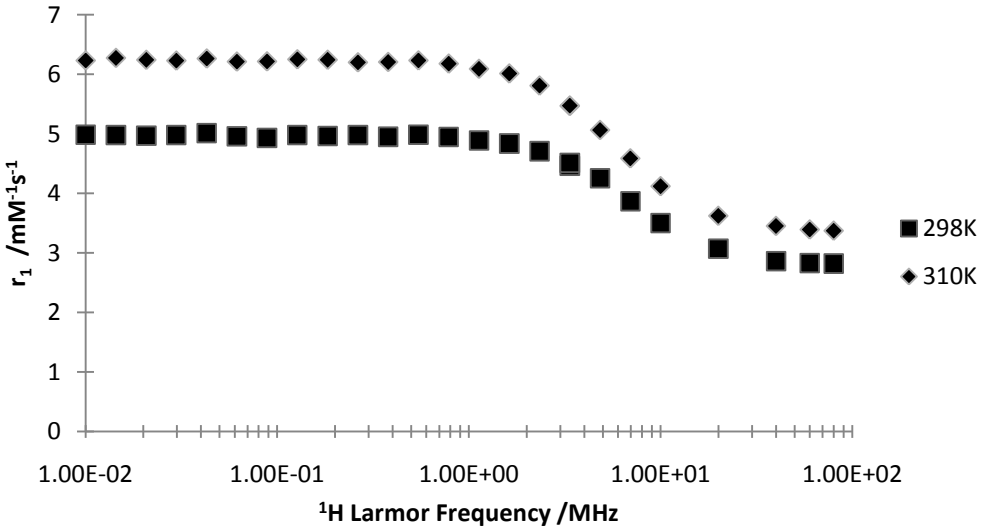

Fig. 4. 3: ^{1}H NMRD profiles obtained at 298K and 310K for 1mM solutions Gd^{III}-L1 complexes, pH ~7.

Nonetheless, the NMRD profile remains valid as no self-aggregation of the complex is expected to occur. The obtained r_1 values at 298 and 310K are lower than those reported for Gd^{III}-DOTA (q=1, 4.2 $mM^{-1}s^{-1}$ at 298K) and other commercially available compounds, thus indicating that less than one water molecule is present in the inner sphere of coordination (0< q< 1) and probably only an outer sphere contribution is involved.[16] This is somehow expected due to the increased steric crowding caused by the presence of the two pyridine-*N*-oxide moieties. However, no further experiments were performed in order to determine the q value, such as the Horrock's method and its subsequent modifications or ^{17}O NMR experiments.

Variable temperature studies were also performed with a 1 mM Gd^{III}-L1 solution at 20 MHz in the 275-350K range. The obtained profile indicates that the system is in a fast water exchange regime, given the positive slope of the curve. This, however, cannot be considered a direct measure of the residence time of the water molecules. Only with simultaneous fitting of the curves obtained by VT-^{17}O NMR and ^{1}H NMRD, under the GSBM framework, could this and other parameters be determined.

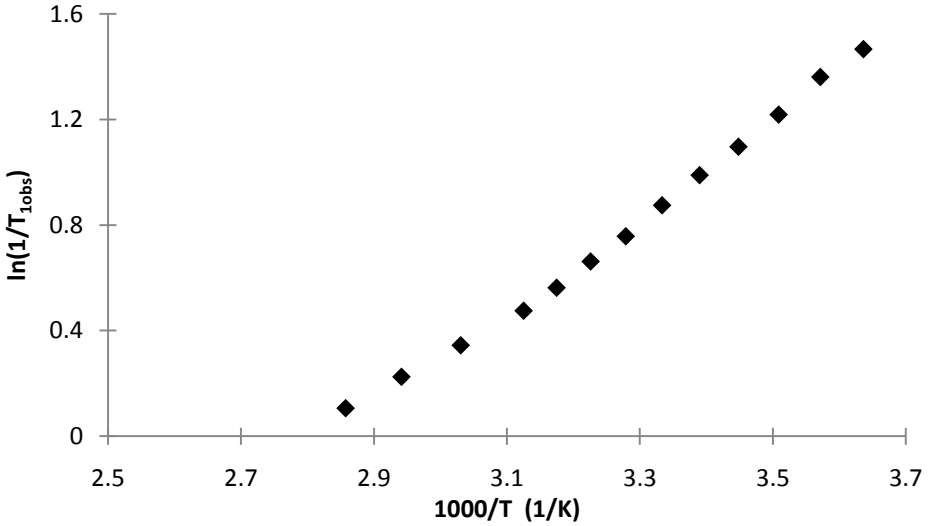

Fig. 4. 4: Observed Longitudinal relaxation times (T_{1obs}) of a 1 mM Gd^{III}-L1 solution (pH ~7) as a function of temperature.

Metal and H^+ assisted dissociation of Ln^{III} ions are one of the major drawbacks in the design of new Gd^{III} chelates since they are key indicators of thermodynamic and kinetic stabilities. A complex suitable for MRI applications must be stable within acid to basic conditions and it must be resistant to transmetallation events in the presence of endogenous ions, such as Zn^{II}, Fe^{II}, Ca^{II} or Cu^{II}.

Transmetallation studies are a very straight approach in the determination of these parameters. If the complex has low thermodynamic stability and low kinetic inertness, the R_{1p} value of a Gd^{III} complex solution in PBS medium is expected to decrease as a function of time in the presence of equimolar amounts of the competing metal ion(s). This happens as the released Gd^{III} ions bind to the PO_4^{3-} ions present in solution, forming a complex with very low solubility ($K_{sp}=10^{-22.26}$ M^2 – see methods).[81] Two arbitrary indexes can be considered: a "kinetic index", defined as the time required to reach 80% of the initial R_{1p} value; and a "thermodynamic index" – defined as the $R_{1p}(t)/R_{1p}(0)$ value after 3 days. In this work, Zn^{II}-assisted dissociation of Gd^{III} ions from the ligand was evaluated.

As it can be seen in Fig. 4. 5, the transmetallation process is not very extensive. The "kinetic index" is > 3000 min and the "thermodynamic index" is > 0.80. These values are quite satisfactory and fall in the range of the ones reported for commercially available compounds based on macrocyclic and acyclic ligands.[81]

In relation to H^+ assisted dissociation, protonation of a macrocyclic nitrogen and the carboxylic groups can lead to Gd^{III} ion release and consequent increase in relaxivity values.[104] The stability of the complex at different pH values was determined by measuring the value of R_1 of a 1 mM Gd^{III}-L1 solution in the 2.41-12.20 range of pH values (Fig. 4. 6). However in this case, the R_{1obs} values did not significantly varied neither in acid or basic conditions thus indicating that no ion dissociation was occurring. Further potentiometric studies would have to be performed in order to have a more qualitative and quantitative understanding of the complex stability.

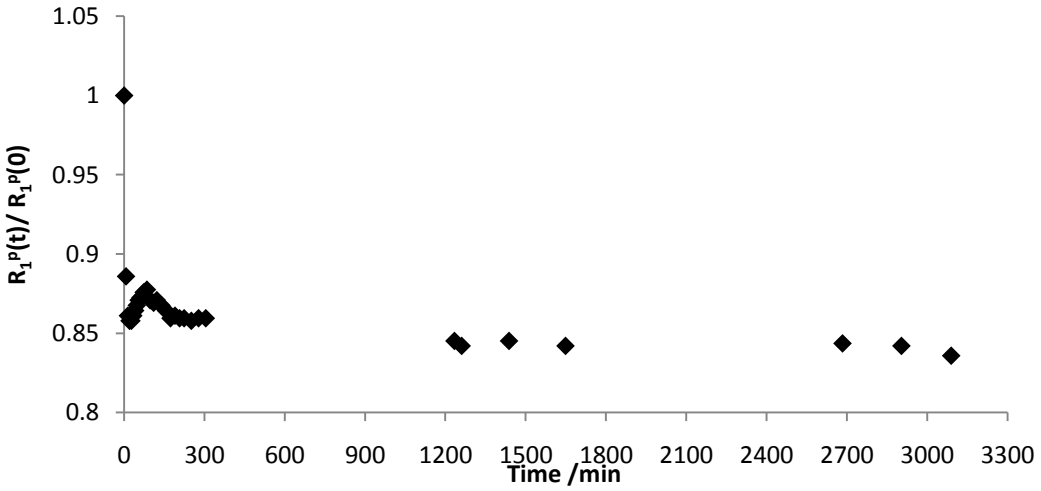

Fig. 4. 5: Evolution of the $R_1^p(t)/ R_1^p(0)$ ratio at 298K of 1 mM Gd^{III}-L1 in 40 mM PBS medium after the addition (t=0) of equimolar amounts of a $ZnCl_2$.

The Gd^{III}-L1 complex has low r_1 values, which compromises its suitability as a MRI contrast agents. Nonetheless, the obtained results gave some insights in the thermodynamic and kinetic stabilities and indicate that this complex might be suitable for biological applications. Furthermore, its suitability for optical applications was also tested, as described below.

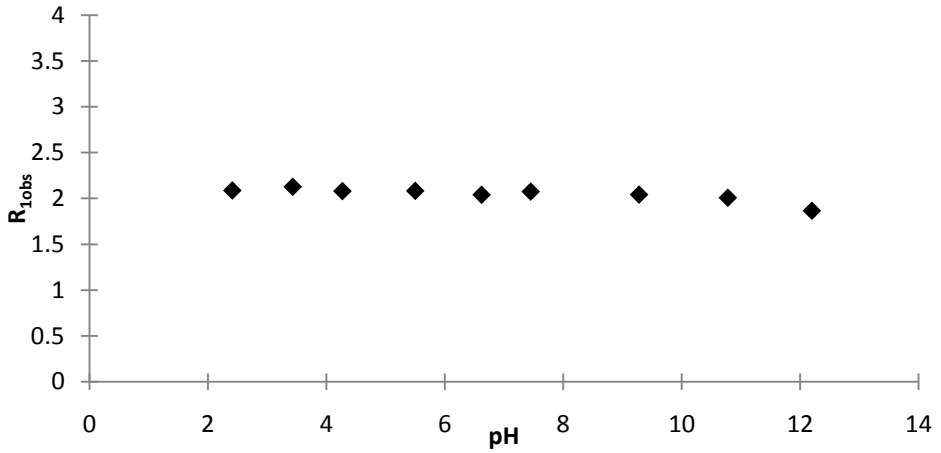

Fig. 4. 6: Observed longitudinal relaxation times (R_{1obs}) of a 1mM Gd^{III}-L1 solution as a function of pH at 298K.

Photophysical Studies

Based on the reported luminescent properties of the analogous DO3A-py^{NO} complexes, it was thought whether this compound could also present the same properties for optical applications. Initially, only the complexes of visible emitters Eu^{III} and Tb^{III} were considered.

First, the UV-Vis absorbance spectra of both Eu^{III} and Tb^{III} complexes were obtained, giving a maximum of absorbance at 260 nm (Fig. 4. 7 A and B, black line in B). It was also observed that the absorption spectrum did not vary among the different Ln^{III}-L1 complexes and only the Tb^{III}-L1 absorption spectrum was presented in all cases. This wavelength value was then used to obtain their emission spectra. Both cases present typical emission profiles of each atom, with six bands for the Eu^{III} complex and four bands for the Tb^{III} complex (Tab. 4. 1). The obtained bands were sharp and well defined thus indicating that an energy transfer process was occurring, given the low molar absorbtivity of the f-f transitions and the concentrations used (0.05 mM). Band profile and assignment was made based on reported literature values.[64]

In order to demonstrate that the ligand was responsible for lanthanide luminescence sensitization, the excitation spectra were obtained by measuring the intensity of the strongest signal for each complex when excited at different wavelengths. In the case of Eu^{III} the observed signal was the one of the $^5D_0 \rightarrow {}^7F_2$ transition band at 615 nm and for Tb^{III} the one corresponding to the $^5D_4 \rightarrow {}^7F_5$ band at 540 nm. Both spectra had a maximum at 260 nm but an unexpected band at 320 nm was also obtained (Fig. 4. 7 and Fig. 4. 8). One possible explanation is that this band corresponds to an energy back-transfer process, since no lanthanide emission was obtained when excitation was made at 320 nm (not shown).

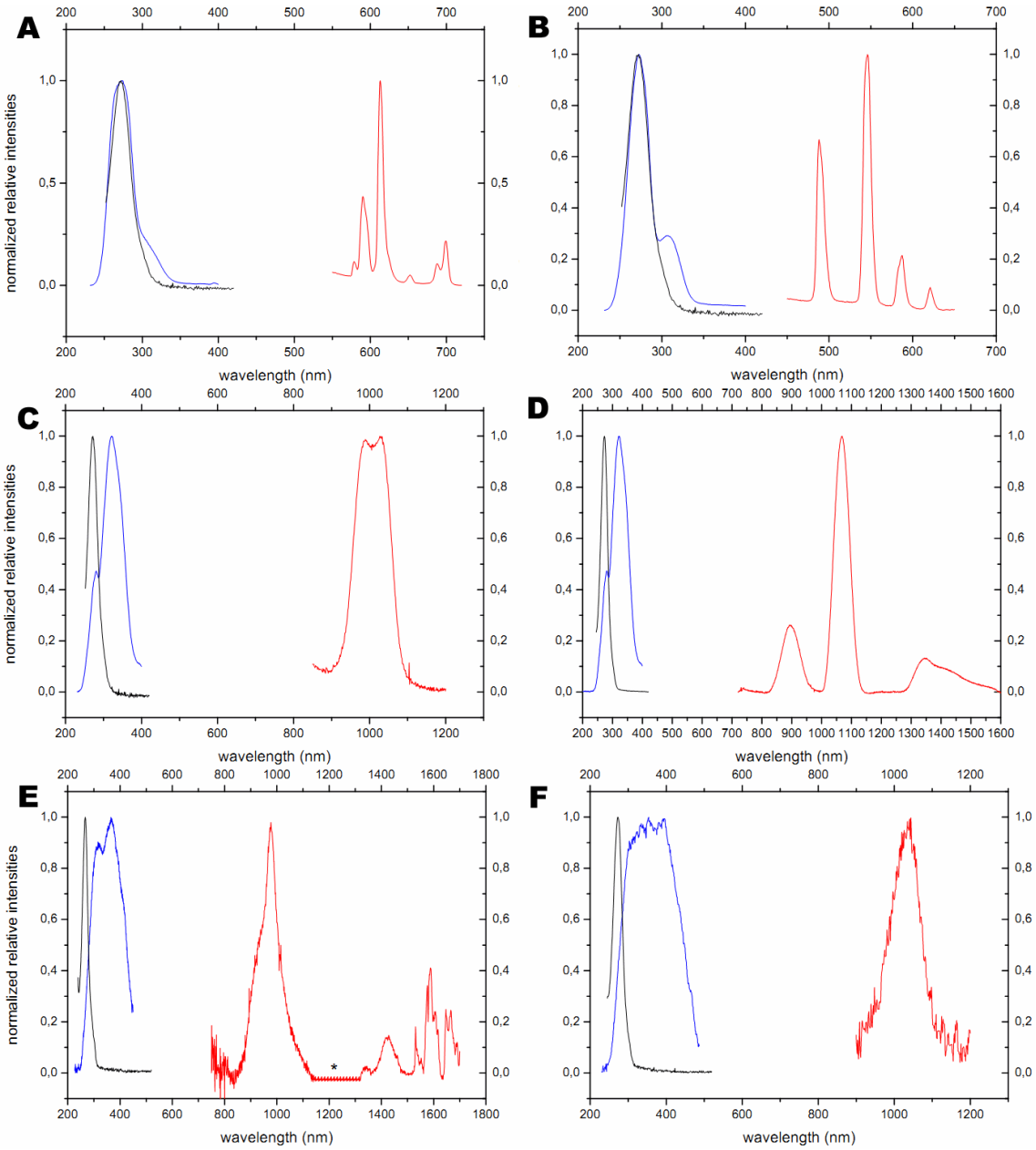

Fig. 4. 7: Excitation (blue) and Emission (red) spectra of Ln^{III}-L1 complexes at 298K, pH ~7 (Ln^{III} = A – Eu^{III}, B – Tb^{III}, C - Yb^{III}; D – Nd^{III}; E - Ho^{III}; F - Pr^{III}). The intensities are normalized to maximum obtained values. Black line corresponds to the absorption spectrum of Tb^{III}-L1 spectrum in all cases.

These results indicated that the ligand L1 had the ability to act as an antenna for lanthanide luminescence in the visible region. For this reason, its ability to sensitize near-infrared emitting Ln^{III} ions was also tested. The corresponding Ln^{III} complexes were then prepared and the same experiments were performed. The emission spectra were obtained by excitation at 260 nm and each lanthanide complex gave characteristic emission bands, with three bands for Nd^{III} and one band for Yb^{III}, Ho^{III} and Pr^{III} (Tab. 4. 1), respectively. The excitation spectra also presented significant shifts for the ligand-centered absorption band, with the highest shifts observed for Ho^{III} and Pr^{III} (Fig. 4. 7 C-F and Fig. 4. 8). In these cases the observed signals were the ones

corresponding to the $^2F_{5/2}\rightarrow{}^2F_{7/2}$ transition at 1000 nm for Yb^{III}-L1, to the $^5F_5\rightarrow{}^5I_7$ transition at 970 nm for Ho^{III}-L1, to the $^1D_2\rightarrow{}^3F_4$ transition at 1050 nm for Pr^{III}-L1 and to the $^4F_{3/2}\rightarrow{}^4I_{11/2}$ transition at 1075 nm for Nd^{III}-L1.

Tab. 4. 1: Observed energy bands of each Ln^{III}-L1 complex and corresponding transitions.

Ln^{III} –L1	Transition(s)	Ground State	λ /nm
Eu^{III}	$^5D_0\rightarrow{}^7F_J$ (J=0-4)	$^7F_0$	580, 590, 615, 650, 690-700
Tb^{III}	$^5D_4\rightarrow{}^7F_J$ (J=6-3)	$^7F_6$	490, 540, 580, 625
Yb^{III}	$^2F_{5/2}\rightarrow{}^2F_{7/2}$	$^2F_{7/2}$	980-1030
Nd^{III}	$^4F_{3/2}\rightarrow{}^4I_J$ (J=9/2-13/2)	$^4I_{9/2}$	900, 1075, 1350
Ho^{III}	$^5F_5\rightarrow{}^5I_7$	$^5I_8$	970
Pr^{III}	$^1D_2\rightarrow{}^3F_4$	$^3H_4$	1050

The ability to sensitize Ho^{III} and Pr^{III} luminescence was somehow unexpected, since the number of reported cases where this had occurred is very limited. Studies where Ho^{III} emission was reported where made in both H_2O and D_2O by Quici *et al.*,[105] in DMSO by Petoud and co-workers[67] and in TRIS-buffered solution by Raymond *et al.*[103] However, it should be noted that the obtained signal is very weak in both cases and the presence of bands in the visible region was not considered. Emission band assignment for these two NIR emitters was based on the works mentioned above.

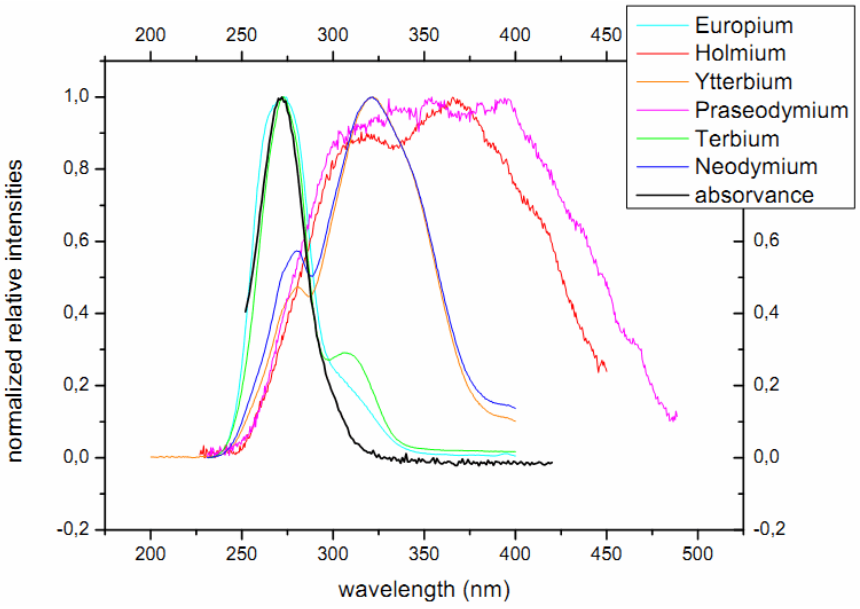

Fig. 4. 8: Detailed superposition of all excitation spectra of Ln^{III}-L1 complexes at 298K, pH ~7.

In order to determine if the ligand is an efficient antenna for lanthanide luminescence, the overall quantum yields of the Ln^{III} complexes were determined. This was done by measuring the intensity of Ln^{III} emission bands and then comparing them to the ones obtained for the reference compound, Ln^{III}-(tropolonate)$_4$ complexes. This compound was reported by Zhang *et al.* and is based on bidentate ligands that bind to the central Ln^{III} ion.[67] The interesting property of this compound is that it also has the ability to sensitize near-infrared Ln^{III} luminescence (Yb^{III}, Nd^{III}, Er^{III}, Tm^{III}, Ho^{III}) in DMSO. The quantum yields were determined by using a comparison method with reported values for another compound (see methods).

Tab. 4. 2: Overall Quantum Yields obtained for Ln^{III}-L1 solutions at 298K, pH~7.

Ln^{III}	Solv.	ΦLn^{III}
Eu^{III}	H_2O	$1.45 \pm 0.01 \times 10^{-1}$
Tb^{III}		$2.91 \pm 0.01 \times 10^{-2}$
Pr^{III}		$2.6 \pm 0.2 \times 10^{-7}$
Ho^{III}		$7.45 \pm 0.03 \times 10^{-8}$
Yb^{III}		$7.3 \pm 0.1 \times 10^{-3}$
Nd^{III}		$1.43 \pm 0.06 \times 10^{-5}$

The obtained values are present in Tab. 4. 2. Comparison with the values reported in the work of Quici *et al*. shows that they fall within the same range, except for the Ho^{III} and Pr^{III} complexes with values 2-3 orders of magnitude lower.[105]

Together with the relaxometric studies, the photophysical data indicate that the presence of a water molecule in the inner coordination sphere of the Ln^{III} is unlikely. The obtained quantum yields are typical of systems were no quencher O-H oscillators are present. This argument is further developed in the following section.

Structural studies

A structural elucidation of Ln^{III} complexes of L1 was attempted by a combination of NMR spectroscopy and computational methods. These studies are quite relevant since the physicochemical and photophysical properties of Ln^{III} complexes of L1 are dependent on its solution structures.

All 1D ^{1}H NMR spectra were obtained at 298K and 333K. Proton signal assignment for L1 (Fig. 4. 9) was based on 2D COSY ^{1}H NMR spectrum (Fig. 4. 10) and comparison with previously

reported spectra of parent DOTA ligand and respective complexes.[25] At 333K significant line broadening and signal merging occurs, thus indicating extended interconversion and dynamic processes at this temperature. For this reason, the 333K spectrum is not presented here.

Tab. 4. 3: ^{1}H shifts (in ppm) for L1 and Lu^{III}-L1 solutions obtained experimentally. Pyridine-N-oxide ^{1}H shifts not included (see Tab. 4. 4).

	δ (ppm)	H's	Class	$J_{H\sim H}$
L1	4.01	4	s	-
	3.5	12	d	16.47
	3.01	4	d	9.31
	2.83	4	d	14.42
Lu^{III}-L1	3.17	2	d	16.86
	3.4	2	d	17.07

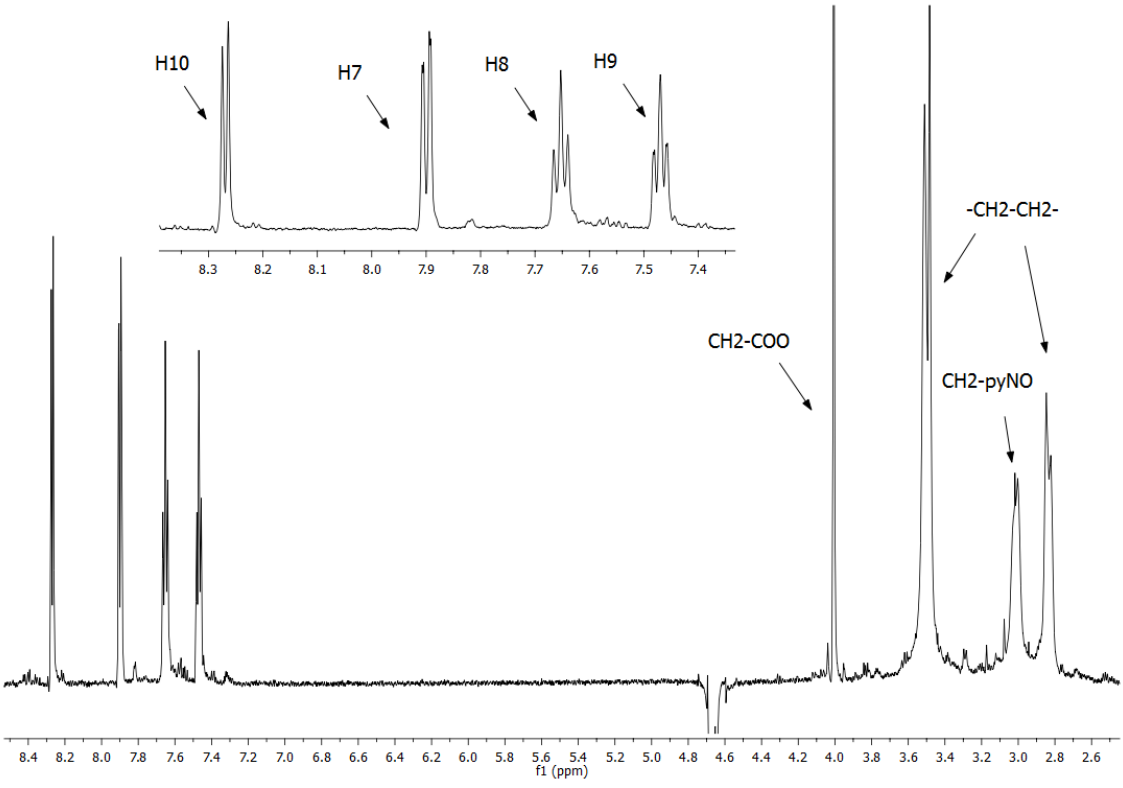

Fig. 4. 9: ^{1}H NMR spectrum of L1 solution at 298K (pyridine-N-oxide signals on inset). At 333K the signals at 2.83 and 3.01 ppm broaden and merge (data not shown).

Considering the spectrum at 298K, the axial and equatorial resonances of the ring ethylenic groups are present at 3.51 and 2.83 ppm. The resonances corresponding to the methylenic protons of the pendant arms are present at 3.01 ppm for the methylpyridine-*N*-oxide pendant

arm and at 4.01 ppm for the acetate pendant arm. The former are present as a multiplet due to unsymmetrical environment caused by the pyridine-*N*-oxide moiety (Tab. 4. 3). The pyridine-*N*-oxide protons give sharp and well defined multiplets in the 7.4-8.4 ppm region of the spectra (Fig. 4. 9– inset and Tab. 4. 4).

Tab. 4. 4: ^{1}H shifts (in ppm) obtained experimentally for pyridine-N-oxide signals in L1, Lu^{III}-L1 and Yb^{III}-L1 solutions with corresponding J_{H-H} couplings (δ_i^{exp} – difference between ^{1}H shifts obtained for Yb^{III}-L1 and L1; δ_i^{dia} - for Lu^{III}-L1 and L1; δ_i^{para} - difference between δ_i^{exp} and δ_i^{dia}. Positive ppm values indicate shifts for higher fields.

	L1		Lu^{III}-L1		Yb^{III}-L1	δ_i^{dia}	δ_i^{exp}	δ_i^{para}
	δ	J_{H-H}	δ	J_{H-H}	δ			
H7	7.9	(dd) 1.66, 7.89	7.67	(dd) 1.83, 7.88	58.95	-0.23	51.05	51.28
H8	7.65	(t) 7.91, 7.91	7.84	(t) 1.13, 7.78	14.13	0.19	6.48	6.29
H9	7.47	(td) 7.09, 1.70	7.69	(m)	1.51	0.22	-5.96	-6.18
H10	8.27	(d) 6.43	8.43	(d) 5.69	-9.13	0.16	-17.4	-17.56

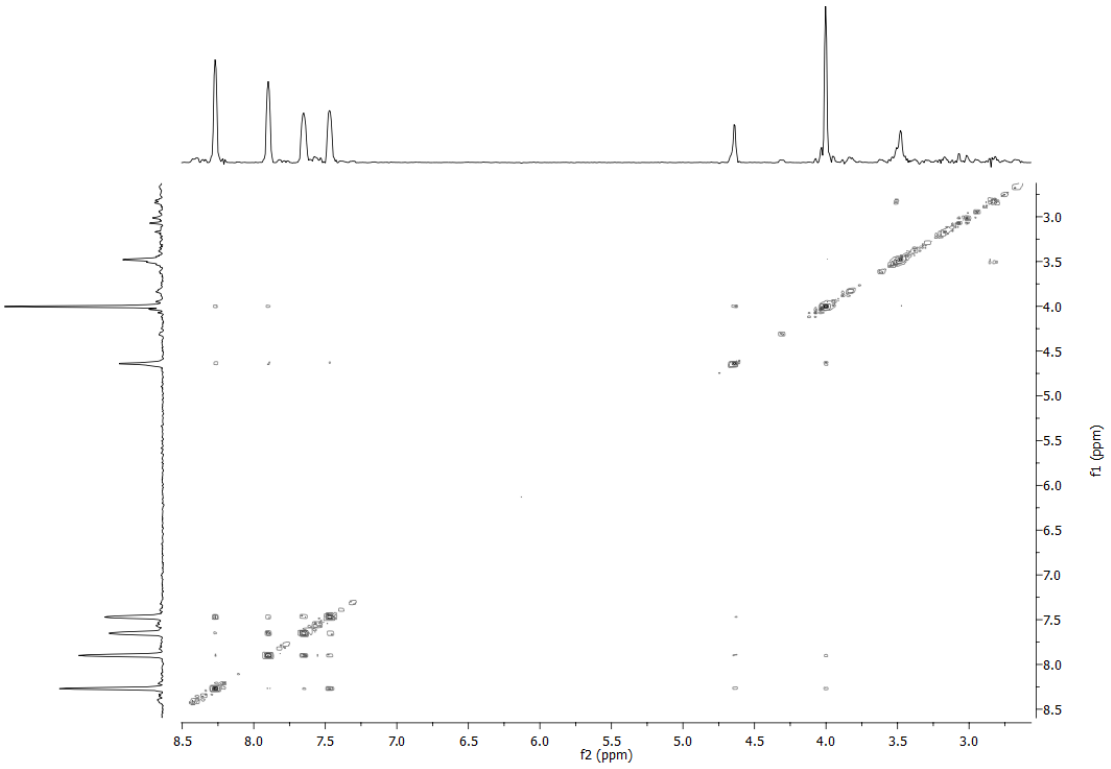

Fig. 4. 10: 2D COSY ^{1}H NMR spectrum of L1 at 298K.

The coordination scheme of Ln^{III} ions was studied with the diamagnetic Lu^{III} complex. The spectrum obtained at 298K (Fig. 4. 11 and 2D COSY Fig. 4. 12) shows shifts for all macrocyclic resonances as well as for the methylenic protons of the pendant arms, making their

assignment impossible except for the acetate protons (H6). This indicates that all four pendant arms are involved in metal ion coordination and in the case of the methylpyridine-*N*-oxide pendant arms, well defined shifts were obtained for their protons (Tab. 4. 4).

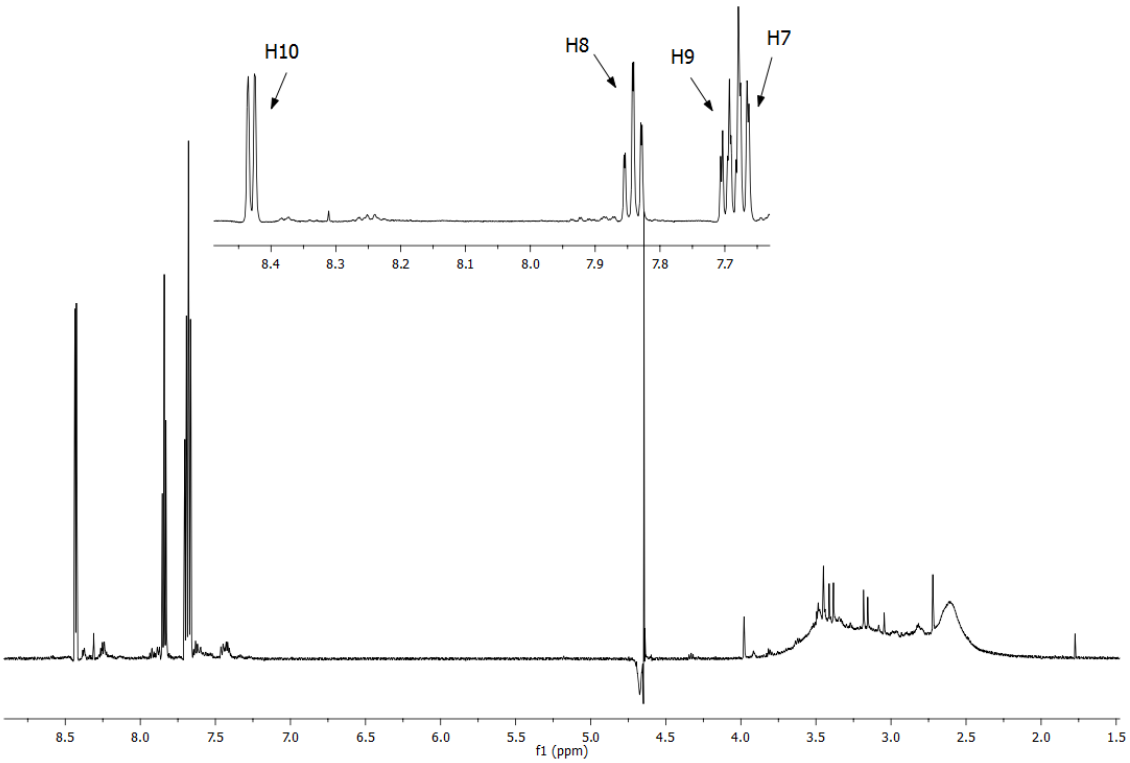

Fig. 4. 11: ^{1}H NMR spectrum of Lu^{III}-L1 complex solution at 298K (pyridine-N-oxide signals on inset).

The Yb^{III}-L1 spectrum at 298K was also obtained (Fig. 4. 13 and 2D COSY Fig. 4. 14). Since the Yb^{III} radius is very similar to the Lu^{III} ion the structure of both complexes should be very similar. The simplified spectrum with 16 resonances is the result of the C2-symmetry of the complex and it also indicates that only one isomer is present at this temperature. Based on the large shifts observed (up to 115 ppm) for the Yb^{III}-L1 complex and the data obtained for analogous CLaNP-5 and DO3A-py^{NO} Ln^{III} complexes, it is presumed that this corresponds to the SAP isomer.

For the ^{1}H NMR spectrum of Yb^{III}-L1 at 333K, resonance merging and broadening occurred, making their interpretation impossible (not shown). However, studies at lower temperatures (down to 238K) could be done in order to evaluate the presence of the TSAP isomer, as it was done in the case of Eu^{III}-DO3A-py^{NO}.[95-97] At these temperatures the interconversion between the two isomers is observable in the NMR time-scale.

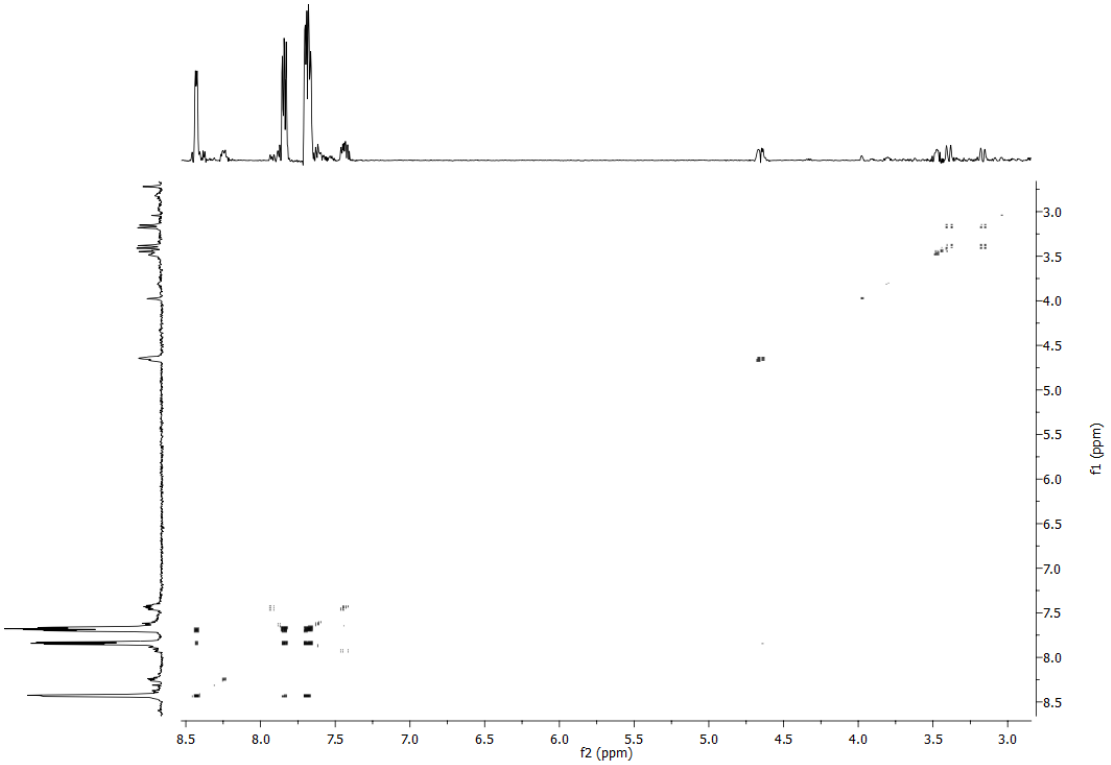

Fig. 4. 12: 2D COSY ^{1}H NMR spectrum of Lu^{III}-L1 complex at 298K.

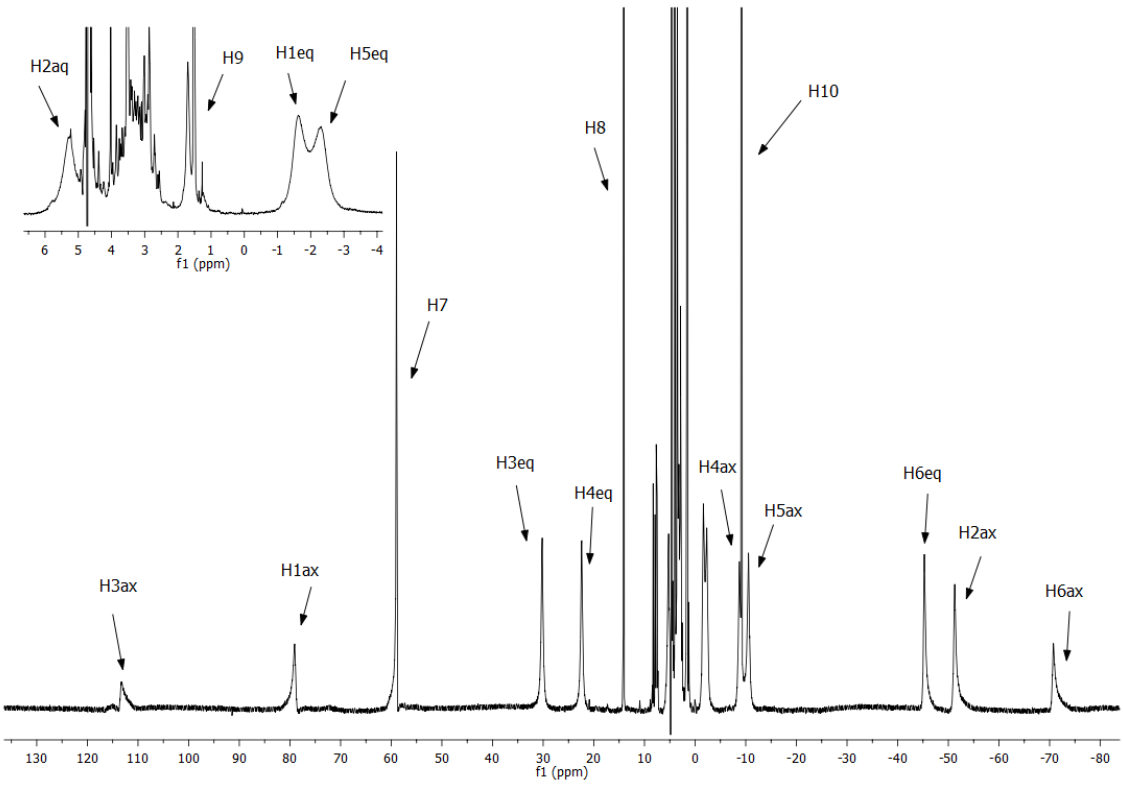

Fig. 4. 13: ^{1}H NMR spectrum of Yb^{III}-L1 complex solution at 298K (diamagnetic region on inset). H$^{7-10}$ signals correspond to pyridine-N-oxide signals.

Similar results were also obtained for the Eu^{III}-L1 spectrum at 298K (Fig. 4. 15). The sixteen resonances are clearly observed in the characteristic range of shifts for Eu^{III}-containing solutions.

There is a tendency for the SAP arrangement to become increasingly predominant along the lanthanide series, with a predominance inversion of SAP isomer over the TSAP isomer occurring in the middle of the series (Nd^{III}-Eu^{III}). For this reason the Yb^{III} and Lu^{III} complexes are usually present in a predominant SAP arrangement and the Nd^{III}-Eu^{III} complexes are present in a mixture of both SAP and TSAP isomers. However, in complexes where the TSAP isomer is strongly disfavored due to steric hindrance, the respective Eu^{III} complex is present as a predominant SAP isomer. Since the ^{1}H NMR spectrum of the Eu^{III}-L1 at 298K indicates the presence of only one isomer, it is most likely that it corresponds to the SAP isomer. Also, by comparing the Eu^{III}-L1 and Eu^{III}-DO3A-py^{NO} (Fig. 4. 15 and Fig. 4. 16) spectra it is again argued that the SAP is the only kind of isomerism present at this temperature in solution. The H7 proton (denoted H231 in the adapted figure) is very sensitive to the chemical environment, namely to the occurrence of two isomers, and in both cases only one resonance is assigned to this nucleus in the same range of frequencies.

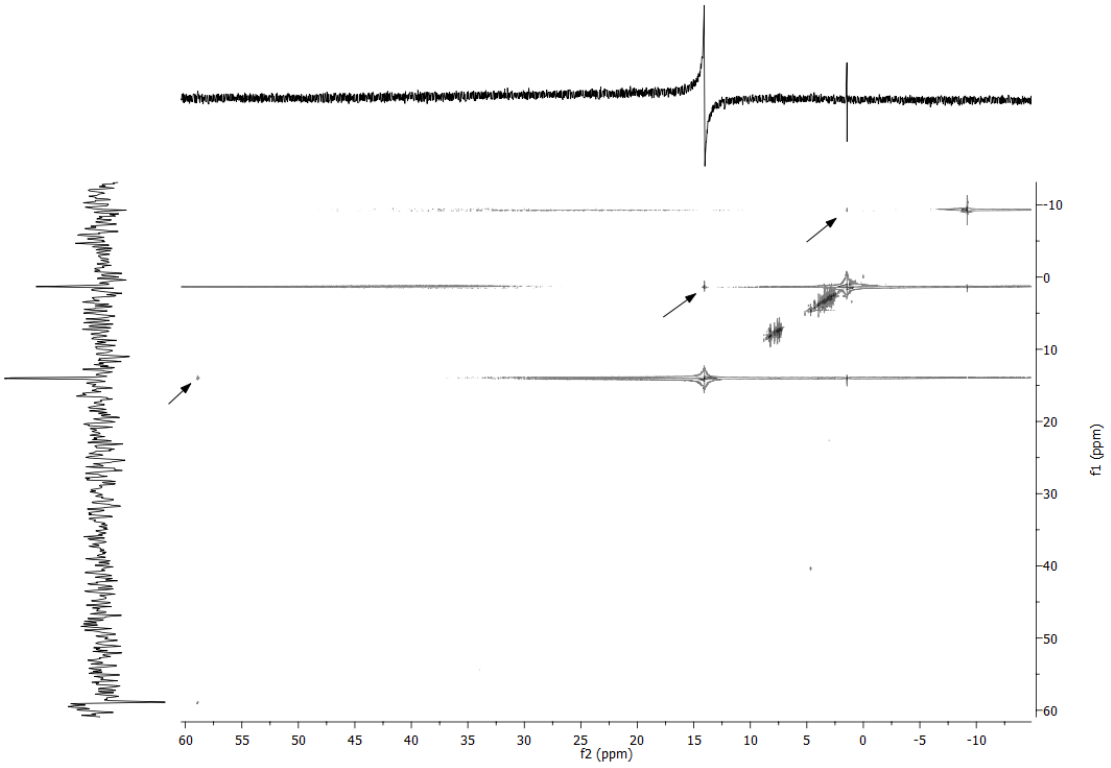

Fig. 4. 14: 2D COSY ^{1}H NMR spectrum of Yb^{III}-L1 complex at 298K. Arrows indicate crosspeaks corresponding to pyridine-N-oxide signals.

Based on the ^{1}H spectra of the complexes described above, only a partial determination of the diamagnetic and paramagnetic shifts was possible, namely for the pyridine-*N*-oxide moiety (Tab. 4. 4). The rest of the observed resonances of the Eu^{III} and Yb^{III} complexes could not be assign at this stage, since no cross-peaks were obtained in the respective 2D COSY spectrum due the fast relaxation of ^{1}H nucleus in the vicinity of the paramagnetic centre. Nonetheless, the involvement of all pendant arms was demonstrated.

In order to obtain a full structural elucidation of the Ln^{III} complexes, computational methods were implemented based on the Yb^{III}-L1 complex. The underlying principle is this: First, a list of paramagnetically shifted resonances (δ_i^{exp}) is obtained from the ^{1}H NMR spectra the Yb^{III}-L1 complex, since they provide information about the dipolar interactions between the Yb^{III} ion and the ligand nuclei (Tab. 4. 5). Second, structural models are generated and the respective theoretical resonance shifts (δ_i^{calc}) of the ligand nuclei are determined (Tab. 4. 5). Finally, an optimal fit is obtained between the experimentally observed shifts and the calculated ones, thus indicating which structural models correspond to the solution structures of the complex.

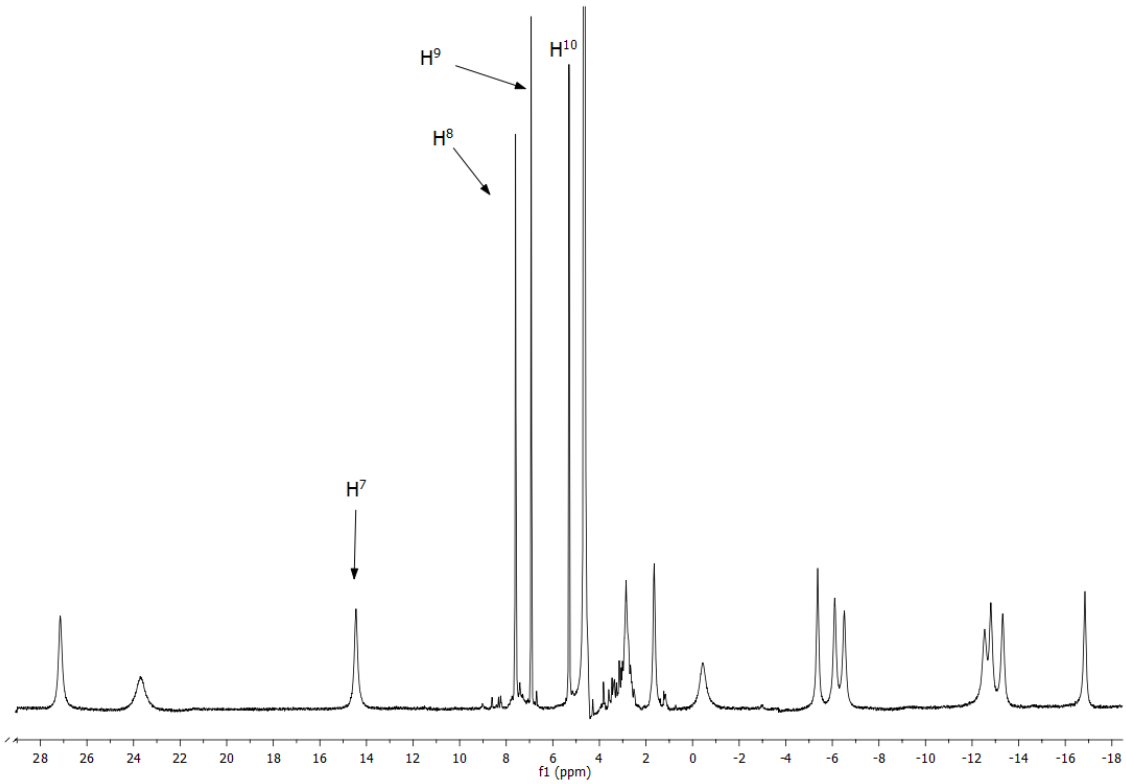

Fig. 4. 15: ^{1}H NMR spectrum of Eu^{III}-L1 complex solution at 298K (pyridine-N-oxide signals on inset). H^{7-10} signals correspond to pyridine-N-oxide signals.

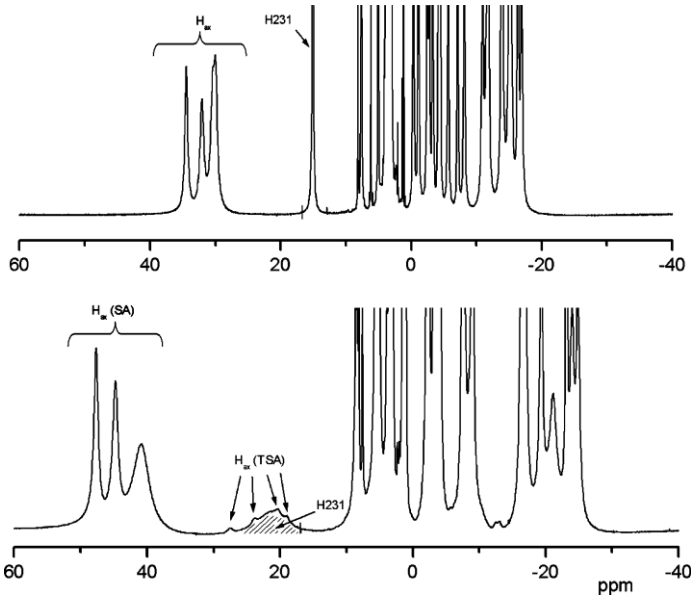

Fig. 4. 16: ^{1}H NMR Spectrum of Eu^{III}-DO3A-py^{NO} at 238K (adapted).[96]

The Yb^{III}-L1 structures with q=0 were characterized by means of DFT calculations (mPWB95 model) performed in aqueous solution. Based on previous experience, the effective core potential (ECP) of Dolg et al. and the related [5s4p3d]-GTO valence basis set was applied in these calculations. This ECP includes 46+4f^{n} electrons in the core, leaving the outermost 11 electrons to be treated explicitly. The use of large core ECPs has been justified by the fact that 4f orbitals do not significantly contribute to bonding due to their limited radial extension as compared to the 5d and 6s shells.

The stereoisomerism of cyclen-based Ln^{III} complexes is relatively well understood, and it has been previously in Chapter 1. Furthermore, the pyridine-N-oxide groups of L1 can coordinate to the Ln^{III} ion by adopting *syn* or *anti* conformations. Thus, four possible diastereoisomeric forms of the Yb^{III}-L1 complex were considered in the DFT calculations: *syn*-Δ(δδδδ), *syn*-Δ(λλλλ), *anti*-Δ(δδδδ) and *anti*-Δ(λλλλ). However, any attempt to model the *anti*-Δ(δδδδ) form of the complex systematically led to conformation *syn*-Δ(δδδδ) during the geometry optimization process, indicating that the *anti*-Δ(δδδδ) form is not a local minimum on the potential energy surface. According to our calculations the *anti*-Δ(λλλλ) form is more stable than the *syn*-Δ(δδδδ) and *syn*-Δ(λλλλ) isomers, the relative free energies of the latter forms with respect to the *anti*-Δ(λλλλ) one amounting to 10.71 and 14.10 kJ·mol^{-1}, respectively.

The minimum energy conformation calculated for Yb^{II}-L1 [*anti*-Δ(λλλλ)] shows a nearly undistorted C2 symmetry, with the symmetry axis being perpendicular to the plane defined by the four nitrogen atoms of the macrocycle and containing the metal ion (Fig. 4. 17). The

coordination of the ligand provides a SAP coordination environment around the metal ion, where the coordination polyhedron can be considered to be comprised by two parallel planes: the oxygen atoms of the ligand define the upper plane, while the nitrogen atoms of the macrocyclic unit delineate the lower plane. The mean twist angle between these two parallel planes is 36.7°, a value that is very similar to those observed for Ln^{III}-DOTA complexes with SAP coordination environment (38-39°). The calculated distances between the Yb^{III} ion and the donor atoms of acetate groups are in excellent agreement with those observed for Yb^{III}-DO3A-py^{NO} in the solid state, while the distances to the oxygen atoms of pyridine-N-oxide groups are ca. 0.05 Å longer in the DFT optimized geometry of Yb^{III}-L1 in comparison to that found in the X-ray structure of Yb-DO3A-py^{NO}. The calculated distances between the Yb^{III} ion and the donor atoms of the cyclen unit are ca. 0.05-0.11 Å longer than those observed for the Yb^{III}-DO3A-py^{NO} analogue.

Tab. 4. 5: Comparison of experimental and calculated ^{1}H shifts (ppm) for Yb^{III}-L1 complex at 298 K (pH = 6.9). [a]

	δ_i^{exp}	δ_i^{calc}
H1ax	79.07	70.81
H1eq	-1.63	-0.57
H2ax	-51.25	-57.70
H2eq	5.23	7.74
H3ax	113.24	114.36
H3eq	30.17	32.81
H4ax	-8.75	-11.97
H4eq	22.39	18.25
H5ax	-10.54	-12.59
H5eq	-2.31	-6.23
H6ax	-70.73	-72.52
H6eq	-45.26	-42.11
H7	58.95	57.94
H8	14.13	17.00
H9	1.51	3.83
H10	-9.13	-5.04

[a] Assignment supported by 2D COSY experiments at 298 K; Calculated values were obtained as described in method and the *anti*-$\Delta(\lambda\lambda\lambda\lambda)$ form of the complex optimized in aqueous solution at the mPWB95/6-31G(d) level.

The calculated DFT geometries of Yb^{III}-L1 and their respective theoretical shifts were used to assess the agreement between the experimental and predicted Yb^{III}-induced paramagnetic shifts by the Kemple procedure. For the macrocyclic proton nuclei the diamagnetic shift was estimated to be 3.0 ppm (since no resonance assignment was possible), while for proton nuclei of the pyridine-*N*-oxide groups the diamagnetic contribution was obtained from shifts observed for the Lu(III) complex (Tab. 4. 5).

The DFT optimized structures of the *syn*-Δ(δδδδ) and *syn*-Δ(λλλλ) isomers provided unacceptable agreements between the experimental and calculated Yb^{III}-induced shifts. On the contrary, the *anti*-Δ(λλλλ) conformation provided an excellent agreement between experimental and calculated shifts (Tab. 4. 5) with $\chi_{zz} - 1/3(\chi_{xx} + \chi_{yy} + \chi_{zz}) = -2877 \pm 46$ ppm·Å^3 and $\chi_{xx} - \chi_{yy} = -1648 \pm 101$ ppm·Å^3. Thus, the analysis of the Yb^{III}-induced paramagnetic shifts unambiguously proves that this complex presents an *anti*-Δ(λλλλ) [or *anti*-Λ(δδδδ)] conformation in aqueous solution, that is to say, an *anti*-SAP conformation. This is somehow unexpected since for the DO3A-py^{NO} complexes the syn-SAP and anti-SAP isomers were present in a dynamical equilibrium at similar experimental conditions. In this case, further steric constrains may lead to the adoption of a single isomer. Based on these results, it was therefore possible to assign all resonances from the Yb^{III}-L1 ^{1}H NMR spectrum ().

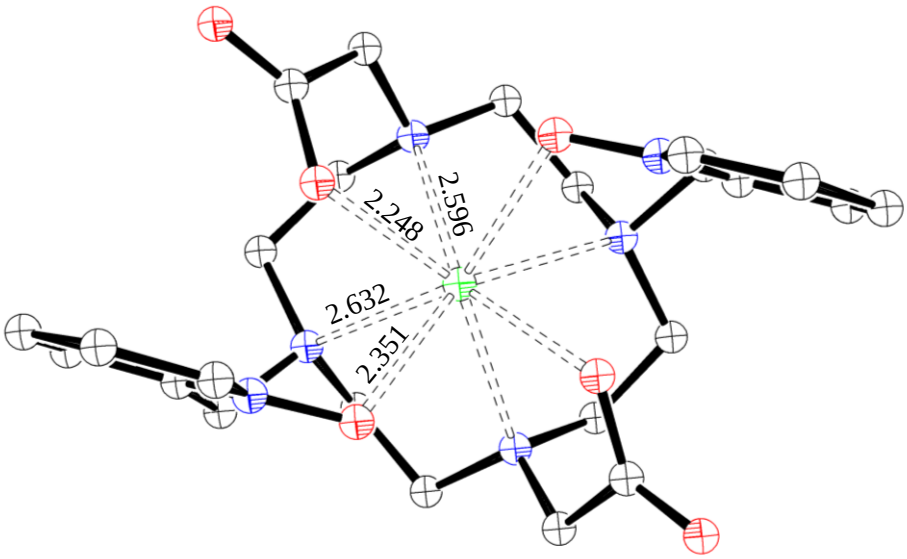

Fig. 4. 17: Calculated minimum energy conformation of Yb^{III}-L1 as optimized in aqueous solution at the mPWB95/6-31G(d) level. Bond distances of the metal coordination environment are given in Å. Hydrogen atoms are omitted for the sake of simplicity.

It should be noted that although there is a good agreement between calculated and solution structures, the absence of a water molecule in the inner coordination sphere is not

proved. Further studies should be performed in order to have a complete structural elucidation of the Ln^{III}-L1 complexes, namely the acquisition of X-ray structures and theoretical calculations of the electronic distributions in the molecule. These studies would allow for a rationalization of the energy-transfer processes involved in these systems that are responsible for their photophysical properties.

4.3 - Conclusions

This work presents preliminary studies on the relaxometric and photophysical properties of the Ln^{III}-L1 complexes. The obtained r_1 values at 298 and 310K are low in relation to the ones of clinically available CAs but its thermodynamic and kinetic stabilities are quite reasonable. The capacity of the L1 ligand to act as an antenna for Eu^{III}, Tb^{III}, Yb^{III}, Nd^{III}, Ho^{III} and Pr^{III} sensitized-emission was confirmed, with reasonable overall quantum yield values.

The ability to sensitize near-IR lanthanide luminescence and the low r_1 value indicate that less than one water molecule is in the inner coordination sphere, although no direct measurements were made. Structural investigations were performed with ^{1}H NMR spectroscopy and DFT calculations and the obtained results indicate that one isomer is predominant at room temperature, namely the *anti*-SAP arrangement.

It should also be considered that bi-functionalization of the ligand can be easily performed by functionalization of the pyridine-*N*-oxide moiety or the acetate pendant arms, as it has been done for the DO3A-py^{NO} and CLaNP-5 analogues. This could lead to the construction of nanosystems based on a polymer scaffold with various LnIII-L units with increasing luminescent and/or relaxometric properties. For example, in the case of DO3A-py^{NO} the carboxylic moiety did not significantly altered the sensitization properties of the ligand, judging by the similar photophysical properties reported for the analogue DO3A-py^{NO} complex. Likewise, in the case of CLaNP-5 the LnIII luminescence was not affected by the introduction of the two 2-(amino-ethyl)methanethiosulfonate moieties. One the other hand, the possibility of creating a responsive agent can also be considered by modulating the energy transfer capability of the bi-functionalized ligand with proper attachment of responsive units that would change the electronic distribution of the complex under environmental stimuli.

Annex I

Cyclen derivatives with three methylphosphonate pendant arms: synthesis and study of the effect of an additional pendant arm on metal complexation

Luís M. P. Lima,[a] Catarina V. Esteves,[a] Rita Delgado,[a,b] Petr Hermann,[c] Jan Kotek,[c] Romana Ševčíková,[d] Radek Ševčík,[d] Přemysl Lubal,*[d] Henrique F. Carvalho,[e] André F. Martins,[e,f] Éva Tóth,[f] and Carlos F. G. C. Geraldes*[e]*

[a] Instituto de Tecnologia Química e Biológica, Universidade Nova de Lisboa, Av. da República, 2780-157 Oeiras, Portugal, [b] Instituto Superior Técnico, DEQB, Universidade Técnica de Lisboa, Av. Rovisco Pais, 1049-001 Lisboa, Portugal, [c] Department of Inorganic Chemistry, Faculty of Science, Univerzita Karlova (Charles University), Hlavova 2030, 12840 Prague 2, Czech Republic, [d] Department of Chemistry, Faculty of Science, Masaryk University, Kotlařská 2, 61137 Brno, Czech Republic, [e] Department of Life Sciences and Center of Neurosciences and Cell Biology, Faculty of Science and Technology, University of Coimbra, Apartado 3046, 3001-401 Coimbra, Portugal, [f] Centre de Biophysique Moléculaire, CNRS, Rue Charles Sadron, 45071 Orléans, France

*To whom correspondence should be addressed. Fax: +351-214411277; Tel: +351-214469737; E-mail: delgado@itqb.unl.pt (R.D.)

July 2011 – Submitted to Journal of Inorganic Chemistry

Abstract. Three compounds based on cyclen and containing three methylphosphonate pendant arms were synthesized, namely (1,4,7,10-tetraazacyclododecane-1,4,7-triyl)tris(methylene)triphosphonic acid (H_6do3p), 3-[4,7,10-tris(phosphonomethyl)-1,4,7,10-tetraazacyclododecan-1-yl]propanoic acid (H_7do3p1pr), and [10-(3-hydroxypropyl)-1,4,7,10-tetraazacyclododecane-1,4,7-triyl]tris(methylene)triphosphonic acid (H_6do3p1ol). X-ray crystal structures were determined for H_6do3p and for the related complex $[Cu(H_2O)(H_4dotp)][Cu(H_2O)_6]$. The acid-base properties of the synthesized ligands were studied in aqueous solution at 298.2 K, by potentiometric and ^{31}P NMR spectroscopic titrations in ionic strength of 0.10 or 0.50 M in $[N(CH_3)_4]NO_3$, respectively. The overall basicity of the three compounds is very high, and their protonation scheme is dominated by proton exchange and intramolecular hydrogen bonding. All three macrocyclic ligands form complexes with thermodynamic stabilities that are moderate for Ca^{2+}, very high for Zn^{2+} and the Ln^{3+}, and extremely high for Cu^{2+}. Kinetic studies showed that the acid-assisted dissociation of Ce^{3+} complexes of these ligands is much faster than metal complexes of related H_8dotp (1,4,7,10-tetraazacyclododecane-1,4,7,10-tetrayl)tetrakis(methylene)tetraphosphonic acid), this effect being less visible in case of Cu^{2+} complex. The lower kinetic inertness of the Ce^{3+} complexes is in agreement with the very fast complex formation. The number of water molecules coordinated to Eu^{3+} complexes, determined by time-resolved luminescence spectroscopy, was estimated at about one. The ^{1}H and ^{31}P NMR spectra of the Eu^{3+}, Yb^{3+} and Lu^{3+} complexes showed that the propionate ligand arm in the $[Ln(do3p1pr)]^{4-}$ complexes and the propanol arm in the $[Ln(do3p1ol)]^{3-}$ complexes are not bound to the Ln^{3+} ion. The $[Ln(do3p)]^{3-}$ and $[Ln(do3p1pr)]^{4-}$ complexes have a clear preference for the TSAP isomer, while both SAP and TSAP isomers are present in the case of the [Ln(do3p1ol)]3– complexes. Despite a water coordination of less than one, the 1H water relaxivity of [Gd(do3p1ol)]3– is quite reasonable, due to self-aggregation and second-sphere contribution.

Introduction

Tetraaza macrocycles are a prominent class of organic ligands due to their remarkable ability to bind strongly to a variety of metal ions with diverse coordination preferences, taking advantage of the pre-organized but sufficiently flexible nature of its skeleton. Derivatives of cyclam (1,4,8,11-tetraazacyclotetradecane) and cyclen (1,4,7,10-tetraazacyclododecane) with *N*-appended coordinating arms are by far the most studied macrocycles of such type, especially those based on the structure of the tetraacetic acid derivative of cyclen, H_4dota.[1,2] This latter compound serves as a model in the design of more efficient ligands for the complexation of Ln^{3+} ions, due to the very high thermodynamic stability and kinetic inertness of such complexes.[3,4] The tetrakis(methylphosphonic acid) analog of H_4dota, H_8dotp, shows an even higher thermodynamic stability but a conversely lower kinetic inertness for its Ln^{3+} complexes, having also been the subject of numerous studies.[5,6] Furthermore, H_4dota and H_8dotp may also exhibit high stability and kinetic inertness for complexes of biologically relevant transition metal ions such as Zn^{2+} and especially Cu^{2+}.[7–9]

Due to the above reasons, numerous analogues of H_4dota and H_8dotp have been developed in the past few decades for potential medical applications. The aim is obtaining ligands whose metal complexes can be used as contrast agents for magnetic resonance imaging (MRI),[4,10–12] and as radiopharmaceuticals in the form of chelates of radionuclides applied in nuclear medicine for diagnosis and therapeutic purposes.[13–15] Effort has been made to design compounds that can be conjugated to a targeting biomolecule via a suitable conjugation moiety from the chelator, to produce bifunctional chelators (BFC) that allow for higher specificity.[13,14]

Specifically for radiopharmaceutical uses, suitable metal ions range from lanthanides (e.g. ^{153}Sm, ^{177}Lu) to transition (e.g. ^{61}Cu, ^{64}Cu) and post-transition metals (e.g. ^{67}Ga, ^{212}Pb).[13–16] Such uses require chelates with high thermodynamic stability and kinetic inertness, as well as fast chelate formation.[11,13,15,16]

One of the methods to improve the properties of cyclen-based ligands is appending a different number of pendant arms containing carboxylate and phosphonate groups in the macrocyclic skeleton and, more recently, different combinations of both types of groups. A H_4dota analogue containing one methylphosphonate pendant, H_5do3a1p, showed very promising results regarding the stability, kinetic, structural and relaxometric properties of its Ln^{3+} complexes, which makes it a promising candidate for the production of contrast agents for MRI.[17–20] Two other analogous ligands with an increasing number of acetate pendants replaced by methylphosphonate ones were later reported, trans-H_6do2a2p [21–23] and H_7do3p1a.[24,25] The first one presented very high thermodynamic stability, its Ln^{3+} complexes having reasonable kinetic inertness and high in vivo stability for Sm^{3+} and Ho^{3+} complexes in particular, while the second one was proved to form Sm^{3+} and Ho^{3+} complexes with suitable in vivo stability and reasonable bone targeting predisposition but has yet to undergo thorough solution studies. The cyclen derivative with only three pendant arms, H_6do3p, has been previously disclosed and briefly studied, having shown to form very stable complexes with Cu^{2+},[26] and also stable complexes with Zn^{2+} and Fe^{3+}.[27]

Recently, a H_4dota analogue with a propionate moiety replacing an acetate pendant arm, H_4do3a1pr, has been reported and found to improve the kinetics of Ln^{3+} complexation.[28,29] Following the evidence of faster complex formation kinetics by elongation of one coordinating pendant arm, and building on the established properties of the H_8dotp chelator, we proposed to start from the structure of the latter compound and replace one of its methylphosphonate pendant arms by another arm that is able to form a 6-membered chelate ring instead of a 5-membered one upon coordination to a metal ion. From the possible donor groups we selected a carboxylate for its proved ability to bind a wide variety of metal ions, and also an alcohol group for its somewhat higher lipophilicity and neutral charge. In this work we report on the synthesis and the detailed solution studies of the two novel ligands, H_7do3p1pr and H_6do3p1ol, and their precursor ligand, H_6do3p, and also of a range of their metal complexes. The X-ray crystal structure of the ligand H_6do3p is reported, as well as that of the related complex $[Cu(H_2O)(H_4dotp)][Cu(H_2O)_6]$. A comparison of the acid-base properties, the thermodynamic stability of selected metal complexes, and of the coordination behaviour of the three ligands towards different metal ions was undertaken, based on potentiometric and NMR spectroscopic studies. The solution structure of the Eu^{3+}, Yb^{3+} and Lu^{3+} complexes was studied using ^1H and ^{31}P NMR spectra. The ^1H and ^{17}O NMR relaxometric properties of the Gd^{3+} complex of H_6do3p1ol were also measured. The acid-assisted dissociation kinetics of Cu^{2+}, Ce^{3+} and Eu^{3+} complexes, as well as the formation kinetics of Ce^{3+} complexes of all ligands, were also investigated. The global results are used to evaluate the influence of the derivatization of the secondary amine of H_6do3p on the coordination properties of metal complexes of the new compounds incorporating an additional carboxyl or hydroxyl moieties.

Scheme 1. Structures of the compounds discussed in this work

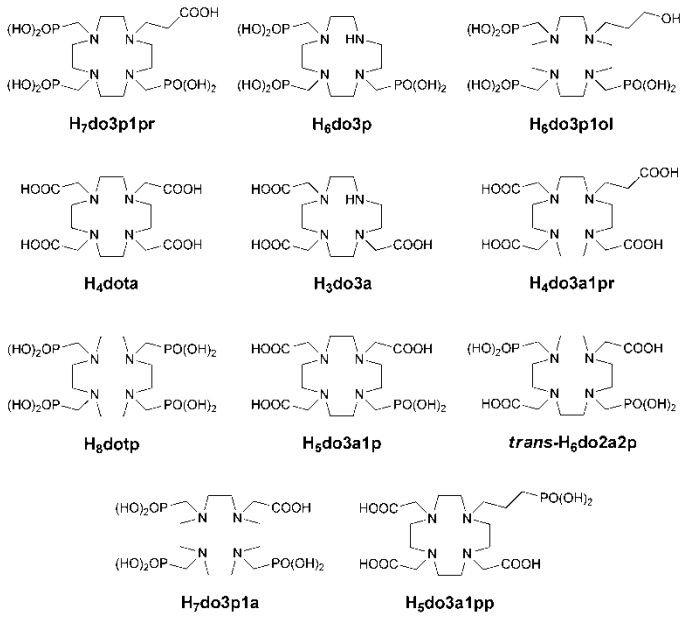

Results and discussion

Synthesis of the macrocyclic compounds. The compounds H_6do3p, H_7do3p1pr and H_6do3p1ol were synthesized, the latter two for the first time in this work, by a parallel methodology starting from cyclen as outlined in Scheme 2. Initially, mono N-alkylation of cyclen was performed by adaptation of a selective reaction procedure recently reported.[30] This method required the use of a 4- to 5-fold excess of cyclen, which could be nonetheless easily recovered by chloroform extraction of the basified aqueous phases originating from the reaction workup. In the case of H_6do3p1ol, the reactive alcohol function of the commercially available alkylation reactant was previously protected with an acetyl group. Next, methylphosphonic ester groups were appended by a Mannich type reaction with paraformaldehyde and triethyl phosphite in anhydrous conditions. Finally, hydrolysis of all acetic and/or methylphosphonic esters in strongly acidic media yielded the final compounds, but it was necessary to adopt different reaction and workup conditions according to the target compound. Indeed, *N*-(2-carboxyethyl) moieties are known to be partially eliminated under strong acid and/or strong heating by a retro-Michaels reaction mechanism.[31] In our case this de-alkylation occurred in variable extent whenever any of the compounds containing the (2-ethoxycarbonyl)ethyl moiety (**1** and **2**) were treated with concentrated acid under heating, but such side-reaction could be avoided as long as that ester moiety was first hydrolysed at r.t. to the corresponding acid. Thus, after careful isolation of the fully esterified precursor of H_7do3p1pr (**2**), its hydrolysis in 20% aq. HCl first at r.t. with subsequent heating to a gentle reflux afforded H_7do3p1pr without noticeable occurrence of de-alkylation. Furthermore, and taking advantage of the mentioned reactivity features, we could obtain the pure H_6do3p by hydrolysis (and simultaneous de-alkylation) of the same precursor (i.e. the ester of H_7do3p1pr, **2**) in 20% aq. HBr under prolonged reflux. To obtain H_6do3p1ol, the hydrolysis was performed in 20% aq. HCl under reflux. In this case, it was necessary to subsequently treat of the reaction mixture by reflux in dilute aqueous sodium hydroxide to revert the partial formation of a chloride derivative of the compound, which is formed by reaction of the alcohol moiety of the target compound with the hydrochloric acid used during hydrolysis.

Scheme 2. Synthetic route [a]

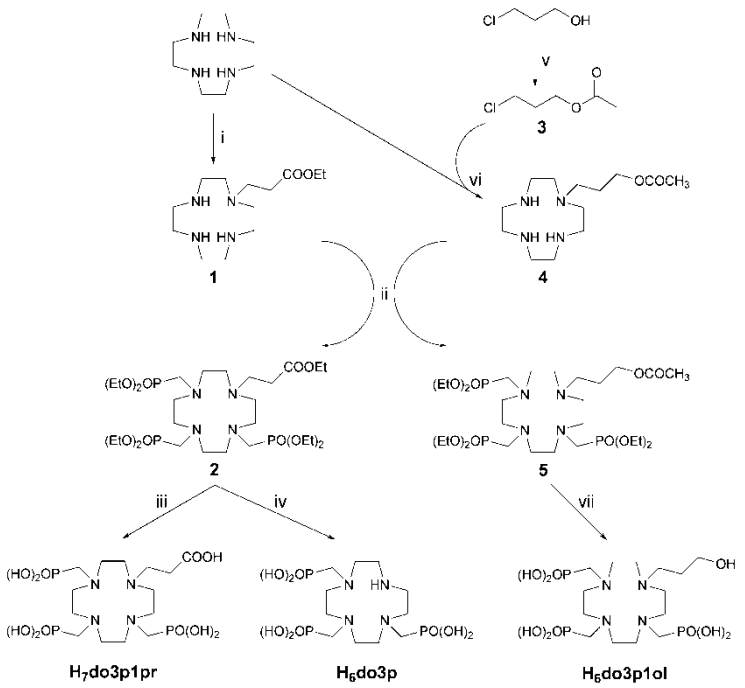

[a] Reagents and conditions: (i) $Br(CH_2)_2COOEt$, $CHCl_3$, NEt_3, reflux, 15 h; (ii) $(HCHO)_n$, $P(OEt)_3$, r.t., 4 d; (iii) aq. HCl 20%, r.t. to reflux, 2 d; (iv) aq. HBr 20%, reflux, 3 d; (v) CH_3COCl, CH_2Cl_2, NEt_3, 5 ºC to r.t., 2.5 h; (vi) $CHCl_3$, NEt_3, reflux, 3 d; (vii) aq. HCl 20%, reflux, 2 d then aq. NaOH 0.2 M, reflux, 12 h.

Purification of all final compounds was done by cationic exchange chromatography. For H_6do3p and H_6do3p1ol, the crude products from the acidic hydrolysis step were first loaded in a strong cationic exchanger, non-aminic impurities were eluted with water and the macrocycles were then eluted with aq. ammonia in the form of ammonium salts. The macrocyclic ammonium salts of H_6do3p and H_6do3p1ol, or the crude product containing H_7do3p1pr from the acidic hydrolysis step, were loaded in a weak cationic exchanger and eluted with water, which isolated the relevant compounds in zwitterionic form free from other macrocyclic by-products that were more retained in the column. Finally, precipitation from a concentrated aqueous solution yielded H_6do3p as a dry

solid, while evaporation and vacuum drying of aqueous solutions yielded H_6do3p1ol as a slightly hygroscopic solid and H_7do3p1pr as a very hygroscopic solid. Both new compounds, H_7do3p1pr and H_6do3p1ol, can be used for the synthesis of bifunctional chelators, by taking advantage of the different reactivity of the alcohol and carboxylate functions with respect to the phosphonate one to append suitable coupling groups on the distinctive pendant arm of each compound.

X-ray crystal structure of H_6do3p. Single crystals were easily obtained in the form of non-stoichiometric hydrate of formula H_6do3p·3.8H_2O, by slow evaporation of a saturated aqueous solution, and the content of solvate water was refined on the basis of X-ray analysis. A similar crystal structure has been previously reported for H_6do3p.[27] However, our structure shows different cell dimensions and belongs to a different space group, besides having significantly better refinement parameters. Additionally, the protonation pattern of the reported structure is also slightly different, although that can be justified by the fact that all protons in the two structures are involved in strong hydrogen bonding interactions.

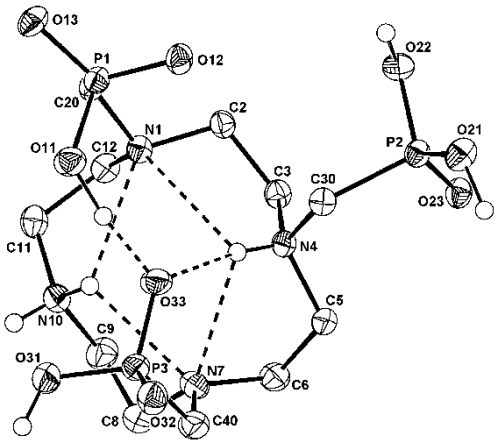

Figure 1. Molecular structure of H_6do3p found in the crystal structure of H_6do3p·3.8H_2O. Hydrogen atoms bound to carbon atoms are omitted for the sake of clarity.

In the crystal structure obtained, shown in Figure 1, the nitrogen atom of the secondary amine N10 and the transannular amine with a methylphosphonate pendant arm N4 are both protonated. The remaining four protons are distributed on the oxygen atoms of the pendant arms, with one proton in each of the phosphonate moieties appended to non-protonated amines N1 and N7, and the two remaining protons in the phosphonate moiety appended at the protonated amine N4. Such a mode of protonation is consistent with the one found in solution for the H_6do3p species (see the discussion of acid-base behaviour below). The four nitrogen atoms form a plane and the whole macrocyclic ring is in a square (3,3,3,3)-B conformation according to the Dale formalism,[32] which is the most usual one for twice-protonated substituted cyclen rings. This macrocyclic conformation is stabilized by a system of intramolecular N–H···N hydrogen bonds with N···N distances in the range 2.88–3.05 Å and N–H···N angles in the range 101–113°. All three pendant arms are pointed to the same direction with respect to the macrocyclic plane; the two pendant arms from amines N1 and N7 are folded above the macrocyclic cavity, while the remaining pendant arm at N4 is turned away; an analogous arrangement was found in the literature for the crystal structure of H_8dotp.[33] The molecular conformation is stabilized by strong cooperative intramolecular hydrogen bonds involving one protonated tertiary amino group and two oxygen atoms from the pendant phosphonate groups, N4–H···O33 with a N···O distance of 2.81 Å and O11–H···O33 with an O···O distance of 2.54 Å, respectively. The ligand molecules are connected via strong hydrogen bonds between protonated and unprotonated phosphonate oxygen atoms with O···O distances in the range 2.46–2.60 Å. The solvate water molecules cross-link the structure with a system of medium–strong hydrogen bonds between water hydrogen and the phosphonate oxygen atoms with O···O distances in the range 2.8–2.9 Å, see Figure 2.

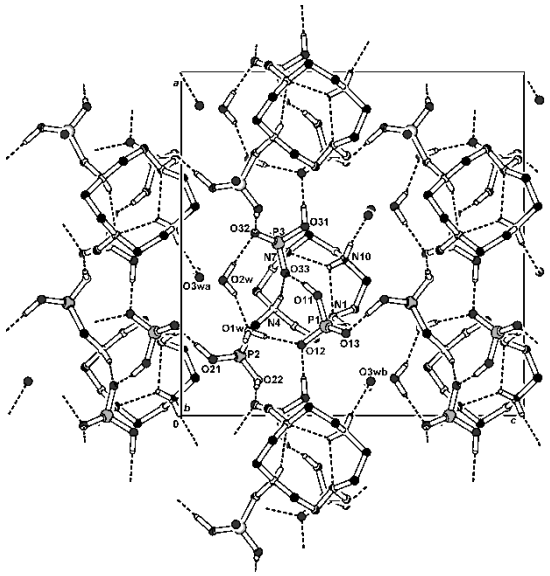

Figure 2. Hydrogen bonding system found in the crystal structure of H_6do3p·3.8H_2O, when viewed along the *b* axis.

X-ray crystal structure of [Cu(H_2O)(H_4dotp)][Cu(H_2O)$_6$]. In the solid-state structure of the complex, the independent unit is formed by one half of the formula unit, with molecules of the macrocyclic complex anion and of a copper hexaaqua cation laying on the two-fold symmetry axes. The central Cu atom in the [Cu(H_2O)(H_4dotp)]$^{2-}$ anion is coordinated with four macrocyclic nitrogen atoms (d_{Cu-N} ~2.03 Å) forming a planar base, and a water molecule in a distant apical position (d_{Cu-O} ~2.27 Å). The central Cu atom lays 0.455(3) Å above the N_4-plane, while all pendant arms are monoprotonated and uncoordinated. Both transannular N–Cu–N$^{\#}$ angles are very similar (~154°) and, as all N–Cu–O1W angles are also very similar (~103°), the coordination sphere has an almost regular square-pyramidal geometry. The structure of the [Cu(H_2O)$_6$]$^{2+}$ cation is octahedral, with tetragonal apical shortening (d_{Cu-O} ~1.99 Å comparing to 2.15 Å observed in the equatorial base) due to the Jahn-Teller effect. The whole structure is stabilized by an extensive network of intermolecular hydrogen bonds, with very strong interaction between protonated and unprotonated phosphonate oxygen atoms from neighboring units ($d_{O\cdots O}$ ~2.55 Å). Selected geometric parameters are listed in Table 1 and the molecular structure of macrocyclic complex anion is shown in Figure 3. A related structure was found for a Ni^{2+} complex of H_8dotp,[34] but in that case with two oxygen atoms of opposite pendant arms *cis*-coordinated to the Ni atom to give octahedral geometry.

Table 1. Selected geometric parameters found in the crystal structure of [Cu(H_2O)(H_4dotp)][Cu(H_2O)$_6$].

[Cu(H_2O)(H_4dotp)]$^{2-}$		[Cu(H_2O)$_6$]$^{2+}$	
	Distances / Å		
Cu1–N1	2.038(4)	Cu2–O1B	1.985(4)
Cu1–N4	2.021(4)	Cu2–O2B	2.152(5)
Cu1–O1A	2.265(6)	Cu2–O3B	2.153(4)
	Angles / °		
N1–Cu1–N4	87.5(2)	O1B–Cu2–O2B	89.7(2)
N1–Cu1–N1$^{\#}$	154.3(2)	O1B–Cu2–O3B	91.0(2)
N1–Cu1–N4$^{\#}$	86.8(2)	O1B–Cu2–O1B$^{\#}$	178.6(2)
N1–Cu1–O1A	102.8(1)	O1B–Cu2–O2B$^{\#}$	89.3(2)
N4–Cu1–N4$^{\#}$	153.9(2)	O1B–Cu2–O3B$^{\#}$	90.1(2)
N4–Cu1–O1A	103.1(1)	O2B–Cu2–O3B	90.2(1)
–	–	O2B–Cu2–O2B$^{\#}$	90.0(2)
–	–	O2B–Cu2–O3B$^{\#}$	179.7(2)
–	–	O3B–Cu2–O3B$^{\#}$	89.6(2)

$^{\#}$ Symmetrically-associated atom (two-fold axis).

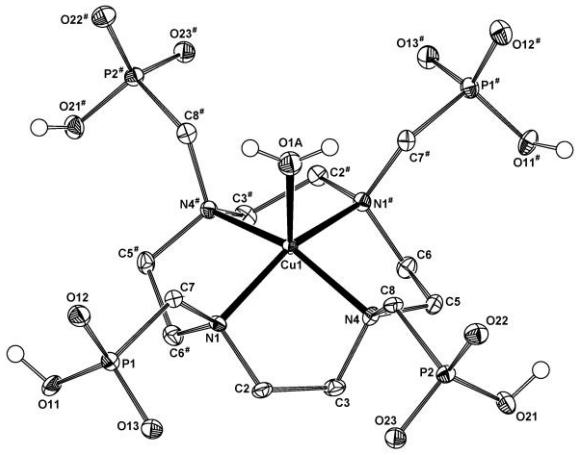

Figure 3. The molecular structure of the $[Cu(H_2O)(H_4dotp)]^{2-}$ anion found in the solid-state structure of $[Cu(H_2O)(H_4dotp)][Cu(H_2O)_6]$. Hydrogen atoms bound to carbon atoms are omitted for the sake of clarity.

Acid-base behaviour. The acid-base properties of $H_7do3p1pr$, H_6do3p and $H_6do3p1ol$ were studied by potentiometric and ^{31}P NMR spectrometric titrations in aqueous solution. The overall protonation constants of the compounds are collected in Table S1 of the Supporting Information. The calculated stepwise constants and the cumulative value of the first four protonation constants for the three compounds, together with literature values for H_6do3p[26,27] and related H_4dota and H_8dotp,[35,36] are presented in Table 2.

Considering the number of amines and acidic groups present in each of the studied compounds, it follows that H_6do3p and $H_6do3p1ol$ have ten basic centres in aqueous solution, while $H_7do3p1pr$ has eleven ones. For these, and while using potentiometric titrations, it was possible to determine accurately four protonation constants for H_6do3p and $H_6do3p1ol$, and five constants for $H_7do3p1pr$. The remaining protonation constants are either very high ($pK_a > 11.5$) or very low ($pK_a < 2$) and thus fall outside the scope of the potentiometric method used. The trend of tetraaza macrocycles with *N*-methylphosphonate pendant arms to exhibit very high protonation constants for the first (one or two) ring amine(s) is well known.[8,19,21,22,35–42] It has been justified by two different phenomena: one is the effect of spreading the high electron density of the fully deprotonated phosphonate group to the nearest nitrogen atom;[8] another is the formation of strong intramolecular hydrogen bonds between a protonated amine and a neighbouring oxygen atom from a phosphonate moiety or between protonated and non-protonated ring amines.[37]

The two highest protonation constants of all three compounds were best determined from "in-cell" ^{31}P NMR titrations in aqueous solution in the alkaline pH region (9–14) at ionic strength of 0.5 M. The ^{31}P NMR spectra of each compound always show two resonances with an integration ratio of 1:2, in agreement with the symmetry of the compounds. Determination of protonation constants from such spectroscopic data was done using both resonances for each compound, and the values of stepwise protonation constants ($\log K_i^H$) obtained were 13.59 and 11.43 for H_6do3p, 13.61 and 11.45 for $H_7do3p1pr$, and 13.61 and 11.66 for $H_6do3p1ol$. These values were then extrapolated to ionic strength 0.1 mol dm^{-3} by application of the Davies equation,[43] and were finally used in the refinement of the remaining protonation constants from the potentiometric data.

The two highest protonation constants for the three studied compounds are quite similar, being somewhat lower than the corresponding constants found for H_8dotp as could be expected from the chemical structure similarity. It was not possible to determine the protonation constant for the propanol moiety of the $H_6do3p1ol$, which indicates that such deprotonation occurs above pH 14 as expected for a primary alcohol. The following three protonation constants for each compound present values that are common for phosphonate moieties and again lower than those of H_8dotp, showing a trend of decreasing values from $H_7do3p1pr$ to $H_6do3p1ol$. Next, $H_7do3p1pr$ presents a constant for the carboxylate moiety which is somewhat higher than could be expected for such functionality appended on a protonated amine. Finally, the lowest constants from each compound can be explained by further protonation on their phosphonate moieties. The complete set of protonation constants demonstrates that all compounds have very high overall basicity, which increases from $H_6do3p1ol$ to H_6do3p and then to $H_7do3p1pr$. For H_6do3p, the protonation constants now determined compare reasonably well with those previously reported,[26,27] considering the different experimental conditions used.

Table 2. Stepwise protonation constants ($\log K_i^H$) of the discussed ligands. $T = 298.2$ K; $I = 0.10$ M in $[N(CH_3)_4]NO_3$.

Equilibrium quotient [a]	$H_7do3p1pr$	H_6do3p	$H_6do3p1ol$	H_4dota	H_8dotp
[HL]/[L][H]	14.00[b]	13.92,[b] 12.9,[c] 13.24[d]	13.94[b]	12.09[e]	14.65[b,f]

$[H_2L]/[LH][H]$	11.78[b]	11.71,[b] 11.4,[c] 11.3[d]	11.93[b]	9.76[e]	12.40[b,f]
$[H_3L]/[LH_2][H]$	9.02	8.99, 8.69,[c] 8.47[d]	8.58	4.56[e]	9.28[f]
$[H_4L]/[LH_3][H]$	7.63	7.40, 7.09,[c] 7.1[d]	7.18	4.09[e]	8.09[f]
$[H_5L]/[LH_4][H]$	6.06	5.51, 5.53,[c] 5.3[d]	5.39	–	6.12[f]
$[H_6L]/[LH_5][H]$	4.64	2.04, 1.42[c]	1.90	–	5.22[f]
$[H_7L]/[LH_6][H]$	2.04	–	–	–	–
$[H_4L]/[L][H]^4$	42.44	42.02	41.63	30.50[e]	44.42[f]

[a] Charges of equilibrium species are omitted for clarity; [b] Determined by ^{31}P NMR spectroscopy; [c] From ref. 26; [d] From ref. 27; [e] From ref. 35; [f] From ref. 36.

To disclose the protonation scheme of H_6do3p, H_7do3p1pr and H_6do3p1ol, they were further studied by additional ^{31}P NMR titrations in aqueous solution over the acid-to-neutral pH range (−1 to 9), where the ionic strength was kept approximately at 0.5 M. In this way it is possible to obtain plots of the pH dependence of the ^{31}P NMR chemical shifts for each compound throughout the whole pH range (Figures 4 and 5, and Figure S1 of the Supporting Information), in order to tentatively assign their protonation sites. A significant amount of data has been reported for the pH dependence of ^{31}P NMR shifts in polyaza macrocycles with methylphosphonate pendants,[19,21,22,24,27,37,38,40,42,44–46] which is used here as the basis of the following discussion.

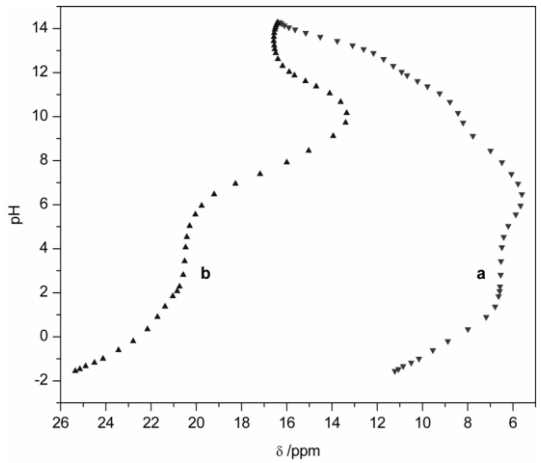

Figure 4. ^{31}P NMR spectroscopic titration of H_7do3p1pr.

Scheme 3. Tentative protonation sequence for H_7do3p1pr

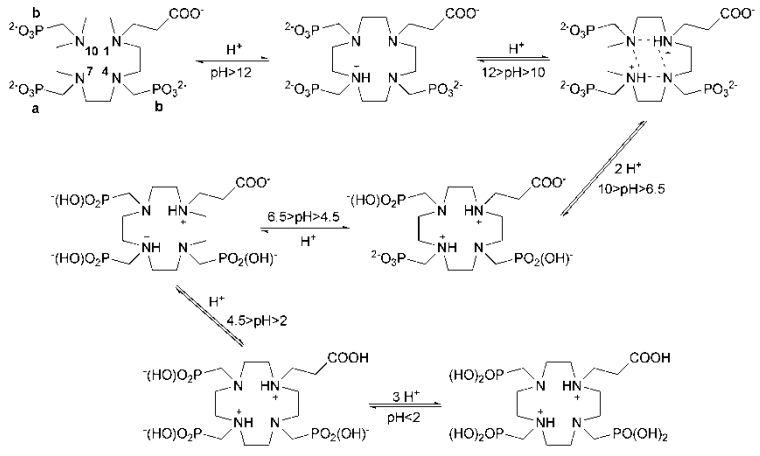

For H_7do3p1pr (Scheme 3), starting from the fully deprotonated species $(do3p1pr)^{7-}$, there is a significant upfield shift of δ_a while δ_b is mostly unchanged (pH > 12). This clearly indicates that protonation starts at the amine N7. Next there is an upfield shift of δ_b and also of δ_a (12 > pH > 10), however these shifts are smaller than those expected for the protonation of an amine with an

appended methylphosphonate moiety. This concurrent change can be understood by admitting the protonation of amine N1 (due to electrostatic repulsion) with formation of hydrogen bonds between the protonated amines and the remaining ones (N4 and N10), thereby delocalizing the positive charge throughout all the ring amines. Next, there is a strong downfield shift of δ_b and a smaller upfield shift of δ_a (10 > pH > 6.5), in a region where only protonation of the phosphonate groups is expected. Protonation of the phosphonates 'b' is therefore undisputed but the shift of δ_a is indicative of more protonation of amine N7, something that can be explained by the dissociation of the hydrogen bonds in the ring leading to an increase of the positive charge on N7 and also N1. Next there is a small downfield shift of δ_a and still of δ_b (6.5 > pH > 4.5), which must then indicate the protonation of phosphonate 'a'. After this there is a region were both δ_a and δ_b remain unchanged (4.5 > pH > 2), which can correspond to the protonation of the carboxylic group that is not expected to influence the phosphorus signals due to the separation between the carboxylate and the phosphonate moieties. Finally, there is a downfield shift of both δ_a and δ_b (pH < 2), which indicates further protonation of all phosphonate groups.

For H_6do3p (Scheme S1), the pH dependence of the ^{31}P NMR chemical shifts is extremely similar to that of H_7do3p1pr throughout the whole pH range, thus a similar protonation scheme is proposed with only two exceptions. At first, the absence of a carboxylate moiety in H_6do3p, which in any case is not reflected in the experimental data for the reason pointed above. Then, at the most acidic range (pH < −1) there is a small upfield shift of δ_b combined with a downfield shift of δ_a, which suggests that protonation of the remaining amines of the ring (N4 and N10) could be starting simultaneously with the end of protonation of the phosphonate groups. It is worth noticing that, in this case, the proposed protonation scheme is in agreement with the protonation mode found in the crystal structure for the zwitterionic species of H_6do3p found in this work and reported elsewhere.[27]

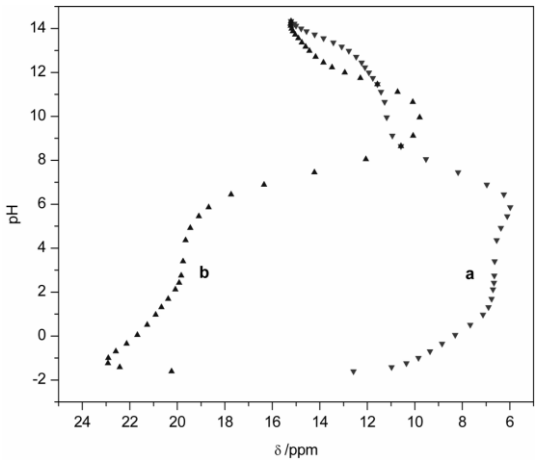

Figure 5. ^{31}P NMR spectroscopic titration of H_6do3p1ol.

For H_6do3p1ol (Scheme 4), starting from the deprotonated species $(do3p1ol)^{6-}$, there is an upfield shift of δ_a and in a smaller degree also of δ_b (pH > 12). This seems to indicate the protonation of amine N7 with probable hydrogen bonds to N4 and N10. Next there is a strong upfield shift of δ_b and a minor one of δ_a (12 > pH > 10), which could indicate that the protonation of a second amine in the ring forces the relocation of the protons to N4 and N10 while hydrogen bonds should now be involving N7. It is likely that N1 is, at this point, also involved in hydrogen bonding with N4 and N10, although it cannot be proven from these data. Next there is a very substantial downfield shift of δ_b and a noticeable upfield shift of δ_a (10 > pH > 6.5). These intense and opposing shifts in a region where only protonation of phosphonate moieties is expected can only be understood if a new relocation of protons on the ring amines is additionally considered. Thus, the downfield shift of δ_b should be explained by protonation of the phosphonate groups 'b' and simultaneous deprotonation of N4 and N10, while the upfield shift of δ_a should be explained by the re-protonation of N7. As a consequence of the redistribution of ring protons, N1 would also become protonated at this point. In the pH < 6.5 range, the change of the chemical shifts of H_6do3p1ol is very similar to the one seen for the H_6do3p, so the assignments proposed above for the latter compound are adopted. In particular, at the most acidic range (pH < −1) there is a more visible upfield shift of δ_b combined with a downfield shift of δ_a, which again points to the protonation of the remaining amines of the ring (N4 and N10) starting simultaneously with the end of protonation of the phosphonate groups.

Scheme 4. Tentative protonation sequence for H_6do3p1ol

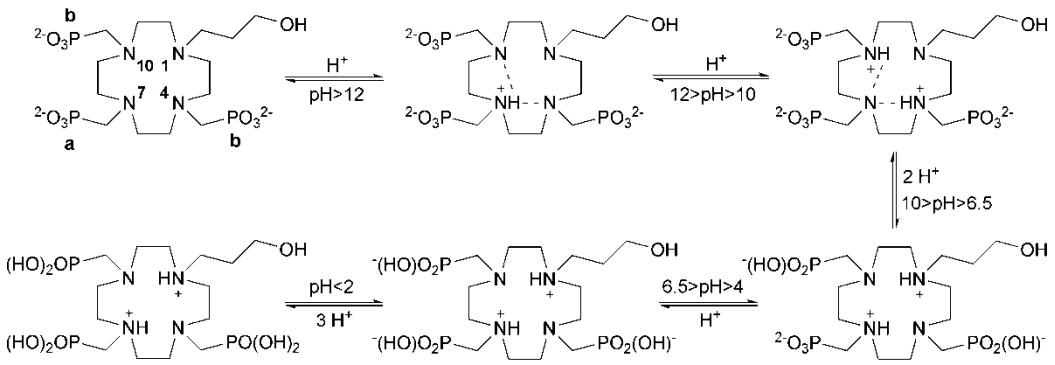

The ^{1}H NMR spectra of all three compounds, H_6do3p, H_7do3p1pr and H_6do3p1ol, were also studied in D_2O solution as a function of temperature (at pD 8.40, 8.60 and 8.00, respectively), where the predominant triprotonated species (H_3L) have two protons located at the ring amines and one proton at the opposite phosphonate groups (P_b). The temperature dependence of the ^{1}H NMR spectra (Figure S16) reflects the temperature-induced change of the restricted dynamics of the protonated species caused by intramolecular hydrogen bonding system between adjacent ring nitrogen atoms and between nitrogen and phosphonate oxygen atoms. At 298 K, the geminal CH_2 protons of the P_b phosphonate and the ring conformation of each half of the molecule are not equivalent, leading to a doubling and/or broadening of the corresponding resonances (*eg.* H_{2ab} in Figure S16). These inequivalences are averaged by internal dynamic processes that become fast in the NMR timescale at 333 K and above, leading to a simplification of the spectra, which at high temperature show six signals for H_6do3p, and an extra two or three signals for the CH_2 groups of the fourth pendant arm of H_7do3p1pr and H_6do3p1ol, respectively.

Thermodynamic stability of metal complexes. The complexes of H_7do3p1pr, H_6do3p and H_6do3p1ol with the Ca^{2+}, Cu^{2+}, Zn^{2+} and some Ln^{3+} metal ions were studied by potentiometric titrations in aqueous solution with ionic strength kept at 0.10 M in $[N(CH_3)_4]NO_3$. Equilibria were attained quickly for each ligand with Ca^{2+}, Cu^{2+} and Zn^{2+}, therefore allowing the study of these complexes by direct 'in-cell' titrations in which a metal-to-ligand ratio of 1:1 was used. For the lanthanide ions, however, the study was hindered by the very low solubility of the triprotonated complex species in the acidic pH range (notably those of H_6do3p and H_6do3p1ol) and also by the somewhat slow formation of the deprotonated complex species at alkaline pH. Both factors, particularly the former one, forced us to work with a metal-to-ligand ratio of 1:2, which hinders the determination of stability constants of possible dinuclear complex species. Nonetheless, this procedure allowed us to perform such studies by direct 'in-cell' titrations as for the other metal ions, although with higher experimental error in the determined values.

The values of the stability constants of H_7do3p1pr, H_6do3p and H_6do3p1ol complexes and the corresponding standard deviations, as obtained from fitting of the experimental data, are collected in Table S2 of the Supporting Information. The calculated stepwise stability constants for the complexes of the three ligands, together with literature values for the related H_4dota and H_8dotp,[6,26,35,41,47–49] are presented in Table 3. While fitting the titration curves, only mononuclear complex species were found to be present under our experimental conditions. This is expected given the metal-to-ligand ratios used in the titrations, as mentioned above. Dinuclear metal complexes are likely to be formed by any one of the studied ligands in the presence of more than one equivalent of most of the metal ions, as it has been found for complexes of similar ligands,[19,21,22] but it was not possible to confirm the presence of such species due to the experimental limitations explained above.

Table 3. Stepwise stability constants (log K_{MH_iL}) of metal complexes of the discussed ligands. T = 298.2 K; I = 0.10 M in $[N(CH_3)_4]NO_3$.

Ion	Equilibrium quotient [a]	H_7do3p1pr	H_6do3p	H_6do3p1ol	H_4dota	H_8dotp
Ca^{2+}	[ML]/[M][L]	12.60	11.89, 10.96[b]	12.33	17.226[c]	11.12[d]
	[MHL]/[ML][H]	9.93	10.14, 9.7[b]	9.97	–	–
	$[MH_2L]/[MHL][H]$	8.37	8.25, 7.9[b]	8.00	–	–
	$[MH_3L]/[MH_2L][H]$	7.33	7.06, 7.05[b]	7.15	–	–
	$[MH_4L]/[MH_3L][H]$	6.91	7.05	6.91	–	–
	[ML]/[MLOH][H]	11.41	12.06	12.13	–	–

Cu^{2+}	[ML]/[M][L]	28.77	28.43, 26.9[e]	27.86	22.25[f]	25.4[g]
	[MHL]/[ML][H]	7.57	7.45	7.47	3.78[f]	7.41[g]
	$[MH_2L]/[MHL][H]$	6.88	6.45	6.39	3.70[f]	6.42[g]
	$[MH_3L]/[MH_2L][H]$	5.38	4.51	4.66	–	6.16[g]
	$[MH_4L]/[MH_3L][H]$	4.19	–	–	–	4.58[g]
	[ML]/[MLOH][H]	12.09	11.84	11.62	–	–
Zn^{2+}	[ML]/[M][L]	22.72	22.34, 21.23[b]	22.27	21.10[f]	24.8[g]
	[MHL]/[ML][H]	8.08	8.17, 7.8[b]	8.21	4.18[f]	7.21[g]
	$[MH_2L]/[MHL][H]$	7.05	6.71, 6.5[b]	6.65	3.51[f]	6.72[g]
	$[MH_3L]/[MH_2L][H]$	5.80	5.42, 5.1[b]	5.23	–	5.06[g]
	$[MH_4L]/[MH_3L][H]$	4.71	–	3.38	–	4.78[g]
	[ML]/[MLOH][H]	11.93	12.11	11.79	–	–
La^{3+}	[ML]/[M][L]	23.4	22.8	22.5	22.9[h]	27.6[i]
	[MHL]/[ML][H]	14.5[j]	14.4[j]	14.1[j]	–	–[k]
	$[MH_2L]/[MHL][H]$				–	–[k]
	$[MH_3L]/[MH_2L][H]$	6.6	6.2	6.1	–	–[k]
	$[MH_4L]/[MH_3L][H]$	4.8	–	–	–	–[k]
	[ML]/[MLOH][H]	11.5	11.1	11.2	–	–
Sm^{3+}	[ML]/[M][L]	24.7	24.1	24.0	23.0[h]	28.1[i]
	[MHL]/[ML][H]	14.8[j]	14.5[j]	14.5[j]	–	–[k]
	$[MH_2L]/[MHL][H]$				–	–[k]
	$[MH_3L]/[MH_2L][H]$	5.6	5.8	5.4	–	–[k]
	$[MH_4L]/[MH_3L][H]$	5.1	–	–	–	–[k]
	[ML]/[MLOH][H]	11.8	11.8	11.1	–	–
Gd^{3+}	[ML]/[M][L]	24.9	24.6	24.4	24.6[h]	28.8[i]
	[MHL]/[ML][H]	15.0[j]	14.6[j]	13.4[j]	–	7.6[i]
	$[MH_2L]/[MHL][H]$				–	6.3[i]
	$[MH_3L]/[MH_2L][H]$	6.5	5.5	6.6	–	5.4[i]
	$[MH_4L]/[MH_3L][H]$	4.2	–	–	–	4.0[i]
	[ML]/[MLOH][H]	11.4	11.1	10.6	–	–
Ho^{3+}	[ML]/[M][L]	25.5	24.9	24.6	24.8[h]	29.2[i]
	[MHL]/[ML][H]	14.5[j]	14.3[j]	13.7[j]	–	–[k]
	$[MH_2L]/[MHL][H]$				–	–[k]
	$[MH_3L]/[MH_2L][H]$	5.6	6.0	6.34	–	–[k]
	$[MH_4L]/[MH_3L][H]$	5.4	–	–	–	–[k]
	[ML]/[MLOH][H]	12.1	11.5	11.3	–	–
Lu^{3+}	[ML]/[M][L]	25.9	25.3	25.0	25.4[h]	29.6[i]
	[MHL]/[ML][H]	15. 3[j]	15.2[j]	15.3[j]	–	8.7[i]
	$[MH_2L]/[MHL][H]$				–	7.0[i]
	$[MH_3L]/[MH_2L][H]$	6.5	5.4	5.1	–	5.5[i]
	$[MH_4L]/[MH_3L][H]$	4.3	–	–	–	4.0[i]

[ML]/[MLOH][H]	10.7	10.9	10.6	–	–

[a] Charges of equilibrium species are omitted for clarity; [b] From ref. 27; [c] From ref. 47; [d] From ref. 41, some protonated and dinuclear species also exist and were used to calculate the pM; [e] From ref. 26; [f] From ref. 35; [g] From ref. 48 with I = 1.0 M; [h] From ref. 49; [i] From ref. 6; [j] Corresponding to a double protonation equilibrium ($[MH_2L]/[ML][H]^2$); [k] Not available, thus corresponding values for the closest lanthanide complexes from ref. 6 were used instead for estimating the pM.

The stability constants found for the Ca^{2+} complexes are somewhat higher than that of H_8dotp but still much lower than that of H_4dota, which is expected given the preference of this metal ion for the carboxylate groups. The Cu^{2+} complexes of all the ligands have very high stability constants derived from the high basicity of the ligands due to the presence of the aminomethylphosphonate groups. With Zn^{2+}, the complexes of all ligands present a rather similar stability that is comparable to that of H_4dota and also H_8dotp. The stability constants for the protonated species of both Cu^{2+} and Zn^{2+} complexes seem to indicate that protonation happens only on the pendant arms, as the values for the protonation constants of MHL and MH_2L species are lower than the first two protonation constants assigned to the phosphonate moieties in the corresponding free ligands. Similar features are observed for H_8dotp, and the same is verified in the solid state as demonstrated above by the structure of $[Cu(H_2O)(H_4dotp)]^{2-}$, Figure 3. This is understandable in view of the preference of these two metal ions for the nitrogen donor atoms. The stability constants obtained for the Ca^{2+}, Cu^{2+} and Zn^{2+} complexes of H_6do3p compare well with those previously reported.[26,27]

The Ln^{3+} complexes of the ligands exhibit very high stability, with constant values that are comparatively very similar, being of the same order of those of H_4dota and lower that those of H_8dotp. Considering that the basicity of these ligands is much higher than H_4dota and almost as high as H_8dotp, the coordination ability of the three studied ligands seems to be somewhat less appropriate for these metal ions than that of the model compounds H_4dota and H_8dotp. In all Ln^{3+} complexes of each ligand, the monoprotonated species (MHL) could not be used in the refinement of equilibrium constants, which is indicative of a very low abundance of such species in solution. Therefore, in these systems only a global constant for the double protonation equilibria could be determined, with log β values around 14–15, which would correspond to two stepwise constants in the range 7–8. Further protonated species of these complexes have log K values around or below 6. These findings suggest that the global constant determined for these complexes corresponds to an almost simultaneous protonation of two ring amines as it was also found for Ln^{3+} complexes of the similar ligand H_5do3a1p.[19] The remaining protonations at lower pH occur on phosphonate groups probably coordinated to the metal centre. Such interpretation is consistent with the commonly accepted mechanism of formation of Ln^{3+} complexes of H_4dota-like ligands[17,21,50] where the Ln^{3+} ions are initially captured by the oxygen donor atoms of the pendant arms and only bind to the nitrogen donors of the ring after full deprotonation of these amines.

The pM values (−log[M]) were calculated for the complexes of the discussed ligands at pH 7.4 (physiological), from the thermodynamic constants in Tables 2 and 3 or from literature ones, and are presented in Table 4. These values are a more accurate way of estimating the complexation efficiency of different ligands as they are based on the global set of stability constants describing each system, and take into account the different basicity properties of each compound. The analysis of the pM values shows at first that the three ligands are very efficient chelators for all metal ions studied except Ca^{2+}, which is mostly free in solution at the pH considered. However, the efficiency of Cu^{2+} chelation is outstandingly high, even higher than for H_4dota and H_8dotp. In contrast, the chelation efficiency for Zn^{2+} and the Ln^{3+} is lower than for the latter ligands. However, the comparison of our results with the ones available in the literature for H_4dota and H_8dotp must be taken cautiously, as the experimental methods and procedures are sometimes significantly different from ours, thus entailing non negligible inconsistencies. Overall, from the three ligands studied, H_7do3p1pr is the most efficient chelator for all metal ions, although there is only a slight difference between them.

Figures 6 and 7 show examples of distribution diagrams for the Cu^{2+} and Lu^{3+} complexes of H_7do3p1pr, and additional examples for this ligand are shown in the Supporting Information. The distribution curves for the systems with other two ligands look very similar to the previous and are thus not shown. These curves show several protonated species existing throughout the whole pH range, as expected from the high number of protonation equilibria allowed by the several functional groups present on the ligands, notably the phosphonate moieties. In the case of the metal complexes, it can be seen that, at the physiological pH, the complexes exist mainly as unprotonated, monoprotonated and diprotonated species, while nearly all metal ions are complexed from below neutral pH except Ca^{2+}.

Table 4. Values of pM [a] calculated for metal complexes of the discussed ligands at pH 7.4, based on the protonation and stability constants of Tables 2 and 3 or on literature ones.

Ion	H_7do3p1pr	H_6do3p	H_6do3p1ol	H_4dota	H_8dotp

Ca^{2+}	5.02	5.01	5.02	10.26[b]	5.01[c]
Cu^{2+}	16.18	16.05	15.74	15.20[d]	15.57[e]
Zn^{2+}	10.57	10.52	10.73	14.05[d]	14.89[e]
La^{3+}	10.52	10.22	10.10	15.85[f]	14.49[g]
Sm^{3+}	11.98	11.56	11.70	15.95[f]	14.76[g]
Gd^{3+}	12.26	12.05	11.91	17.55[f]	15.46[g]
Ho^{3+}	12.60	12.26	12.11	17.75[f]	16.49[g]
Lu^{3+}	13.53	13.12	13.15	18.35[f]	17.29[g]

[a] Values calculated for 100% excess of ligand concentration at $c_M = 1.00\times10^{-5}$ M; [b] From ref. 47; [c] From ref. 41; [d] From ref. 35; [e] From ref. 48 with $I = 1.0$ M; [f] From ref. 49;; [g] From ref. 6

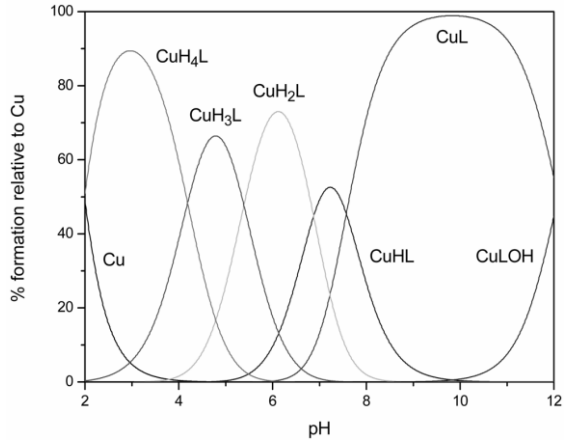

Figure 6. Species distribution diagram for the Cu^{2+} complex of H_7do3p1pr at $c_M = c_L = 1.0\times10^{-3}$ M.

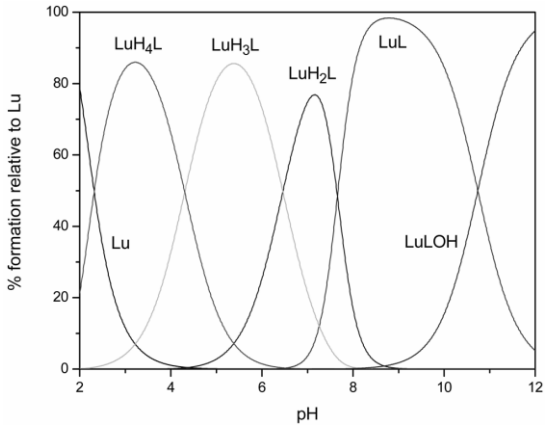

Figure 7. Species distribution diagram for the Lu^{3+} complex of H_7do3p1pr at $c_M = c_L = 1.0\times10^{-3}$ M.

An important question that remains unanswered in these studies is whether the carboxylate and alcohol groups in H_7do3p1pr and H_6do3p1ol participate in the coordination of any of the metal ions once these are encapsulated into the macrocyclic framework, especially in the case of Ln^{3+} ions. Although the ligand H_7do3p1pr presents the highest stability constants and pM values with the latter metal ions, the differences are relatively small and could well be just a consequence of the dissimilar basicity of the ligands. A better understanding of the metal coordination behaviour of these ligands is given by the following studies.

Dissociation kinetics study of Cu^{2+} complexes. To characterize the Cu^{2+} complexes their UV-Vis spectra were measured in aqueous solution. The absorption band maxima are in the 320–330 nm range in the UV region and at 620 nm in the visible region (see Figures S6 and S7) indicating that these Cu^{2+} complexes have the same structure.

The acid-assisted dissociation of the Cu^{2+} complexes was studied in the presence of high concentration of HCl (see Figures 8 and 9). As it can be seen, the Cu^{2+} complex of H_6do3p1ol is more kinetically inert than those of H_6do3p and H_7do3p1pr. In addition, there is no shift of the absorption maximum of the complexes in both UV and visible regions (see Figures S8–S12) during the

progress of the decomplexation reaction, indicating that the structures of the kinetic intermediates (if any) are the same as those of the starting complex.

Scheme 5. Proposed reaction scheme of dissociation of Cu^{2+} complexes of H_6do3p, H_6do3p1ol (m = 3, n = 4) and H_7do3p1pr (m = 4, n = 5)

$$[CuL]^{n-} + m\,H^+ \underset{}{\overset{\text{fast}}{\rightleftharpoons}} [CuH_mL]^{m-n}$$

$$[CuH_mL]^{m-n} + H^+ \underset{\text{fast}}{\overset{K}{\rightleftharpoons}} [CuH_{m+1}L]^{m+1-n}$$

$$[CuH_mL]^{m-n} \xrightarrow[\text{slow}]{k_1} Cu^{2+} + [H_{m+1}L]^{m-1-n}$$

$$[CuH_{m+1}L]^{m+1-n} \xrightarrow[H^+]{k_2\ \text{slow}} Cu^{2+} + [H_{m+2}L]^{m-n}$$

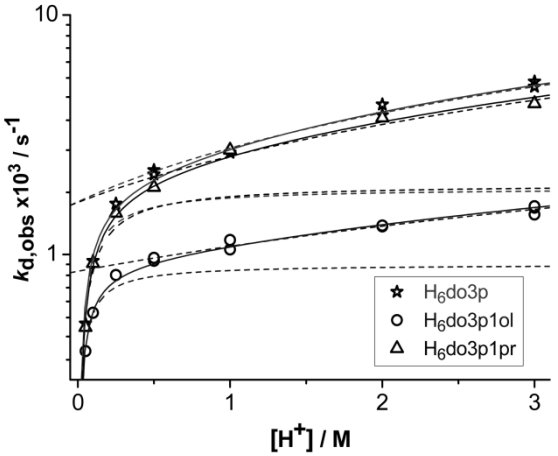

Figure 8. Comparison of the decomplexation rate constants for Cu^{2+} complexes of the three studied ligands at 298.2 K. The fitting using Eq. (1) is represented in solid lines, and the limiting cases of Eqs. (2b) and (2c) with the parameters given in Table 4 are represented in dashed lines.

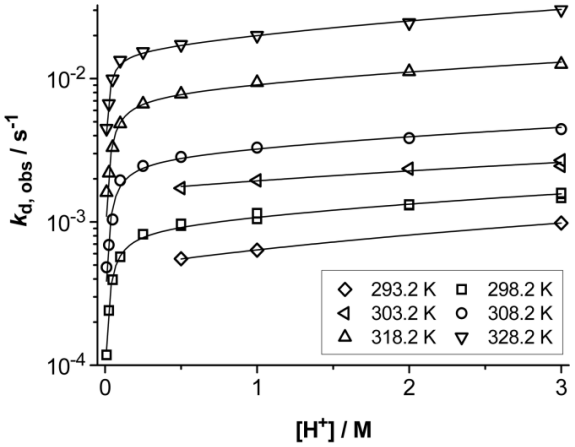

Figure 9. Dependence of the pseudo-first-order rate constants for the Cu^{2+} complex of H_6do3p1ol in solution, as a function of the acidity at different temperatures. The experimental points were fitted by Eq. (1) with the parameters given in Table 5.

Assuming the reaction mechanism proposed in Scheme 5, the following empirical rate law was derived:[51]

$$k_{d,obs} = \frac{k_1 \times K \times [H^+] + k_2 \times K \times [H^+]^2}{1 + K \times [H^+]} = \frac{K \times [H^+](k_1 + k_2 \times [H^+])}{1 + K \times [H^+]} \quad (1)$$

There are several limiting cases leading to a simplification of equation (1):

$1 >> K \times [H^+]$, $$k_{d,obs} = k_1 \times K \times [H^+] + k_2 \times K \times [H^+]^2 \quad (2a)$$

$1 << K \times [H^+]$, $$k_{d,obs} = k_1 + k_2 \times [H^+] \quad (2b)$$

$k_1 >> k_2 \times [H^+]$, $$k_{d,obs} = \frac{k_1 \times K \times [H^+]}{1 + K \times [H^+]} \quad (2c)$$

The pseudo-first-order rate constants were measured at different HCl concentration (Figures 8 and 9) in order to determine the parameters of Eq. (1). At higher acid concentration, the simplified rate-law equation (2b) can be used for the estimation of the k_1 and k_2 rate constants, while the thermodynamic constant K can be obtained from the measurements at lower acid concentration using Eq. (2c), see Figure 8. All the values were compiled in Table S3, and representative ones are shown together with the activation parameters in Table 5.

Table 5. Kinetic parameters [a] for acid-assisted dissociation of Cu^{2+} complexes (I = 3.0 M (Na,H)Cl).

Temperature	Rate constants			Thermodynamic constant
/ K	$k_1 \times 10^3$ / s^{-1}	$k_2 \times 10^3$ / M^{-1} s^{-1}	k_2 / k_1	K / M^{-1}
H_6do3p				
288.2	0.75(2)	0.525(9)	0.70(2)	n.d.
293.2	1.2(1)	0.79(8)	0.7(1)	n.d.
298.2	1.9(1)	1.12(9)	0.59(6)	10(3)
308.2	6.3(3)	2.9(3)	0.46(6)	8(1)
318.2	14.2(5)	6.9(5)	0.48(4)	10(1)
$\Delta H^{\neq}$ / kJ mol^{-1}	75(3)	63(2)	–	–
$\Delta S^{\neq}$ / J mol^{-1} K^{-1}	−47(9)	−88(8)	–	–
H_6do3p1ol				
293.2	0.466(3)	0.172(1)	0.369(3)	n.d.
298.2	0.91(2)	0.23(2)	0.25(2)	16(2)
303.2	1.6(1)	0.34(5)	0.21(3)	n.d.
308.2	2.81(9)	0.62(4)	0.22(2)	16(2)
318.2	7.8(2)	1.9(2)	0.24(2)	16(2)
328.2	15.4(3)	5.1(2)	0.33(1)	37(5)
$\Delta H^{\neq}$ / kJ mol^{-}	78(3)	78(5)	–	–
$\Delta S^{\neq}$ / J mol^{-1} K^{-}	−42(10)	−55(15)	–	–
H_7do3p1pr				
288.2	0.69(4)	0.31(3)	0.46(5)	7(1)
298.2	1.9(1)	0.9(1)	0.47(8)	8(2)
308.2	4.9(2)	2.4(2)	0.49(5)	11(2)
318.2	13.2(6)	6.2(1)	0.47(2)	11(2)
328.2	27.3(7)	11.8(5)	0.43(2)	13(1)
$\Delta H^{\neq}$ / kJ mol^{-1}	70(1)	70(2)	–	–
$\Delta S^{\neq}$ / J mol^{-1} K^{-1}	−61(4)	−70(7)	–	–

[a] The standard deviations are given in parentheses.

Both k_1 and k_2 rate constants are 2–4 times lower for the Cu^{2+} complex of H_6do3p1ol than for those of H_6do3p and H_7do3p1pr. However, this trend is opposite if the ratio of both constants is considered (Table 5). This fact is also reflected in the activation parameters of the three complexes, showing that both dissociation reaction pathways should have a similar mechanism. Although the $\Delta H^{\neq}$ values are of the same order of magnitude for the three complexes, the highest one was found for the $[Cu(do3p1ol)]^{4-}$. Both reaction steps for all studied complexes (Table 5) do have a strongly associative character, probably with a significant participation of the bulk water molecules coming from the solvent. Water molecule(s) probably participate in the proton transfer from a pendant arm (rate constant k_1) or in the direct proton attack (rate constant k_2) to nitrogen atoms of the macrocyclic cavity. The $[Cu(do3p1ol)]^{4-}$ complex is the one that least favours both reaction pathways, probably due to the presence of the pendant arm

without acid-base behaviour. In addition, the differences between the kinetic inertness of Cu^{2+} complexes of ligands having three or more phosphonate pendant arms (H_6do3p, H_8dotp, H_6do3p1ol, H_7do3p1a) are smaller than between those having three or more acetate arms (H_3do3a, H_4dota, H_5do3a1p), for which the proton-transfer pathway is also preferred.

Spectroscopic and kinetic study of Ln^{3+} complexes. The Ln^{3+} complexes were characterized in aqueous solution by molecular absorption (Ce) or luminescence (Eu) spectroscopies. The Ce^{3+} complexes of all three studied ligands showed the maximum of their absorption bands at 300 nm, which is comparable to those of the Ce^{3+} complexes of analogous ligands: $[Ce(H_2O)(dotp)]^{5-}$ at 300 nm,[52] $[Ce(H_2O)(do3p1a)]^{4-}$ at 305 nm,[24] $[Ce(H_2O)(trans\text{-}do2a2p)]^{3-}$ at 310 nm,[21] and $[Ce(H_2O)(dota)]^{-}$ at 322 nm.[21] This fact is an indirect proof that all phosphonate pendant arms are coordinated to Ce^{3+} ion. Luminescence spectroscopy showed that the Eu^{3+} complexes of all studied ligands exhibit a I_{615}/I_{594} ratio higher than one, see Figures S13–S15, as in the case of the $[Eu(dotp)]^{5-}$ complex.[53] However, the characteristic emission band at 615 nm is split for the complexes of H_6do3p and H_6do3p1ol, leading to the decrease of the I_{615}/I_{594} ratio. The number of coordinated water molecules is about one for the H_6do3p complex and less than one for the H_6do3p1ol complex (in agreement with the data for the Gd^{3+} complex, see below), as shown in Table S4. This also agrees with the assumption that the number of water molecules in the [Eu(do3a)] complex is about two, and in the $[Eu(dotp)]^{5-}$ complex it is zero,[53] suggesting that the smaller acetate arms enable the accommodation of more water molecules in the Eu^{3+} complexes. The higher number of water molecules in the Eu^{3+} complex of H_7do3p1pr suggests the protonation of the propionate pendant arm. However, the calculation of the hydration number using improved formulas,[17,21,53] which take into account the second sphere effects, led to lower values for all three complexes. The most significant effect was observed for the complex of H_7do3p1pr, for which a value close to one was found (see Table S4).

The formation of Ce^{3+} complexes of the macrocycles was studied in ligand excess ($c_L = 2\times c_{Ce}$ = 0.4 mM, I = 0.1 M KCl, T = 298.2 K) in the 4.5–6.5 pH range. This reaction was found to be relatively fast and therefore it was suitable to be studied by conventional molecular absorption spectroscopy. The second-order rate formation constants were estimated to be in the 0.5–1.0 M^{-1} s^{-1} range for all three complexes, and they do not exhibit any pH dependence in the used pH range. This indicates that protonated species H_5L, H_4L and H_3L (and H_6L in the case of H_7do3p1pr; the charges are omitted for clarity) have almost the same reactivity. These findings are in agreement with the results obtained in the study of Ce^{3+} complexes of H_7do3p1a.[24]

The acid-assisted dissociation reaction of Ce^{3+} and Eu^{3+} complexes was studied at low temperature (278.2 K), since this reaction was too fast at r.t. In order to compare the reactivity of Ln^{3+} complexes, the pseudo-first-order rate constants, $k_{d,obs}$, were determined in 0.01 M $HClO_4$ for the Ce^{3+} and Eu^{3+} complexes (see Table 6). The values are much higher for these complexes than for those of H_7do3p1a and H_8dotp measured at T = 298.2 K and at the same acidity medium.[21,24] Under these experimental conditions, both Ln^{3+} complexes of H_7do3p1a have comparable values of $k_{d,obs}$, (about 2.35×10^{-6} s^{-1}); however, the Ce^{3+} complex of H_8dotp is more inert (4.6×10^{-7} s^{-1}) than the Eu^{3+} one of the same ligand (1.27×10^{-5} s^{-1}). The comparison of values for Ln^{3+} complexes of H_6do3p and H_7do3p1a for lower temperature show a five-order decrease of decomplexation rate when one acetate pendant arm is added to the macrocyclic framework of H_6do3p. The same but in a smaller extent was observed for the Gd^{3+} complexes of H_3do3a and H_4dota (Table 6). A similar difference can also be found for the Eu^{3+} complexes of H_7do3p1a and H_7do3p1pr (7.12×10^{-8} *vs.* 0.031 s^{-1}, see Table 5). However, it was not observed in the Eu^{3+} complexes of H_7do3a1p,[24] or in the analogous ligand H_5do3a1pp that has one methylphosphonate pendant arm replaced by the longer propylphosphonate.[54] This behaviour suggests that the propanol and propionate pendant arms in the complexes of H_7do3a1p and H_5do3a1pp are probably not coordinated to the Ln^{3+}, as also proposed from NMR experiments (see below).

Table 6. Kinetic inertness of Ln^{3+} complexes (c_{LnL} = 1 mM, $[H^+]$ = 0.01 M).

Ln^{3+}	Ligand	$k_{d,obs}$ / s^{-1}	T / K	Ref.
Ce^{3+}	H_6do3p	0.019	278.2	This work [a]
Eu^{3+}	H_6do3p	0.070	278.2	This work [a]
Ce^{3+}	H_6do3p1ol	0.168	278.2	This work [a]
Eu^{3+}	H_6do3p1ol	0.024	278.2	This work [a]
Ce^{3+}	H_7do3p1pr	0.012	278.2	This work [a]
Eu^{3+}	H_7do3p1pr	0.031	278.2	This work [a]
Ce^{3+}	H_7doa3p	1.70×10^{-7}	278.2	21,24 [a]
Eu^{3+}	H_7doa3p	7.12×10^{-8}	278.2	21,24 [a]
Ce^{3+}	H_7doa3p	2.4×10^{-6}	298.2	21,24
Eu^{3+}	H_7doa3p	2.3×10^{-6}	298.2	21,24

Ce^{3+}	H_7dotp	4.6×10^{-7}	298.2	21,52
Eu^{3+}	H_7dotp	1.27×10^{-5}	298.2	21
Gd^{3+}	H_3do3a	7.0×10^{-4}	298.2	19
Gd^{3+}	H_4dota	8.4×10^{-8}	298.2	19
Eu^{3+}	H_5do3ap	9.6×10^{-7}	298.2	17,21
Eu^{3+}	H_5do3app	1.16×10^{-6}	298.2	55

[a]This work, recalculation from activation parameters taken from ref. 21.

The acid-assisted dissociation of the Ce^{3+} complexes was also studied at different acid concentrations (Figure 10). The following empirical rate-law was used to fit the experimental points (Eq. 3):

$$k_{\mathrm{d,obs}} = \frac{k_0 + k_1 \times K \times [\mathrm{H}^+]}{1 + K \times [\mathrm{H}^+]} = \frac{k_0 + K^{\mathrm{H}} \times [\mathrm{H}^+]}{1 + K \times [\mathrm{H}^+]} \qquad (3)$$

where k_0, k_1 and K are parameters defined in Scheme 6. The parameters obtained from non-linear least-squares fitting procedure are given in Table 7.

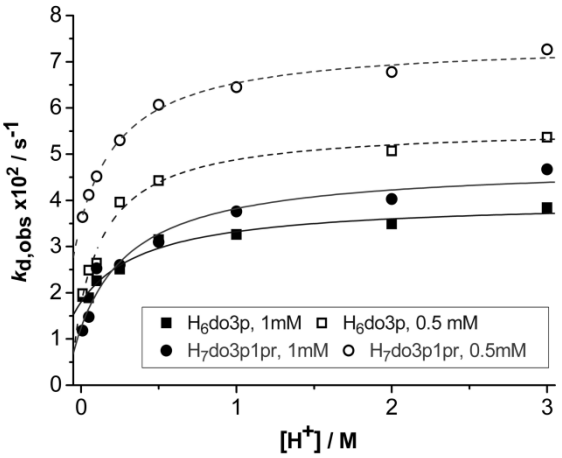

Figure 7. Dependence of observed rate constants for acid-assisted dissociation of the Ce^{3+} complexes on proton concentration at two different overall complex concentrations (I = 3.0 M (Na,H)ClO_4, T = 278.2 K).

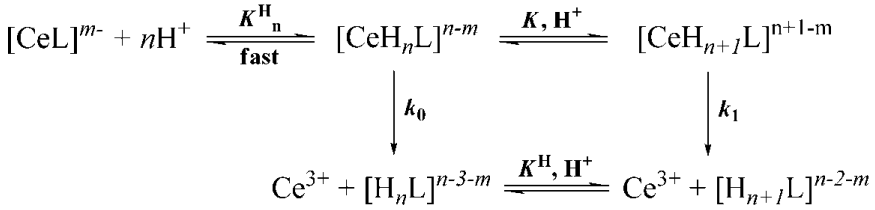

Scheme 6. Proposed reaction scheme for the dissociation of Ce^{3+} complexes of H_6do3p (m = 3, n = 3) and H_7do3p1pr (m = 4, n = 4).

Table 7. Kinetic parameters [a] for acid-assisted dissociation of Ce^{3+} complexes (I = 3.0 M (Na,H)ClO_4), T = 278.2 K.

Complex	c / mM	k_0 / s^{-1}	K^{H} / M^{-1} s^{-1}	k_1 / s^{-1}	K / M^{-1}
$[Ce(do3p)]^{3-}$	1.0	0.0180(12)	0.090(27)	0.040(12)	2.25(76)
	0.5	0.0175(20)	0.246(56)	0.056(14)	4.4(11)
$[Ce(do3p1pr)]^{4-}$	1.0	0.0124(28)	0.129(52)	0.048(30)	2.7(13)
	0.5	0.0354(12)	0.247(36)	0.075(11)	3.32(53)

[a]The standard deviations are given in parentheses.

It was observed that a white precipitate of the ligand in zwitterionic form occurs usually at the end of the dissociation reaction, probably due to the low temperature employed in the study. The points where the precipitate was present were not considered in the fitting of kinetic data. In acidic medium, the Ln^{3+} complexes are protonated and polymeric structures might be formed *via* protonated and unprotonated phosphonate groups.[55] This was tested by studying the dissociation kinetics at various overall Ce^{3+} complex concentrations. This self-aggregation was also observed by NMR spectroscopy in slightly basic medium, see below. In order to decrease the extent of the polymerization, the measurements at lower complex concentrations lead to a faster complex decomposition (Figure 10 and Table 7), thus, supporting this hypothesis.[21] While the acceleration of the dissociation for the Ce^{3+} complex of H_6do3p can be mostly attributed to the increase of its protonation constant *K*, the increase for the Ce^{3+} complex of H_7do3p1pr is caused by the higher values of both parameters, *k* and *K*, probably as a consequence of the acid-base behaviour of the propionate arm.

NMR studies of lanthanide(III) complexes. The ^{1}H NMR spectra of the $[Ln(do3p)]^{3-}$, $[Ln(do3p1pr)]^{4-}$ and $[Ln(do3p1ol)]^{3-}$ complexes (Ln = Lu, Eu and Yb) were studied as a function of temperature in D_2O solution at pD (8.5–9.5) corresponding to the formation of the fully deprotonated ML species (Figure S17–S19). They showed resonances with linewidths that are strongly temperature dependent in the 298–353 K interval. A complete structural study of these complexes was not possible to undertake, as it depended on the full assignment of the spectra. Therefore, the main aim of the current study was to investigate whether or not all the pendant arms of the ligands are involved in the coordination to the Ln^{3+} ion.

The Ln^{3+} complexes of tetraazamacrocyclic ligands, such as H_8dotp, trans-H_6do2a2p or H_4dota, can form two diastereomers in solution, arising from combination of the conformation of the macrocyclic ethylene chelate rings (δ/λ) and the helicity of the phosphonate/acetate pendant arms (Λ/Δ).[21,22,56,57,58] This leads to two cordination geometries: square antiprismatic (SAP) forming the enantiomeric pair Δ(λλλλ)/Λ(δδδδ□□) and twisted square antiprismatic (TSAP) with the enantiomeric pair Δ(δδδδ)/Λ(λλλλ). The ^{1}H NMR spectra of the diamagnetic $[Lu(do3p)]^{3-}$, $[Lu(do3p1pr)]^{4-}$ and $[Lu(do3p1ol)]^{3-}$ complexes at different temperatures (Figure S17) have some similarities to those described for $[Ln(trans\text{-}do2a2p)]^{3-}$.[21,22,56] Therefore, it may be concluded that the Lu^{3+} ion is coordinated through the four macrocyclic nitrogen atoms and an oxygen atom of each of the three pendant arm phosphonate groups in the $[Lu(do3p)]^{3-}$ complex, with the possibility of extra coordination of the fourth pendant arm in the $[Lu(do3p1pr)]^{4-}$ and $[Lu(do3p1ol)]^{3-}$ complexes.

The resonances of the methylene CH_2 protons of the ring and phosphonate pendant arms show very similar temperature dependence, being quite broad at 298 K and displaying very significant sharpening at 333 K and above. This reflects the intramolecular dynamic isomerization process of the complexes between SAP and TSAP structures, which becomes fast on the NMR time scale at temperature higher than 333 K. This process has been found before for other Ln^{3+} complexes of tetraaza ligands with mixed carboxylate and phosphonate pendant arms, such as $[Ln(\textit{trans}\text{-}do2a2p)]^{3-}$,[21,22,56] but is absent in $[Ln(dotp)]^{5-}$ complexes which occur in solution exclusively in the TSAP geometry.[57] The same NMR spectra indicate that the propionate and propanol pendant arms of $[Lu(do3p1pr)]^{4-}$ and $[Lu(do3p1ol)]^{3-}$, respectively, are not coordinated to the Lu^{3+} ions since the geminal CH_2 protons at each of their carbon atoms are equivalent and originate sharp multiplets, as expected for freely rotating unbound groups (Figure S17). If they were bound to the Lu^{3+} ion, they would originate clearly detectable AB or AX multiplet patterns, as observed before for ion-bound acetate and phosphonate pendant arms.[21,22,57] The $C_{(17)}H_2$ protons of $[Lu(do3p1pr)]^{4-}$, adjacent to the terminal carboxylate group of the fourth arm, originate two partially overlapping sharp triplets (Figure S17), reflecting the presence of the SAP and TSAP isomers of the complex in solution.

The ^{31}P NMR spectra of the Lu^{3+} and Yb^{3+} complexes of the three ligands consist of two resonances with 1:2 relative intensities, corresponding to the P_a and P_b ligand phosphonates, and their shifts are summarized in Table S4. Those shifts are almost the same in all three Lu^{3+} complexes, reflecting the equivalent binding of the three phosphonate groups to the central ion. The large ^{31}P paramagnetic shifts observed for the P_a and P_b atoms of the pendant arms induced by the paramagnetic Yb^{3+} ion in the three complexes unequivocally confirm their metal binding in all cases, as expected.

The ^{1}H NMR resonances of the Yb^{3+} and Eu^{3+} complexes of H_6do3p, H_7do3p1pr and H_6do3p1ol show a clear temperature dependence (Figure S18 and S19). The paramagnetically shifted resonances for the H_6do3p and H_7do3p1pr complexes are quite broad and most are not observed at 298 K and become visible and sharper at higher temperatures (353 K). The opposite is observed for the H_6do3p1ol complexes, where the shifted resonances are even sharper at r.t. and their number corresponds to a slow exchange process between SAP/TSAP isomers present in solution, while those resonances dramatically broaden out at higher temperatures. This effect reflects a dynamic equilibrium between the SAP and TSAP isomers present is solution. Due to the symmetry of the complexes, the four axial ring protons originate three shifted resonances with 1:1:2 relative intensities for each isomer. Figure 11 shows representative spectra of the Yb^{3+} and Eu^{3+} complexes of H_6do3p, H_7do3p1pr and H_6do3p1ol in conditions where they are

sharp. On the basis of previously published data for the complexes of H_8dotp, H_4dota, trans-H_6do2a2p and other H_4dota-like ligands with mixed pendant arms,[21,22,57–60] the three low field ^{1}H NMR resonances from the axial ring protons have shifts in the range characteristic of a TSAP isomer for the $[Yb(do3p)]^{3-}$, $[Eu(do3p)]^{3-}$ and $[Yb(do3p1pr)]^{4-}$ complexes at 353 K, and this isomer predominates in solution. However, for the $[Eu(do3p1ol)]^{3-}$ complex, these protons lead at 298 K to two sets of resonances assigned to SAP and TSAP isomers present in approximately 1:1 ratio. The paramagnetic shifts of the fourth pendant arms in the complexes are relatively small and compatible with not being coordinated to the paramagnetic center.

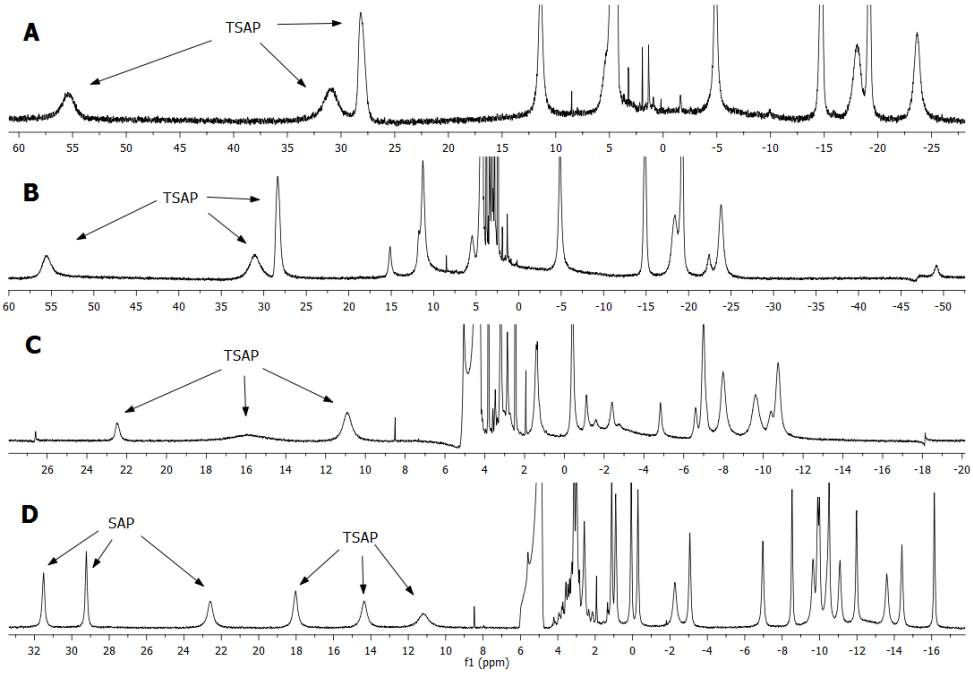

Figure 11. ^{1}H NMR spectra in 10 mM D_2O solution of: A) $[Yb(do3p)]^{3-}$ at 353 K (pD = 8.90), B) $[Yb(do3p1pr)]^{4-}$ at 353 K (pD = 9.02), C) $[Eu(do3p)]^{3-}$ at 353 K (pD = 9.23), D) $[Eu(do3p1ol)]^{3-}$ at 298 K (pD = 9.03).

^{17}O NMR and ^{1}H NMRD Studies. The relaxation effect of the $[Gd(do3p1ol)]^{3-}$ complex was studied in aqueous solution by measuring the magnetic field dependence of the longitudinal water proton relaxivity (r_1) (nuclear magnetic relaxation dispersion – NMRD curves) at 298 K (Figure 12) as well as the temperature dependence of the water ^{17}O NMR longitudinal ($1/T_{1r}$) and transverse ($1/T_{2r}$) relaxation rates and chemical shifts ($\Delta\omega_r$) (Figure S20).

Although the parameters that describe its water exchange, rotation, electronic relaxation and proton relaxivity could not be quantitatively characterized from the experimental data,[3] some qualitative conclusions can be drawn. The ^{17}O NMR data show that there is either no water or at least less than one water molecule in the inner sphere of the complex. In fact, the observed reduced ^{17}O NMR chemical shifts ($\Delta\omega_r$) of water, which depend on the contact shift induced by Gd^{3+} on the ^{17}O nucleus of the coordinated water molecule(s) and which are proportional to the inner-sphere water coordination number (q), are close to zero (< 200 Hz) instead of being around 8–10×10^5 Hz as expected for Gd^{3+} complexes with q = 1. In addition, the reduced transverse relaxation rates ($1/T_{2r}$) are also much lower than those for typical q = 1 complexes.[3,61–66] The shape of the temperature dependence of ($1/T_{2r}$) indicates that the water exchange is in the fast exchange regime. The ^{1}H NMRD curve shows that the proton r_1 relaxivities are low at low magnetic fields, but a small peak is observed at higher field, corresponding to a frequency of about 60 MHz. This suggests there must be some residual inner-sphere water ($0 < q < 1$) in the $[Gd(do3p1ol)]^{3-}$ complex, in agreement with the hydration number calculated for the $[Eu(do3p1ol)]^{3-}$ complex (Table 6), although a relaxation contribution from water molecules in the second coordination sphere of the complex[67] could also lead to this observation, as found for the tetraphosphonate/tetraphosphinate complexes such as $[Gd(dotp)]^{5-}$.[68] The presence of the high-field relaxivity peak reflects that there is definitely a self-aggregation in the $[Gd(do3p1ol)]^{3-}$ solutions, as it has been observed before for other Gd^{3+} macrocyclic phosphonate complexes.[69] It is also in agreement with the observation of different decomplexation rate of the Ce^{3+} complexes at different overall complex concentrations (see above).

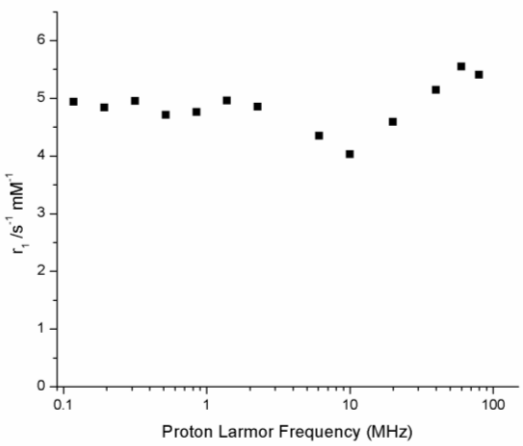

Figure 12. ^{1}H NMRD curve for an aqueous solution of the $[Gd(do3p1ol)]^{-3}$ complex (at 298 K, c = 4.56 mM, pH = 6.5).

Conclusions

Three macrocyclic compounds based on cyclen and containing three methylphosphonate pendant arms, H_6do3p, H_7do3p1pr and H_6do3p1ol, were synthesized and characterised, the latter two for the first time. All three compounds show a very high basicity, as expected from the presence of three methylphosphonate pendant arms. Their protonation sequence could be tentatively assigned from the pH dependence of the ^{31}P NMR chemical shifts, which proved the occurrence of proton exchange between the various basic sites and also suggested the occurrence of strong hydrogen bonding interactions between ring amines at very high pH. These internal hydrogen bonds lead to slow intramolecular interconversions of some protonated species in solution. All ligands were shown to form complexes of reasonable thermodynamic stability with Ca^{2+} and very high stability with Zn^{2+} and the Ln^{3+} ions, while complexes of Cu^{2+} exhibit an even higher stability. In general, the trend in the increase of the complex stability constants for each metal ion follows the trend in the increase of ligand basicity, except in the case of Ca^{2+} where an inversion between the complexes of H_6do3p and H_6do3p1ol was found, which could possibly be justified by the presence of an additional oxygen donor atom that better suits this metal ion.

The kinetic study of acid-assisted dissociation of the Cu^{2+} complexes showed that the $[Cu(do3p1ol)]^{4-}$ is more kinetically inert than the other two complexes. This seems to indicate that the propanol group of H_6do3p1ol in the complex is not involved in the key proton-transfer step of the dissociation reaction, unlike what probably happens to the propionate group in $[Cu(do3p1pr)]^{5-}$. On the other hand, in the $[Cu(do3p)]^{4-}$ complex, the kinetic inertness decrease is due to the presence of the secondary amine. Some of the pendant arms of the ligands are evidently not coordinated to the Cu^{2+} centre, and this can also influence the kinetic inertness of the complexes. The studied Ln^{3+} complexes also have a lower kinetic inertness when compared with analogous complexes of H_8dotp. Indeed, the lower rigidity and lower denticity of the ligands, where propanol/propionate pendant arms are not bound to the Ln^{3+} metal, lead to fast formation as well as low kinetic inertness of the complexes. One coordinated water molecule helping to transfer one proton to the ligand nitrogen atom(s) might be the crucial point to explain the reaction mechanism. Nonetheless, the kinetic inertness of the Ln^{3+} complexes is strengthened by the complex association via phosphonates in different protonation stages.

A ^{1}H and ^{31}P NMR studies of both diamagnetic (Lu^{3+}) and paramagnetic (Eu^{3+}, Yb^{3+}) complexes clearly showed that all three methylphosphonate arms coordinate the metal centres in all studied complexes and also show unambiguously that the propionate arm in the $[Ln(do3p1pr)]^{4-}$ complexes and the propanol arm in the $[Ln(do3p1ol)]^{3-}$ complexes are free and point away from the metal site. The TSAP isomer is predominant in solution for the $[Ln(do3p)]^{3-}$ and $[Ln(do3p1pr)]^{4-}$ (Ln = Eu, Yb) complexes, like for $[Ln(trans\text{-}do2a2p)]^{3-}$ and $[Ln(dotp)]^{5-}$,[21,22,56] while the SAP and TSAP isomers are equally present for the $[Ln(do3p1ol)]^{3-}$ (Ln = Eu, Yb) complexes. The inner-sphere hydration state of the complexes is variable. The luminescence study on the Eu^{3+} complexes points to q values of ~1 for H_6do3p, ~0.5 for H_6do3p1ol and ~1 for H_7do3p1pr, in agreement with the relaxivity data for the $[Gd(do3p1ol)]^{3-}$ complex showing the presence of less than one inner-sphere water molecule. However, the relaxivity of the complex is increased by self-aggregation and possibly also by a contribution from second-sphere water molecules interacting with the phosphonate groups.

Finally, the present study shows that removing one pendant arm of a tetrasubstituted cyclen ligand from the coordination sphere of its Ln^{3+} complexes leads to lower thermodynamic stability and kinetic inertness. This clearly indicates that the appending of a targeting biomolecule to one pendant arm of the chelator to form a BFC must not prevent the coordination of this arm to the metal ion.

Experimental Section

A. Synthesis. A1. Reagents and methods. Cyclen (1,4,7,10-tetraazacyclododecane) was obtained from Chematech, paraformaldehyde, ethyl 3-bromopropionate and triethyl phosphite were obtained from Sigma-Aldrich, and 3-chloropropan-1-ol and acetyl chloride were obtained from Merck. All reagents obtained from commercial sources were used as received. Organic solvents were dried by standard methods.[70] Elemental analyses and electrospray ionization mass spectra (ESI-MS) were performed by the Analytical Services Unit of ITQB-UNL/IBET. The ^{1}H, $^{13}C\{^{1}H\}$, and $^{31}P\{^{1}H\}$ Nuclear Magnetic Resonance (NMR) spectra for ligand characterization and pH titration studies were recorded on a Bruker Avance III 400 MHz spectrometer, operating at frequencies of 400.14 (^{1}H), 100.61 (^{13}C) and 161.99 (^{31}P) MHz, at probe temperature of 298.2 K. Chemical shifts (δ) are given in ppm and coupling constants (J) in Hz. Tetramethylsilane (TMS) or tert-butyl alcohol were used as internal references for ^{1}H and ^{13}C spectra in $CDCl_3$ or D_2O, respectively, while H_3PO_4 was used as external reference (inner-capillary method) for ^{31}P spectra. Resonance assignments are based on peak integration and multiplicity, and on 2D homo- and heteronuclear correlation experiments.

A2. Ethyl 3-(1,4,7,10-tetraazacyclododecan-1-yl)propanoate, 1. Cyclen (5.34 g, 31 mmol) was dissolved in chloroform (120 mL) and triethylamine (1.29 mL, 9.3 mmol) was added. Ethyl 3-bromopropionate (0.99 mL, 7.75 mmol) was then added and the solution was gently refluxed under nitrogen for 15 h. The reaction mixture was cooled and extracted with aq. NaOH (1 M, 3×40 mL) and water (3×40 mL). The organic phase was separated, evaporated to dryness, redissolved in chloroform (40 mL) and extracted again with aq. NaOH (1 M, 2×40 mL) and water (2×40 mL). The organic phase was then dried with anhydrous sodium sulfate, filtered, evaporated to dryness and the residue was dried under vacuum, yielding 1.32 g (63%) of pure mono-alkylated cyclen as a colorless oil. NMR: δ_H (400 MHz, $CDCl_3$, TMS) 1.18 (3H, t, O–CH_2–CH_3), 2.41 (2H, t, CH_2–CO), 2.45–2.75 (18H, m, ring and pendant N–CH_2), 4.07 (2H, q, O–CH_2–CH_3); δ_C (101 MHz, $CDCl_3$, TMS) 14.1 (1C, s, O–CH_2–CH_3), 32.6 (1C, s, CH_2–CO), 44.8, 45.9, 46.8, 51.1 (4×2C, s, ring N–CH_2), 49.8 (1C, s, pendant N–CH_2), 60.2 (1C, s, O–CH_2–CH_3), 172.5 (1C, s, C=O).

A3. Ethyl 3-{4,7,10-tris[(diethoxyphosphoryl)methyl]-1,4,7,10-tetraazacyclododecan-1-yl}propanoate, 2. Compound **1** (1.28 g, 4.7 mmol) was dissolved in triethyl phosphite (2.58 mL, 14.8 mmol). Paraformaldehyde was then added (0.49 g, 15.5 mmol) in small portions over 1 h. The solution was finally stirred at r.t. for an additional 4 d. The volatiles were evaporated; the product was co-evaporated with toluene (3×50 mL) and dried under vacuum for several hours to yield 3.34 g of a clear oil. This product, containing also a minor amount of a diethyl hydroxymethylphosphonate by-product (ca. 8% based on ^{31}P NMR peak integration, overall yield of 2 is 90%), was used without further purification in the following hydrolysis step to remove both carboxylate and phosphonate ethyl esters. NMR: δ_H (400 MHz, $CDCl_3$, TMS) 1.21 (3H, t, C–O–CH_2–CH_3), 1.28 (18H, t, P–O–CH_2–CH_3), 2.38 (2H, t, CH_2–CO), 2.54 (4H, m, ring N–CH_2), 2.71 (2H, t, N–CH_2–CH_2–CO), 2.80 (12H, m, ring N–CH_2), 2.87 (6H, d, $^{2}J_{HP}$ 8.4, N–CH_2–P), 4.07 (14H, m, C–O–CH_2–CH_3 and P–O–CH_2–CH_3); δ_C (101 MHz, $CDCl_3$, TMS) 13.5 (1C, s, C–O–CH_2–CH_3), 15.7 (6C, d, $^{3}J_{CP}$ 5.5, P–O–CH_2–CH_3), 31.6 (1C, s, CH_2–CO), 49.8, 49.9 (1+2C, d, $^{1}J_{CP}$ 154.3, N–CH_2–P), 50.2 (1C, s, N–CH_2–CH_2–CO), 51.9 (2C, s, ring N–CH_2), 52.5, 52.7, 52.8 (3×2C, d, $^{3}J_{CP}$ 6.3, ring P–CH_2–N–CH_2), 59.3 (1C, s, C–O–CH_2–CH_3), 60.8 (6C, d, $^{2}J_{CP}$ 6.6, P–O–CH_2–CH_3), 171.7 (1C, s, C=O); δ_P (162 MHz, $CDCl_3$, H_3PO_4) 26.99 (2P, s), 27.02 (1P, s).

A4. 3-[4,7,10-tris(phosphonomethyl)-1,4,7,10-tetraazacyclododecan-1-yl]propanoic acid, H_7do3p1pr. Compound **2** (1.34 g, ca. 1.7 mmol at 92% purity) was dissolved in aq. HCl (20%, 50 mL) and the solution was stirred at r.t. for 12 h and then heated to gentle reflux for an additional 36 h. The suspension was filtered, volatiles were evaporated and the product was co-evaporated with water (3×50 mL) to remove the excess of acid. The product was dissolved in a small amount of water, loaded in a weak cationic exchange column (Amberlite CG-50, 20×4.5 cm, H^+-form) and eluted with water (800 mL) in fractions of ca. 20 mL. The fractions containing only the desired compound were combined, treated with charcoal (0.3 g), filtered, and the solution was evaporated to obtain a hygroscopic transparent oil, which after drying under vacuum yielded 0.52 g (58%) of pure H_7do3p1pr in the zwitterionic form. MS: m/z 527.1 $(M+H)^+$. NMR: δ_H (400 MHz, DCl in D_2O, pD=1.2, tert-butyl alcohol) 2.39 (2H, t, CH_2–CO), 2.72 (4H, d, $^{2}J_{HP}$ 11.2, N–CH_2–P), 2.76, 2.93, 3.10, 3.39 (16H, m, ring N–CH_2), 3.46 (2H, d, $^{2}J_{HP}$ 11.7, N–CH_2–P), 3.62 (2H, t, N–CH_2–CH_2–CO); δ_C (101 MHz, DCl in D_2O, pD=1.2, tert-butyl alcohol) 36.6 (1C, s, CH_2–CO), 42.8, 49.6 (2×2C, s, ring N–CH_2), 49.9 (1C, d, $^{1}J_{CP}$ 137.9, N–CH_2–P), 50.3 (2C, d, $^{1}J_{CP}$ 132.4, N–CH_2–P), 51.1, 51.4 (2×2C, s, ring N–CH_2), 57.1 (2C, s, N–CH_2–CH_2–CO), 176.3 (1C, s, C=O); δ_P (162 MHz, DCl in D_2O, pD=1.2, H_3PO_4) 6.97 (1P, s), 21.64 (2P, s).

A5. (1,4,7,10-tetraazacyclododecane-1,4,7-triyl)tris(methylene)triphosphonic acid, H_6do3p. Compound **2** (1.89 g, ca. 2.4 mmol at 92% purity) was dissolved in aq. HBr (20%, 50 mL) and the solution was refluxed for 3 d. The suspension was filtered, volatiles were evaporated and the product was co-evaporated with water (3×50 mL) to remove the excess of acid. The product was dissolved in a small amount of water, loaded in a strong cationic exchange column (Dowex 50W×4, 20×2.5 cm, H^+-form), and eluted with water (300 mL) followed by 5% aq. ammonia solution (500 mL). The water fractions contained only inorganic impurities, while the combined ammonia fractions containing macrocyclic compounds were evaporated to dryness and co-

evaporated with water (3×50 mL) to remove the excess of ammonia. The resulting oil was dissolved in a minimal volume of water, loaded in a weak cationic exchange column (Amberlite CG-50, 20×4.5 cm, H^+-form) and eluted with water (600 mL) in fractions of ca. 20 mL. The fractions containing only the desired compound were combined and the solution was treated with charcoal (0.4 g), filtered, and concentrated in the evaporator. After cooling and overnight standing a white solid precipitated, which after filtration and drying under vacuum yielded 0.71 g (65%) of pure H_6do3p in the zwitterionic form. Calcd. for $C_{11}H_{29}N_4O_9P_3$: C, 29.08; H, 6.43; N, 12.33. Found: C, 29.10; H, 6.73; N, 12.30. MS: m/z 455.1 $(M+H)^+$. NMR: δ_H (400 MHz, KOD in D_2O, pD=11.6, tert-butyl alcohol) 2.73 (4H, d, $^2J_{HP}$ 9.9, N–CH_2–P), 2.90, 2.98, 3.04 (3×4H, t, ring N–CH_2), 3.08 (2H, d, $^2J_{HP}$ 10.8, N–CH_2–P), 3.24 (4H, t, ring N–CH_2); δ_C (101 MHz, KOD in D_2O, pD=11.6, tert-butyl alcohol) 44.4, 50.5, 51.0 (3×2C, s, ring N–CH_2), 51.1 (1C, d, $^1J_{CP}$ 125.4, N–CH_2–P), 52.2 (2C, s, ring N–CH_2), 53.2 (2C, d, $^1J_{CP}$ 136.1, N–CH_2–P); δ_P (162 MHz, KOD in D_2O, pD=11.6, H_3PO_4) 10.42 (1P, s), 15.68 (2P, s).

A6. 3-chloropropyl acetate, 3. A solution of acetyl chloride (1.43 mL, 20 mmol) in dichloromethane (10 mL) was added dropwise (30 min.) to a solution of 3-chloropropan-1-ol (1.67 mL, 20 mmol) and triethylamine (3.46 mL, 25 mmol) in dichloromethane (15 mL), while cooling the mild exotherm with an ice water bath (ca. 5 ºC). The reaction was then continued at r.t. for another 2 h. The resulting solution was added to water (25 mL), vigorously stirred for 10 min. and then extracted with dichloromethane. The organic phase was dried with anhydrous sodium sulfate, filtered and evaporated. The clear yellowish liquid obtained was then dried under limited reduced pressure (>50 mmHg) to remove the remaining volatile impurities, yielding 2.62 g (96%) of the title compound as a liquid. NMR data: δ_H (400 MHz, $CDCl_3$, TMS) 1.97 (3H, s, CO–CH_3), 2.02 (2H, m, CH_2–CH_2–CH_2), 3.55 (2H, t, Cl–CH_2–CH_2), 4.13 (2H, t, CH_2–CH_2–O); δ_C (101 MHz, $CDCl_3$, TMS) 20.6 (1C, s, CO–CH_3), 31.4 (1C, s, CH_2–CH_2–CH_2), 41.1 (1C, s, Cl–CH_2–CH_2), 60.9 (1C, s, CH_2–CH_2–O), 170.5 (1C, s, C=O).

A7. 3-(1,4,7,10-tetraazacyclododecan-1-yl)propyl acetate, 4. Cyclen (3.44 g, 20 mmol) was dissolved in chloroform (50 mL) and triethylamine (0.83 mL, 6 mmol) was added. 3-chloropropyl acetate (compound **3**, 0.96 g, 5 mmol) was then added and the solution was gently refluxed under nitrogen for 3 d. The reaction mixture was cooled and extracted with aq. NaOH (1 M, 3×20 mL) and water (3×20 mL). The organic phase was separated, evaporated to dryness, re-dissolved in chloroform (30 mL) and extracted again with aq. NaOH (1 M, 2×20 mL) and water (2×20 mL). The organic phase was then dried with anhydrous sodium sulfate, filtered, evaporated to dryness and dried under vacuum, yielding 0.71 g (52%) of pure mono-alkylated cyclen as yellowish oil. NMR data: δ_H (400 MHz, $CDCl_3$, TMS) 1.74 (2H, m, CH_2–CH_2–CH_2), 1.96 (3H, s, CO–CH_3), 2.40–2.75 (18H, m, ring and pendant N–CH_2), 4.07 (2H, t, CH_2–CH_2–O); δ_C (101 MHz, $CDCl_3$, TMS) 20.7 (1C, s, CO–CH_3), 26.2 (1C, s, CH_2–CH_2–CH_2), 44.9, 45.9, 46.8, 51.3 (4×2C, s, ring N–CH_2), 50.4 (1C, s, pendant N–CH_2), 62.2 (1C, s, CH_2–CH_2–O), 170.6 (1C, s, C=O).

A8. 3-{4,7,10-tris[(diethoxyphosphoryl)methyl]-1,4,7,10-tetraazacyclododecan-1-yl}-propyl acetate, 5. Compound **4** (0.66 g, 2.4 mmol) was dissolved in triethylphosphite (1.32 mL, 7.6 mmol). Paraformaldehyde was then added (0.24 g, 7.9 mmol) in small portions over 1 h. The solution was finally stirred at r.t. for an additional 3 d. The volatiles were evaporated, and the product was co-evaporated with toluene (3×50 mL) and dried under vacuum to yield 1.72 g of a clear oil. This product, containing also a minor amount of a diethyl hydroxymethylphosphonate by-product (ca. 7% based on ^{31}P NMR peak integration, overall yield of **5** is 92%), was used without further purification in the following hydrolysis step to remove both carboxylate and phosphonate ethyl esters. NMR: δ_H (400 MHz, $CDCl_3$, TMS) 1.26 (18H, t, P–O–CH_2–CH_3), 1.69 (2H, m, CH_2–CH_2–CH_2), 1.97 (3H, s, CO–CH_3), 2.38 (2H, pendant N–CH_2), 2.51, 2.78 (4+12H, t, ring N–CH_2), 2.86 (6H, d, $^2J_{HP}$ 8.4, N–CH_2–P), 3.97 (2H, t, CH_2–CH_2–O), 4.06 (12H, m, P–O–CH_2–CH_3); δ_C (101 MHz, $CDCl_3$, TMS) 15.5 (6C, s, P–O–CH_2–CH_3), 19.9 (1C, s, CO–CH_3), 25.5 (1C, s, CH_2–CH_2–CH_2), 49.8, 49.9 (2+1C, d, $^1J_{CP}$ 154.4, N–CH_2–P), 51.2 (1C, s, pendant N–CH_2), 51.6, 52.1, 52.3, 52.4 (4×2C, s, ring N–CH_2), 60.3 (6C, d, $^2J_{CP}$ 5.7, P–O–CH_2–CH_3), 61.9 (1C, s, CH_2–CH_2–O), 169.9 (1C, s, C=O); δ_P (162 MHz, $CDCl_3$, H_3PO_4) 25.70 (1P, s), 25.76 (2P, s).

A9. [10-(3-hydroxypropyl)-1,4,7,10-tetraazacyclododecane-1,4,7-triyl]tris(methyle-ne)triphosphonic acid, H_6do3p1ol. Compound **5** (1.63 g, ca. 2.1 mmol at 93% purity) was dissolved in aq. HCl (20%, 50 mL) and the solution was refluxed for 2 d. The volatiles were evaporated and the product was co-evaporated with water (3×50 mL) to remove the excess of acid. The product was then dissolved in diluted aq. NaOH (0.2 M, 50 mL) and this solution was refluxed for another 12 h. The suspension was filtered, volatiles were evaporated and the oil obtained was then purified by ion exchange chromatography as described for H_6do3p. The fractions from the weak cationic exchange column containing only the desired compound were combined, treated with charcoal (0.5 g), filtered, evaporated and dried under vacuum to yield 0.76 g (71%) of an off-white solid of pure H_6do3p1ol in the zwitterionic form. Calcd. for $C_{14}H_{35}N_4O_{10}P_3$: C, 32.82; H, 6.89; N, 10.93. Found: C, 32.50; H, 6.88; N, 10.98. MS: m/z 513.1 $(M+H)^+$. NMR: δ_H (400 MHz, DCl in D_2O, pD=1.8, tert-butyl alcohol) 1.79 (2H, m, CH_2–CH_2–O), 2.65 (4H, d, $^2J_{HP}$ 11.1, N–CH_2–P), 2.79 (2H, t, pendant N–CH_2), 2.89, 3.16, 3.22 (6+4+2H, t, ring N–CH_2), 3.35 (2H, t, CH_2–CH_2–O), 3.39 (2H, d, $^2J_{HP}$ 12.3, N–CH_2–P), 3.45 (4H, t, ring N–CH_2); δ_C (101 MHz, DCl in D_2O, pD=1.8, tert-butyl alcohol) 24.4 (1C, s, CH_2–CH_2–O), 49.6 (1C, s, pendant N–CH_2), 50.2

(1C, d, $^1J_{CP}$ 132.4, N–CH_2–P), 50.6 (2C, d, $^1J_{CP}$ 136.1, N–CH_2–P), 49.7, 49.9, 51.1, 51.3 (6C, s, ring N–CH_2), 51.8 (1C, s, CH_2–CH_2–O), 58.3 (2C, s, ring N–CH_2); δ_P (162 MHz, DCl in D_2O, pD=1.8, H_3PO_4) 6.68 (1P, s), 20.35 (2P, s).

B. X-ray crystallography. Single crystals of H_6do3p·3.8H_2O were obtained in the form of small colorless prisms on standing of a concentrated aqueous solution of the free ligand over a few days. Single crystals of [Cu(H_2O)(H_4dotp)][Cu(H_2O)$_6$] were obtained at random as small blue prisms, on standing over several months of a concentrated acidic solution (pH 2–3) containing excess of $Cu(ClO_4)_2$ and a mixture of H_7do3p and H_8dotp coming from preliminary synthetic work. Selected crystals were mounted on a glass fiber in random orientation and cooled to 150(1) K. The diffraction data were collected employing a Nonius Kappa CCD diffractometer (Enraf-Nonius) using Mo-K_α (λ = 0.71073 Å) at 150(1) K (Cryostream Cooler Oxford Cryosystem) and analyzed using the HKL DENZO program package[71,72] for H_6do3p·3.8H_2O, and Bruker APEX/SAINT software[73] for [Cu(H_2O)(H_4dotp)][Cu(H_2O)$_6$]. The structures were solved by direct methods and refined by full-matrix least-squares techniques (SIR92,[74] SHELXS97[75] and SHELXL97[75]). The used scattering factors for neutral atoms were included in the SHELXL97 program. In the case of [Cu(H_2O)(H_4dotp)][Cu(H_2O)$_6$], a semi-empirical absorption correction was carried out using SADABS.[76] Selected experimental data are listed in Table 8.

Table 8. Experimental crystallographic data for the reported crystal structures.

Compound	H_6do3p·3.8H_2O	[Cu(H_2O)(H_4dotp)][Cu(H_2O)$_6$]
Formula	$C_{11}H_{36.6}N_4O_{12.8}P_3$	$C_{12}H_{42}Cu_2N_4O_{19}P_4$
M_r	522.75	797.46
Color	colorless	blue
Habit	prism	prism
Crystal size (mm)	0.15×0.18×0.25	0.13×0.25×0.36
Crystal system	orthorhombic	orthorhombic
Space group	*Pna*2$_1$ (no. 33)	*Pcca* (no. 54)
a (Å)	16.6902(2)	15.7326(11)
b (Å)	8.0162(5)	11.2581(7)
c (Å)	16.7793(4)	15.6342(11)
U (Å^3)	2244.94(15)	2769.1(3)
Z	4	4
D_{calc} (g cm^{-3})	1.547	1.913
μ (mm^{-1})	0.334	1.858
F(000)	1112	1648
GOF on F^2	1.046	1.258
Total refl.	4185	3033
Obsd. refl. [I>2σ(I)]	3818	2471
Parameters	281	187
R; *R*'[I>2σ(I)]	0.0396; 0.0329	0.0712; 0.0563
wR; *wR*'[I>2σ(I)]	0.0814; 0.0776	0.1328; 0.1281
Largest diff. peak/hole (e·Å^{-3})	0.221/–0.287	1.069/–0.684
CCDC reference number	CCDC XXXXXX	CCDC XXXXXX

In the crystal structure of H_6do3p·3.8H_2O, all non-hydrogen atoms were refined anisotropically. The independent unit contains a ligand molecule and several water solvate molecules. Two molecules were refined with full occupancy, and one of the remaining water molecules was best refined disordered in two positions with relative 55:45 occupancy. However, some other weak maxima of residual electronic density close to each other pointed to another disordered water molecule. This disorder cannot be reliably fitted as there were several maxima with a low intensity, so, this electronic density was squeezed off using PLATON.[77] By the electronic count, the squeezed density corresponds to approx. 0.8 water molecule. All hydrogen atoms were found in the electronic difference map, except those belonging to disordered water molecule; however, they were located in theoretical positions (C–H) or were kept in their original positions (O–H, N–H) to keep low number of refined parameters.

In the crystal structure of [Cu(H_2O)(H_4dotp)][Cu(H_2O)$_6$], all non-hydrogen atoms were refined anisotropically. All hydrogen atoms were found in the electronic difference map, and were placed in theoretical positions (C–H) or were kept in their original positions (O–H). The highest difference maxima (1.07 and 0.75 e·Å^{-3}) lay very close to copper cations (~1.1 Å), thus they cannot be any real atoms and are attributed to artifacts.

C. Potentiometric measurements. Purified water was obtained from a Millipore Milli-Q demineralization system. Stock solutions of H_6do3p, H_7do3p1pr and H_6do3p1ol were prepared at *ca.* 2×10^{-3} M. The [N(CH_3)$_4$]NO_3 was prepared by neutralisation of a commercial [N(CH_3)$_4$]OH solution with HNO_3. Metal ion solutions were prepared in water at 0.025–0.050 M from analytical grade nitrate salts of the metals (kept in excess of HNO_3 in the case of lanthanides), and standardized by titration with Na_2H_2edta.[78] Carbonate-free solutions of the titrant [N(CH_3)$_4$]OH were obtained at ca. 0.10 M by treating freshly prepared silver oxide with a solution of N(CH_3)$_4$I under nitrogen. These solutions were standardized by application of Gran's method[79] and were discarded as soon as the concentration of carbonate reached *ca.* 1% of the total amount of base. For backtitrations a 0.100 M standard solution of HNO_3 was prepared from a commercial ampoule.

The potentiometric setup used for conventional titrations has been described before.[38] Measurements were carried out at 298.2 ± 0.1 K in solutions with ionic strength kept at 0.10 ± 0.01 M with [N(CH_3)$_4$]NO_3, and atmospheric CO_2 was excluded from the cell during titrations by passing purified N_2 across the top of the experimental solutions. The [H^+] of the solutions was determined by measurement of the electromotive force of the cell, $E = E^{o\prime} + Q \log[H^+] + E_j$. The term pH is defined as $-\log [H^+]$. $E^{o\prime}$ and Q were determined by titrating a solution of known hydrogen-ion concentration at the same ionic strength in the acid pH region. The liquid-junction potential, E_j, was found to be negligible under the experimental conditions used. The value of $K_w = [H^+][OH^-]$ was found to be equal to 10$^{-13.80}$ by titrating a solution of known hydrogen-ion concentration at the same ionic strength in the alkaline pH region, considering $E^{o\prime}$ and Q valid for the entire pH range. Measurements during conventional titrations were carried out with ca. 0.05 mmol of ligand in a total volume of *ca.* 30 mL, in the absence of metal ions and in the presence of each metal ion at *ca.* 0.9 equiv. (or 0.5 equiv. for the Ln^{3+}) relative to the ligand. For all metal ions except Ca^{2+}, a backtitration was performed at the end of each direct titration in order to check if equilibrium was attained throughout the full pH range. Each titration curve consisted typically of 70–90 points in the 2.5–11.5 pH region and a minimum of two replicate titrations were performed for each system.

D. Kinetic measurements. The dissociation kinetics of Cu^{2+} complexes ($c_{CuL} \approx 1.0\times10^{-4}$ M) was studied under the pseudo-first order experimental conditions ($[H^+]_{tot} >> c_{CuL}$) and the ionic strength 3.00 M (Na,H)Cl. The temperature was changed in the 288–328 K range in order to estimate the activation parameters. Analogously, the dissociation kinetics of Ce^{3+} and Eu^{3+} complexes were studied at ionic strength 3.00 M (Na,H)ClO_4. The Cu^{2+} complexes were prepared by mixing $CuCl_2$ and ligand solutions in 1:1.2 molar ratio followed by stepwise neutralisation of the stock solution of complex formed at pH 7.5–9.0. The same procedure was followed for the preparation of solutions of Ce^{3+} and Eu^{3+} complexes.

The absorbance kinetic measurements were carried out on double-beam UV4 (PYE UNICAM, UK) and diode-array HP8453A (Agilent, USA) spectrophotometers. The luminescence spectra were measured on AMINCO-BOWMAN 2 (Thermo Electronic, USA).

E. NMR measurements. For determination of the two highest protonation constants of H_6do3p, H_7do3p1pr and H_6do3p1ol, ^{31}P NMR spectra of aqueous solution of the ligands were recorded, *ca.* 20 points per titration over the pH 9–14 range at 298.2 K. A ligand solution was prepared at 0.010 M and the titrant was a fresh 25% (wt.) aqueous solution of [N(CH_3)$_4$]OH (Aldrich) and was standardized by titration with a 1.0 M HNO_3 solution. The titration was carried out in a closed titration cell and the titrant was added with a Crison microBU 2031 automatic burette. The pH was measured with an Orion 420A measuring instrument fitted with a Metrohm 6.0210.100 combined electrode after calibration of the electrode with commercial buffer solutions of standard pH (at 298.2 K) of 7.96 and 11.88. Atmospheric CO_2 was excluded from the cell during the titration by passing purified nitrogen across the top of the experimental solution. The measurements were carried out with 0.03 mmol of ligand in a total volume of *ca.* 5 mL and the

ionic strength of the titration solution was kept at 0.50 M with $[N(CH_3)_4]NO_3$. Following each addition of titrant, the pH was measured after equilibration and a sample of solution was placed in a 5 mm NMR tube adapted with an internal capillary tube containing D_2O and H_3PO_4 for locking and referencing purposes. After recording each ^{31}P NMR spectrum, the sample volume was returned to the titration cell.

The Ln^{3+} complexes of the ligands were prepared by mixing aqueous solutions of anhydrous chloride salts of the concerned metal ion and ligands in a 1:1.1 molar ratio, followed by mild heating and slow addition of a diluted KOH solution until pH 8.0–9.0 was reached (which corresponds to a maximum abundance of the ML complex species in all cases). The solutions were then evaporated to dryness and redissolved in D_2O at *ca.* 1×10^{-2} M, with the final pD of the samples adjusted at *ca.* 9 by addition of diluted DCl or KOD solutions. Ligand samples used for comparison purpose were prepared in D_2O at *ca.* 1×10^{-2} M with the pD similarly adjusted at *ca.* 8.5.

The ^1H and ^{31}P NMR spectra of the Ln^{3+} complexes were performed at 298, 333 and 353 K on a Varian Unity 500 spectrometer operating at 499.83 (^1H) and 202.33 MHz (^{31}P). The ^{31}P NMR spectra were also acquired on a Bruker Avance III 400 MHz operating at 161.99 MHz. The 2D ^1H gradient correlated (gCOSY) and DQF-COSY spectra were obtained on a Varian VNMRS 600 MHz NMR spectrometer operating at 599.72 MHz using a 5-mm pulse field gradient (PFG) triple resonance probe. D_2O was used as internal reference for ^1H spectra in D_2O, while 85% H_3PO_4 in water with some drops of D_2O was used as external reference (inner-capillary method) for ^{31}P.

F. ^{17}O NMR and ^1H NMRD Experiments. F1. Sample Preparation. The $[Gd(do3p1ol)]^{3-}$ complex for ^{17}O NMR and ^1H NMRD was prepared by mixing $GdCl_3$ and ligand solutions as described above. After treatment with Chelex 100, the absence of free Gd^{3+} was checked by testing with xylenol orange.[80] The ^{17}O-enriched water (^{17}O content: 11.4%) was added to the solution for the ^{17}O NMR measurements to improve the sensitivity. The final solution concentration for ^{17}O NMR was 26.86 mM at pH = 7.45, as measured by a bulk magnetic susceptibility measurement,[81] and 4.56 mM at pH 6.5 for the ^1H NMRD experiments at 298 K.

F2. ^{17}O NMR experiments. Variable-temperature ^{17}O NMR measurements were performed on a Bruker Avance-500 (11.7 T, 500 MHz) spectrometer and BVT-3000 temperature control unit was used to stabilize the temperature. The samples were sealed in glass spheres that fitted into 10 mm o.d. NMR tubes, to eliminate susceptibility corrections to the chemical shifts.[82] Longitudinal relaxation rates $1/T_{1r}$ were measured by the inversion-recovery pulse sequence and transverse relaxation rates $1/T_{2r}$ by the Carr-Purcell-Meiboom-Gill spin-echo technique. Acidified water of pH 3.4 was used as an external reference.

F3. ^1H NMRD Measurements. The measurements were performed at 298 K by using a Stelar Spinmaster FFC NMR relaxometer (0.01–20 MHz) equipped with a VTC90 temperature control unit. At higher fields, the ^1H relaxivity measurements were performed on a Bruker Electromagnet at the frequencies of 20 MHz, 40 MHz, 60 MHz and 80 MHz. In each case, the temperature was measured by a substitution technique.

G. Calculation of thermodynamic equilibrium constants. Spectroscopic data from the ^{31}P NMR titrations in water were used to calculate the two highest protonation constants of H_6do3p, $H_7do3p1pr$ and $H_6do3p1ol$ at ionic strength 0.50 M by refinement with the HYPNMR program.[83] The values herein obtained were then extrapolated to ionic strength 0.10 M using the Davies equation[43] and these adjusted values were finally used in the determination of the remaining protonation constants of the ligand. The calculation of overall equilibrium constants β_i^H and $\beta_{M_mH_hL_l}$ (being $\beta_{M_mH_hL_l} = [M_mH_hL_l]/[M]^m[H]^h[L]^l$ and $\beta_{MH_{-1}L} = \beta_{ML(OH)}\times K_w$) was done by refinement of the potentiometric data from with the HYPERQUAD program.[84] Species distribution diagrams were plotted from the calculated constants with the HYSS program.[85] Differences, in log units, between the values of protonated (or hydrolysed) and non-protonated constants provide the stepwise (log *K*) reaction constants (being $K_{M_mH_hL_l} = [M_mH_hL_l]/[M_mH_{h-1}L_l][H]$). The errors quoted are the standard deviations of the overall stability constants calculated by the fitting program from all the experimental data for each system.

Acknowledgement. The authors acknowledge Fundação para a Ciência e a Tecnologia (FCT), with co-participation of the European Community funds FEDER, POCI, QREN and COMPETE for the financial support under project PTDC/QUI/67175/2006. C. F. G. C. Geraldes thanks the Gabinete de Relações Internacionais da Ciência e Ensino Superior (GRICES) of Portugal (PESSOA project) for support. The NMR spectrometers used are part of the National NMR Network and were purchased in the framework of the National Program for Scientific Re-equipment, contract REDE/1517/RMN/2005, with funds from POCI 2010 (FEDER) and FCT. The Analytical Services Unit of ITQB-UNL/IBET and M. C. Almeida are acknowledged for providing data for elemental analysis and ESI-MS. L. M. P. Lima thanks FCT for the Ph.D. fellowship (SFRH/BD/18522/2004) and H. F. Carvalho thanks the EU COST D38 Action for a travel grant. P. Lubal thanks the Ministry of Education, Youth and Sports of the Czech Republic (project ME09065), GRICES for a travel grant, and EU (COST D38, CEITEC CZ.1.05/1.1.0/02.0068). P. Hermann and J. Kotek

thank the Grant Agency of the Czech Republic (203/09/1056, 207/11/1437), the Ministry of Education, Youth and Sports of the Czech Republic (MSM0021620857), and EU (COST D38, BM 607 and CM802).

Supporting Information Available: Overall protonation and stability constants, ^{31}P NMR titration curve and tentative protonation sequence for H_6do3p, representative speciation diagrams in solution, UV-Vis spectra of the Cu^{2+} complexes, rate constants for the acid-assisted dissociation of Cu^{2+} and Ce^{3+} complexes, time course of acid-assisted dissociation of the Cu^{2+} complexes, hydration numbers for the Eu^{3+} complexes, emission and 3D luminescence spectra of the Eu^{3+} complexes, NMR spectra and data for the ligands and its Ln^{3+} complexes, ^{17}O NMR data for the Gd^{3+} complex of H_6do3p1ol. This material is available free of charge via the Internet at http://pubs.acs.org.

References

(1) Meyer, M.; Dahaoui-Gindrey, V.; Lecomte C.; Guilard, R. *Coord. Chem. Rev.* 1998, *178–180*, 1313–1405.

(2) Wainwright, K. P. *Coord. Chem. Rev.* **1997**, *166*, 35–90.

(3) *The Chemistry of Contrast Agents in Medical Magnetic Resonance Imaging*; Merbach, A. E., Tóth, É., Eds.; John Wiley & Sons: Chichester, 2001.

(4) Bianchi, A.; Calabi, L.; Corana, F.; Fontana, S.; Losi, P.; Maiocchi, A.; Paleari, L.; Valtancoli, B. *Coord. Chem. Rev.* **2000**, *204*, 309–393.

(5) Burai, L.; Király, R.; Lázár, I.; Brücher, E. *Eur. J. Inorg Chem.* **2001**, 813–820.

(6) Sherry, A. D.; Ren, J.; Huskens, J.; Brücher, E.; Tóth, É.; Geraldes, C. F. C. G.; Castro, M. M. C. A.; Cacheris, W. P. *Inorg. Chem.* **1996**, *35*, 4604–4612.

(7) Anderegg, G.; Arnaud-Neu, F.; Delgado, R.; Felcman, J.; Popov, K. *Pure Appl. Chem.* **2005**, *77*, 1445–1495.

(8) Lukeš, I.; Kotek, J.; Vojtíšek, P.; Hermann, P. *Coord. Chem. Rev.* **2001**, *216–217*, 287–312.

(9) Lubal, P.; Kývala, M.; Hermann, P.; Holubová, J.; Rohovec, J.; Havel, J.; Lukeš, I. *Polyhedron* **2001**, *20*, 47–55.

(10) Kubíček, V.; Tóth, É. *Adv. Inorg. Chem.* **2009**, *61*, 63–129.

(11) Hermann, P.; Kotek, J.; Kubíček, V.; Lukeš, I. *Dalton Trans.* **2008**, 3027–3047.

(12) Woods, M.; Woessner, D. E.; Sherry, A. D. *Chem. Soc. Rev.* **2006**, *35*, 500–511.

(13) Liu, S. *Adv. Drug Del. Rev.* **2008**, *60*, 1347–1370.

(14) Woods, M.; Kovacs, Z.; Sherry, A. D. *J. Supramol. Chem.* **2002**, *2*, 1–15.

(15) Liu, S.; Edwards, D. S. *Bioconjugate Chem.* **2001**, *12*, 7–34.

(16) Liu, S. *Chem. Soc. Rev.* **2004**, *33*, 445–461.

(17) Táborský, P.; Svobodová, I.; Lubal, P.; Hnatejko, Z.; Lis, S.; Hermann, P. *Polyhedron* **2007**, *26*, 4119–4130.

(18) Rudovský, J.; Cígler, P.; Kotek, J.; Hermann, P.; Vojtíšek, P.; Lukeš, I.; Peters, J. A.; Vander Elst, L.; Muller, R. N. *Chem. Eur. J.* **2005**, *11*, 2373–2384.

(19) Táborský, P.; Lubal, P.; Havel, J.; Kotek, J.; Hermann, P.; Lukeš, I. *Collect. Czech. Chem. Commun.* **2005**, *70*, 1909–1942.

(20) Vojtíšek, P.; Cígler, P.; Kotek, J.; Rudovský, J.; Hermann, P.; Lukeš, I. *Inorg. Chem.* **2005**, *44*, 5591–5599.

(21) Campello, M. P. C.; Lacerda, S.; Santos, I. C.; Pereira, G. A.; Geraldes, C. F. G. C.; Kotek, J.; Hermann, P.; Vaněk, J.; Lubal, P.; Kubíček, V.; Tóth, É.; Santos, I. *Chem. Eur. J.* **2010**, *16*, 8446–8465.

(22) Kálmán, F. K.; Baranyai, Z.; Tóth, I.; Bányai, I.; Kíraly, R.; Brücher, E.; Aime, S.; Sun, X.; Sherry, A. D.; Kovács, Z. *Inorg. Chem.* **2008**, *47*, 3851–3862.

(23) Campello, M. P.; Marques, F.; Gano, L.; Lacerda, S.; Santos, I. *Radiochim. Acta* **2007**, *95*, 329–334.

(24) Campello, M. P.; Balbina, M.; Santos, I.; Lubal, P.; Ševčík, R.; Ševčíková, R. *Helv. Chim. Acta* **2009**, *92*, 2398–2413.

(25) Gano, L.; Marques, F.; Campello, M. P.; Balbina, M.; Lacerda, S.; Santos, I. *Q. J. Nucl. Med. Mol. Imaging* **2007**, *51*, 6–15.

(26) Sun, X.; Wuest, M.; Kovacs, Z.; Sherry, A. D.; Motekaitis, R.; Wang, Z.; Martell, A. E.; Welch, M. J.; Anderson, C. J. *J. Biol. Inorg. Chem.* **2003**, *8*, 217–225.

(27) Kreher, U.; Hearn, M. T. W.; Spiccia, L. *Aust. J. Chem.* **2009**, *62*, 1583–1592.

(28) Balogh, E.; Tripier, R.; Fousková, P.; Reviriego, F.; Handel, H.; Tóth, É. *Dalton Trans.* **2007**, 3572–3581.

(29) Keire, D. A.; Jang, Y. H.; Li, L.; Dasgupta, S.; Goddard III, W. A.; Shively, J. E. *Inorg. Chem.* **2001**, *40*, 4310–4318.

(30) Massue, J.; Plush, S. E.; Bonnet, C. S.; Moore, D. A.; Gunnlaugsson, T. *Tetrahedron Lett.* **2007**, *48*, 8052–8055.

(31) Barefield, E. K.; Foster, K. A.; Freeman, G. M.; Hodges, K. D. *Inorg. Chem.* **1986**, *25*, 4663–4668.

(32) Dale, J. *Acta Chem. Scand.* **1973**, *27*, 1115–1158.

(33) Lázár, I; Hrncir, D. C.; Kim, W.-D.; Kiefer, G.; Sherry, A. D. *Inorg. Chem.* **1992**, *31*, 4422–4424.

(34) Kong, D.; Medvedev, D. G.; Clearfield, A. *Inorg. Chem.* **2004**, *43*, 7308–7314.

(35) Chaves, S.; Delgado, R.; Fraústo da Silva, J. J. R. *Talanta* **1992**, *39*, 249–254.

(36) Marques, F.; Gano, L.; Campello, M. P.; Lacerda, S.; Santos, I.; Lima, L. M. P.; Costa, J.; Antunes, P.; Delgado, R. *J. Inorg. Biochem.* **2006**, *100*, 270–280.

(37) Kotek, J.; Vojtíšek, P.; Císařová, I.; Hermann, P.; Jurečka, P.; Rohovec, J.; Lukeš, I. *Collect. Czech. Chem. Commun.* **2000**, *65*, 1289–1316.

(38) Lima, L. M. P.; Delgado, R.; Drew, M. G. B.; Brandão, P.; Félix, V. *Dalton Trans.* **2008**, 6593–6608.

(39) Delgado, R.; Félix, V.; Lima L. M. P.; Price, D. W. *Dalton Trans.* **2007**, 2734–2745.

(40) Burai, L.; Ren, J.; Kovács, Z.; Brücher, E.; Sherry, A. D. *Inorg. Chem.*, **1998**, *37*, 69–75.

(41) Delgado, R.; Siegfried, L. C.; Kaden, T. A. *Helv. Chim. Acta* **1990**, *73*, 140–148.

(42) Lima, L. M. P.; Delgado, R.; Plutnar, J.; Hermann, P.; Kotek, J. *Eur. J. Inorg. Chem.* **2011**, 527–538.

(43) *Pettit, L. D.;* Sukhno, I.; Buzko, V. *Aq. Solutions programs suite*, Academic Software, IUPAC, 2004.

(44) Försterová, M.; Svobodová, I.; Lubal, P.; Táborský, P.; Kotek, J.; Hermann, P.; Lukeš, I. *Dalton Trans.* **2007**, 535–549.

(45) Guerra, K. P.; Delgado, R.; Lima, L. M. P.; Drew, M. G. B.; V. Félix, *Dalton Trans.* **2004**, 1812–1822.

(46) Geraldes, C. F. G. C.; Sherry, A. D.; Cacheris, W. P. *Inorg. Chem.* **1989**, *28*, 3336–3341.

(47) Delgado, R.; Fraústo da Silva, J. J. R. *Talanta* **1982**, *29*, 815–822.

(48) Kabachnik, I. M.; Medved, T. Y.; Belskii, F. I.; Pisareva, S. A. *Izv. Akad. Nauk. (USSR) Ser. Khim.* **1984**, *4*, 844–849.

(49) Cacheris, W. P.; Nickle, S. K.; Sherry, A. D. *Inorg. Chem.* **1987**, *26*, 958–960.

(50) Moreau, J. ; Guillon, E.; Pierrard, J.-C. ; Rimbault, J. ; Port, M. ; Aplincourt, M. *Chem. Eur. J.* **2004**, *10*, 5218–5232.

(51) Kotek, J.; Lubal, P. ; Hermann, P.; Císařová, I.; Lukeš, I.; Godula, T.; Svobodová, I.; Táborský, P.; Havel, J. *Chem. Eur. J.* **2003**, *9*,233–248.

(52) Svobodová, I.; Piskula, Z.; Lubal, P.; Lis, S.; Hermann, P. *J. Alloy Comp.* **2008**, *451*, 42–45.

(53) Táborský, P.; Svobodová, I.; Hnatejko, Z.; Lubal, P.; Lis, S.; Försterová, M.; Hermann, P.; Lukeš, I.; Havel, J. *J. Fluorescence* **2005**, *15*, 507–512.

(54) Mamedov, I.; Táborský, P.; Lubal, P.; Laurent, S.; Vander Elst, L.; Mayer, H. A.; Logothetis, N. K.; Angelovski, G. *Eur. J. Inorg. Chem.* **2009**, 3298–3306.

(55) Yang, T.-H.; Zhou, K.; Bao, S.-S.; Zhu, C.-J.; Zheng, L.-M. *Inorg. Chem. Comm.* **2008**, *11*, 1075-1078.

(56) Purgel, M.; Baranyai, Z.; de Blas, A.; Rodríguez-Blas, T.; Bányiai, I.; Platas-Iglesias, C.; Tóth, I. *Inorg. Chem.* **2009**, *49*, 4370–4382.

(57) Geraldes, C. F. G. C.; Sherry, A. D.; Kiefer, G. E. *J. Magn. Reson.* **1992**, *97*, 290–304.

(58) Aime, S.; Botta, M.; Fasano, M.; Marques, M. P. M.; Geraldes, C. F. G. C.; Pubanz, D.; Merbach, A. E. *Inorg. Chem.* **1997**, *36*, 2059–2068.

(59) Lebdušková, P.; Hermann, P.; Helm, L.; Tóth, É.; Kotek, J.; Binnemans, K.; Rudovský, J.; Lukeš, I.; Merbach, A.E. *Dalton Trans*. **2007**, 493–501.

(60) Vitha, T.; Kubíček, V.; Kotek, J.; Hermann, P.; Vander Elst, L.; Muller, R. N.; Lukeš, I.; Peters, J. A. *Dalton Trans*. **2009**, 3204–3214.

(61) Ruloff, R.; Tóth, É.; Scopelliti, R.; Tripier, R.; Handel, H.; Merbach, A. E. *Chem. Commun.* **2002**, 2630–2631.

(62) Burai, L.; Tóth, É.; Merbach, A. E. *Chem. Commun.* **2003**, 2680–2681.

(63) Laus, S.; Ruloff, R.; Tóth, É.; Merbach, A. E. *Chem. Eur. J.* **2003**, *9*, 3555–3566.

(64) Torres, S.; Martins, J. A.; André, J. P.; Pereira, G. A.; Kiraly, R.; Brücher, E.; Helm, L.; Tóth, É.; Geraldes, C. F. G. C. *Eur. J. Inorg. Chem*. **2007**, 5489–5499.

(65) Silvério, S.; Torres, S.; Martins, A. F.; Martins, J. A.; André, J. P.; Helm, L.; Prata, M. I. M.; Santos, A. C.; Geraldes, C. F. G. C. *Dalton Trans*. **2009**, 4656–4670.

(66) Ferreira, M. F.; Martins, A. F.; Martins, J. A.; Ferreira, P. M.; Tóth, É.; Geraldes, C. F. G. C. *Chem. Commun*. **2009**, 6475–6477.

(67) Botta, M. *Eur. J. Inorg. Chem*. **2000**, 399–407.

(68) Geraldes, C. F. G. C.; Brown III, R. D.; Cacheris, W. P.; Koening, S. H.; Sherry, A. D.; Spiller, M. *Magn. Reson. Med.* **1989**, *9*, 94–104.

(69) Kotková, Z.; Pereira, G. A.; Djanashvili, K.; Kotek, J.; Rudovský, J.; Hermann, P.; Vander Elst, L.; Muller, R. N.; Geraldes, C. F. G. C.; Lukeš, I.; Peters, J. A. *Eur. J. Inorg. Chem*. **2009**, 119–136.

(70) Perrin, D. D., Armarego, W. L. F. *Purification of Laboratory Chemicals*; Pergamon: Oxford, 3rd ed., 1988.

(71) Otwinovski, Z; Minor, W. *HKL Denzo and Scalepack Program Package*; Nonius BV: Delft, The Netherlands, 1997.

(72) Otwinovski, Z.; Minor, W. *Methods Enzymol.* **1997**, *276*, 307–326.

(73) *APEX* and *SAINT*, Bruker AXS Inc., Madison, WI, U.S.A., 2004.

(74) Altomare, A.; Burla, M. C.; Camalli, M.; Cascarano, G.; Giacovazzo, C.; Guagliardi, A.; Polidori, G. *J. Appl. Crystallogr.* **1994**, *27*, 435–435.

(75) Sheldrick, G. M. *SHELXS97 and SHELSL97, A Computer Programs for Solution and Refining of Crystal Structures*; University of Göttingen, Göttingen, Germany, 1997.

(76) Sheldrick, G. M. *SADABS*, Bruker AXS Inc., Madison, WI, U.S.A., 2004.

(77) Spek, A. L. *PLATON – A Multipurpose Crystallographic Tool*. Utrecht University, Utrecht, The Netherlands, 2005.

(78) Schwarzenbach, G., Flaschka, W. *Complexometric Titrations*; Methuen & Co: London, 1969.

(79) Rossotti, F. J.; Rossotti, H. J. *J. Chem. Educ.* **1965**, *42*, 375–378.

(80) Brunisholz, G.; Randin, M. *Helv. Chim. Acta* **1959**, *42*, 1927–1938.

(81) Corsi, D. M.; Platas-Iglesias, C.; van Bekkum, H.; Peters, J. A. *Magn. Reson. Chem.* **2001**, *39*, 723–726.

(82) Hugi, A. D.; Helm, L.; Merbach, A. E. *Helv. Chim. Acta* **1985**, *68*, 508–521.

(83) Frassineti, C.; Ghelli, S.; Gans, P.; Sabatini, A.; Moruzzi, M. S.; Vacca, A. *Anal. Biochem.* **1995**, *231*, 374–382.

(84) Gans, P.; Sabatini, A.; Vacca, A. *Talanta* **1996**, *43*, 1739–1753.

(85) Alderighi, L.; Gans, P.; Ienco, A.; Peters, D.; Sabatini, A.; Vacca, A. *Coord. Chem. Rev.* **1999**, *184*, 311–318.

REFERENCES

1. Jacques V, Desreux JF. New Classes of MRI Contrast Agents. *Topics in Current Chemistry*. 2002;221(Contrast Agents I):123-164.

2. Anon. BRAIN: CT, MRI - a knol by Christopher Hess. Available at: http://knol.google.com/k/brain-ct-mri#. [Accessed August 7, 2011].

3. Gil VMS, Geraldes CFGC. *Ressonância Magnética Nuclear - Fundamentos, Métodos e Aplicações*. Coimbra: Fundação Calouste Gulbenkian; 2002:1012.

4. Anon. The Basics of MRI. Available at: http://www.cis.rit.edu/htbooks/mri/.

5. Norris DG. Principles of magnetic resonance assessment of brain function. *Journal of magnetic resonance imaging : JMRI*. 2006;23(6):794-807.

6. Ogawa S, Lee T-M, Nayak AS, Glynn P. Oxygenation-sensitive contrast in magnetic resonance image of rodent brain at high magnetic fields. *Magnetic Resonance in Medicine*. 1990;14(1):68-78.

7. Wise RG, Tracey I. The role of fMRI in drug discovery. *Journal of magnetic resonance imaging : JMRI*. 2006;23(6):862-76.

8. Anon. No Title. Available at: http://www.fmrib.ox.ac.uk/education/fmri/.

9. Anon. Brain Imaging and Spectroscopy: Projects. Available at: http://www.mr.ethz.ch/brain/brain_proj.html [Accessed August 17, 2011].

10. Kurhanewicz J, Swanson MG, Nelson SJ, Vigneron DB. Combined magnetic resonance imaging and spectroscopic imaging approach to molecular imaging of prostate cancer. *Journal of magnetic resonance imaging : JMRI*. 2002;16(4):451-63.

11. Basser PJ, Pajevic S, Pierpaoli C, Duda J, Aldroubi A. In Vivo Fiber Tractography Using DT-MRI Data. 2000;632:625- 632.

12. Golman K, Zandt R in ’t, Thaning M. Real-time metabolic imaging. *Proceedings of the National Academy of Sciences of the United States of America*. 2006;103(30):11270-5.

13. Anon. NIBIB - Super-Cool Imaging Technique Identifies Agressive Tumors: December 22, 2009. Available at: http://www.nibib.nih.gov/HealthEdu/eAdvances/22Dec09.

14. Cacheris WP, Quay SC, Rocklage SM. The relationship between thermodynamics and the toxicity of gadolinium complexes. *Magnetic Resonance Imaging*. 1990;8(4):467-481.

15. Sherry a D, Caravan P, Lenkinski RE. Primer on gadolinium chemistry. *Journal of magnetic resonance imaging : JMRI*. 2009;30(6):1240-8.

16. Hermann P, Kotek J, Kubícek V, Lukes I. Gadolinium(III) complexes as MRI contrast agents: ligand design and properties of the complexes. *Dalton transactions (Cambridge, England : 2003)*. 2008;9226(23):3027-47.

17. Aime S, Calabi L, Cavallotti C, et al. [Gd-AAZTA]-: a new structural entry for an improved generation of MRI contrast agents. *Inorganic chemistry*. 2004;43(24):7588-90.

18. Raymond KN, Pierre VC. Next generation, high relaxivity gadolinium MRI agents. *Bioconjugate chemistry*. 2005;16(1):3-8.

19. Ferreira MF, Martins AF, Martins J a, et al. Gd(DO3A-N-alpha-aminopropionate): a versatile and easily available synthon with optimized water exchange for the synthesis of high relaxivity, targeted MRI contrast agents. *Chemical communications (Cambridge, England)*. 2009;(42):6475-7.

20. Helm L. Relaxivity in paramagnetic systems: Theory and mechanisms. *Progress in Nuclear Magnetic Resonance Spectroscopy*. 2006;49(1):45-64.

21. Borel A, Helm L, Merbach AE. Molecular dynamics simulations of MRI-relevant GdIII chelates: direct access to outer-sphere relaxivity. *Chemistry (Weinheim an der Bergstrasse, Germany)*. 2001;7(3):600-10.

22. Aime S, Botta M, Fasano M, Crich SG, Terreno E. H and 17 O-NMR relaxometric investigations of paramagnetic contrast agents for MRI . Clues for higher relaxivities. *Coordination Chemistry Reviews*. 1999;186:321 - 333.

23. Aime S, Botta M, Ermondi G. NMR study of solution structures and dynamics of lanthanide(III) complexes of DOTA. *Inorganic Chemistry*. 1992;31(21):4291-4299.

24. Bari L Di, Salvadori P. Static and Dynamic Stereochemistry of Chiral Ln DOTA Analogues. *Chemphyschem : a European journal of chemical physics and physical chemistry*. 2011;12(8):1490-7.

25. Aime S, Botta M, Fasano M, et al. Conformational and Coordination Equilibria on DOTA Complexes of Lanthanide Metal Ions in Aqueous Solution Studied by (1)H-NMR Spectroscopy. *Inorganic chemistry*. 1997;36(10):2059-2068.

26. Benetollo F, Bombieri G, Calabi L, Aime S, Botta M. Structural variations across the lanthanide series of macrocyclic DOTA complexes: insights into the design of contrast agents for magnetic resonance imaging. *Inorganic chemistry*. 2003;42(1):148-57.

27. Purgel M, Baranyai Z, Blas A de, et al. An NMR and DFT investigation on the conformational properties of lanthanide(III) 1,4,7,10-tetraazacyclododecane-1,4,7,10-tetraacetate analogues containing methylenephosphonate pendant arms. *Inorganic chemistry*. 2010;49(9):4370-82.

28. Vojtísek P, Cígler P, Kotek J, et al. Crystal structures of lanthanide(III) complexes with cyclen derivative bearing three acetate and one methylphosphonate pendants. *Inorganic chemistry*. 2005;44(16):5591-9.

29. Kotek J, Rudovsk\`y J, Hermann P, Lukeš I. Three in One: TSA, TSA', and SA Units in One Crystal Structure of a Yttrium (III) Complex with a Monophosphinated H4dota Analogue. *Inorganic chemistry*. 2006;45(7):3097–3102.

30. Lukeš I, Kotek J, Vojtíšek P, Hermann P. Complexes of tetraazacycles bearing methylphosphinic/phosphonic acid pendant arms with copper(II), zinc(II) and lanthanides(III). A comparison with their acetic acid analogues. *Coordination Chemistry Reviews*. 2001;216-217:287-312.

31. Kotková Z, Pereira G a, Djanashvili K, et al. Lanthanide(III) Complexes of Phosphorus Acid Analogues of H 4 DOTA as Model Compounds for the Evaluation of the Second-Sphere Hydration. *European Journal of Inorganic Chemistry*. 2009;2009(1):119-136.

32. Sherry a D, Ren J, Huskens J, et al. Characterization of Lanthanide(III) DOTP Complexes: Thermodynamics, Protonation, and Coordination to Alkali Metal Ions. *Inorganic Chemistry*. 1996;35(16):4604-4612.

33. Rohovec J, Vojtíšek P, Hermann P, et al. Synthesis, crystal structures and NMR and luminescence spectra of lanthanide complexes of 1,4,7,10-tetraazacyclododecane with N-

methylene(phenyl)phosphinic acid pendant arms †. *Journal of the Chemical Society, Dalton Transactions*. 1999;(20):3585-3592.

34. Aime S, Batsanov AS, Botta M, et al. Nuclear magnetic resonance, luminescence and structural studies of lanthanide complexes with octadentate macrocyclic ligands bearing benzylphosphinate groups. *Journal of the Chemical Society, Dalton Transactions*. 1997;(19):3623-3636.

35. Pasha A, Tircsó G, Benyó ET, Brücher E, Sherry AD. Synthesis and Characterization of DOTA-(amide)(4) Derivatives: Equilibrium and Kinetic Behavior of Their Lanthanide(III) Complexes. *European journal of inorganic chemistry*. 2007;2007(27):4340-4349.

36. Kálmán FK, Baranyai Z, Tóth I, et al. Synthesis , Potentiometric , Kinetic , and NMR Studies of with Ca (II), Cu (II), Zn (II) and Lanthanide (III) Ions 3851. *Inorganic chemistry*. 2008;47(9):3851-3862.

37. Laurent S, Elst LV, Muller RN. Comparative study of the physicochemical properties of six clinical low molecular weight gadolinium contrast agents. *Contrast media & molecular imaging*. 2006;1(3):128-37.

38. Acta HC, Kiraly R, Carvalho RA, et al. Tetraazacyclododecane-1 , 4 , 7 , 10-tetraacetic Acid) Substituted at One Acetate Pendant Arm : 1 H-NMR and Potentiometric Studies of the Ligand and Its Lanthanide (III) Complexes. *Helvetica Chimica Acta*. 2005;88.

39. Wang Y-M, Lee C-H, Liu G-C, Sheu R-S. Synthesis and complexation of Gd3+, Ca2+, Cu2+ and Zn2+ by 3,6,10-tri(carboxymethyl)-3,6,10-triazadodecanedioic acid. *Journal of the Chemical Society, Dalton Transactions*. 1998;(24):4113-4118.

40. Balogh E, Tripier R, Fousková P, et al. Monopropionate analogues of DOTA4- and DTPA5-: kinetics of formation and dissociation of their lanthanide(III) complexes. *Dalton transactions (Cambridge, England : 2003)*. 2007;(32):3572-81.

41. Balogh E, Tripier R, Ruloff R, Tóth E. Kinetics of formation and dissociation of lanthanide(III) complexes with the 13-membered macrocyclic ligand TRITA4-. *Dalton transactions (Cambridge, England : 2003)*. 2005;(6):1058-65.

42. Congreve A, Parker D, Gianolio E, Botta M. Steric control of lanthanide hydration state: fast water exchange at gadolinium in a mono-amide “DOTA” complex. *Dalton transactions (Cambridge, England : 2003)*. 2004;(9):1441-5.

43. Jebasingh B, Alexander V. Synthesis and relaxivity studies of a tetranuclear gadolinium(III) complex of DO3A as a contrast-enhancing agent for MRI. *Inorganic chemistry*. 2005;44(25):9434-43.

44. Silvério S, Torres S, Martins AF, et al. Lanthanide chelates of (bis)-hydroxymethyl-substituted DTTA with potential application as contrast agents in magnetic resonance imaging. *Dalton transactions (Cambridge, England : 2003)*. 2009;(24):4656-70.

45. Datta A, Raymond KN. Gd-hydroxypyridinone (HOPO)-based high-relaxivity magnetic resonance imaging (MRI) contrast agents. *Accounts of chemical research*. 2009;42(7):938-47.

46. Dunand FA, Aime S, Merbach AE. First 17 O NMR Observation of Coordinated Water on Both Isomers of [Eu(DOTAM)(H 2 O)] 3+ : A Direct Access to Water Exchange and its Role in the Isomerization 1. *Journal of the American Chemical Society*. 2000;122(7):1506-1512.

47. Dunand FA, Aime S, Lausanne D. First 17 O NMR Observation of Coordinated Water on Both Isomers of [Eu (DOTAM)(H 2 O)] 3 + : A Direct Access to Water Exchange and its Role in the Isomerization 1. *Physiology*. 2000;1(5):1506-1512.

48. Moreau J, Pierrard J-C, Rimbault J, et al. Thermodynamic and structural properties of Eu3+ complexes of a new 12-membered tetraaza macrocycle containing pyridine and N-glutaryl groups as pendant arms: characterization of three complexing successive phases. *Dalton transactions (Cambridge, England : 2003)*. 2007;(16):1611-20.

49. Bellin M-france. MR contrast agents , the old and the new. *European Journal of Radiology*. 2006;60:314-323.

50. Terreno E, Castelli DD, Viale A, Aime S. Challenges for molecular magnetic resonance imaging. *Chemical reviews*. 2010;110(5):3019-42.

51. Langereis S, Dirksen A, Hackeng TM, Genderen MHP van, Meijer EW. Dendrimers and magnetic resonance imaging. *New Journal of Chemistry*. 2007;31(7):1152.

52. Polásek M, Hermann P, Peters J a, Geraldes CFGC, Lukes I. PAMAM dendrimers conjugated with an uncharged gadolinium(III) chelate with a fast water exchange: the influence of chelate charge on rotational dynamics. *Bioconjugate chemistry*. 2009;20(11):2142-53.

53. Shultz MD, Wilson JD, Fuller CE, et al. Metallofullerene-based Nanoplatform for Brain Tumor Brachytherapy and Longitudinal Imaging in a Murine Orthotopic Xenograft Model. *Radiology*. 2011.

54. Geraldes CFGC, Laurent S. Classification and basic properties of contrast agents for magnetic resonance imaging. *Contrast media & molecular imaging*. 2009;4(1):1-23.

55. Karfeld-Sulzer LS, Waters E a, Kohlmeir EK, et al. Protein polymer MRI contrast agents: Longitudinal analysis of biomaterials in vivo. *Magnetic resonance in medicine : official journal of the Society of Magnetic Resonance in Medicine / Society of Magnetic Resonance in Medicine*. 2011;65(1):220-8.

56. Lelyveld VS, Brustad E, Arnold FH, Jasanoff A. Metal-substituted protein MRI contrast agents engineered for enhanced relaxivity and ligand sensitivity. *Journal of the American Chemical Society*. 2011;133(4):649-51.

57. Shapiro MG, Westmeyer GG, Romero P a, et al. Directed evolution of a magnetic resonance imaging contrast agent for noninvasive imaging of dopamine. *Nature biotechnology*. 2010;28(3):264-70.

58. Westmeyer GG, Durocher Y, Jasanoff A. A secreted enzyme reporter system for MRI. *Angewandte Chemie (International ed. in English)*. 2010;49(23):3909-11.

59. Westmeyer GG, Jasanoff A. Genetically controlled MRI contrast mechanisms and their prospects in systems neuroscience research. *Magnetic resonance imaging*. 2007;25(6):1004-10.

60. Ziv K, Meir G, Harmelin A, et al. Ferritin as a reporter gene for MRI: chronic liver over expression of H-ferritin during dietary iron supplementation and aging. *NMR in biomedicine*. 2010;23(5):523-31.

61. Terashima M, Uchida M, Kosuge H, et al. Human ferritin cages for imaging vascular macrophages. *Biomaterials*. 2011;32(5):1430-7.

62. Frullano L, Meade TJ. Multimodal MRI contrast agents. *Journal of biological inorganic chemistry : JBIC : a publication of the Society of Biological Inorganic Chemistry*. 2007;12(7):939-49.

63. Bonnet CS, Tóth É. Towards highly efficient, intelligent and bimodal imaging probes: Novel approaches provided by lanthanide coordination chemistry. *Comptes Rendus Chimie*. 2010;13(6-7):700-714.

64. Bünzli J-CG. Lanthanide luminescence for biomedical analyses and imaging. *Chemical reviews*. 2010;110(5):2729-55.

65. Eliseeva SV, Bünzli J-CG. Lanthanide luminescence for functional materials and bio-sciences. *Chemical Society reviews*. 2010;39(1):189-227.

66. Uh H, Petoud S. Novel antennae for the sensitization of near infrared luminescent lanthanide cations. *Comptes Rendus Chimie*. 2010;13(6-7):668-680.

67. Zhang J, Badger PD, Geib SJ, Petoud S. Sensitization of near-infrared-emitting lanthanide cations in solution by tropolonate ligands. *Angewandte Chemie (International ed. in English)*. 2005;44(17):2508-12.

68. Weissleder R, Ntziachristos V. Shedding light onto live molecular targets. *Nature medicine*. 2003;9(1):123-8.

69. Corsi DM, Platas-Iglesias C, Bekkum HV, Peters J a. Determination of paramagnetic lanthanide(III) concentrations from bulk magnetic susceptibility shifts in NMR spectra. *Magnetic Resonance in Chemistry*. 2001;39(11):723-726.

70. Peters JA, Huskens J, Raber DJ. Lanthanide induced shifts and relaxation rate enhancements. *Progress in Nuclear Magnetic Resonance Spectroscopy*. 1996;28(3-4):283-350.

71. Forsberg JH, Delaney RM, Zhao Q, Harakas G, Chandran R. Analyzing Lanthanide-Induced Shifts in the NMR Spectra of Lanthanide(III) Complexes Derived from 1,4,7,10-Tetrakis(N,N-diethylacetamido)-l,4,7,lO-tetraazacyclododecane. *Inorganic Chemistry*. 1995;(34):3705-3715.

72. Terazzi E, Rivera J-P, Ouali N, Piguet C. A justification for using NMR model-free methods when investigating the solution structures of rhombic paramagnetic lanthanide complexes. *Magnetic resonance in chemistry : MRC*. 2006;44(5):539-52.

73. Lisowski J, Sessler JL, Lynch V, Mody TD. 1H NMR Spectroscopic Study of Paramagnetic Lanthanide(III) Texaphyrins. Effect of Axial Ligation. *Journal of the American Chemical Society*. 1995;117(8):2273-2285.

74. Barge A, Cravotto G, Gianolio E, Fedeli F. How to determine free Gd and free ligand in solution of Gd chelates . A technical note. *Contrast media & molecular imagingMolecular Imaging*. 2006;188(September):184-188.

75. Pereira G, Ball L, Sherry AD, Peters J, Geraldes CFGC. NMR Characterization of Lanthanide(3+) Complexes of Tetraazatetrakisphosphinato and Tetraazatetrakisphosphonato Ligands. *Helvetica Chimica Acta*. 2009;92(11):2532-2551.

76. Becke AD. Density-functional thermochemistry. IV. A new dynamical correlation functional and implications for exact-exchange mixing. *The Journal of Chemical Physics*. 1996;104(3):1040.

77. Adamo C, Barone V. Exchange functionals with improved long-range behavior and adiabatic connection methods without adjustable parameters: The mPW and mPW1PW models. *The Journal of Chemical Physics*. 1998;108(2):664.

78. Frisch, M. J.; Trucks, G. W.; Schlegel, H. B.; Scuseria, G. E.; Robb, M. A.; Cheeseman, J. R.; Scalmani, G.; Barone, V.; Mennucci, B.; Petersson, G. A.; Nakatsuji, H.; Caricato, M.; Li, X.; Hratchian, H. P.; Izmaylov, A. F.; Bloino, J.; Zheng, G.; Sonnenb DJG. Gaussian 09, Revision A.01. 2009.

79. Dolg M, Stoll H, Savin A, Preuss H. Energy-adjusted pseudopotentials for the rare earth elements. *Theoretica Chimica Acta*. 1989;75(3):173-194.

80. Tomasi J, Mennucci B, Cammi R. Quantum mechanical continuum solvation models. *Chemical reviews*. 2005;105(8):2999-3093.

81. Laurent S, Vander Elst L, Henoumont C, Muller RN. How to measure the transmetallation of a gadolinium complex. *Contrast media & molecular imaging*. 2010;5(6):305-8.

82. Rudovský J, Hermann P, Botta M, Aime S, Lukes I. Dendrimeric Gd(III) complex of a monophosphinated DOTA analogue: optimizing relaxivity by reducing internal motion. *Chemical communications (Cambridge, England)*. 2005;(18):2390-2.

83. Táborský P, Svobodová I, Lubal P, et al. Formation and dissociation kinetics of Eu(III) complexes with H5do3ap and similar dota-like ligands. *Polyhedron*. 2007;26(15):4119-4130.

84. Campello MPC, Lacerda S, Santos IC, et al. Lanthanide(III) complexes of 4,10-bis(phosphonomethyl)-1,4,7,10-tetraazacyclododecane-1,7-diacetic acid (trans-H6do2a2p) in solution and in the solid state: structural studies along the series. *Chemistry (Weinheim an der Bergstrasse, Germany)*. 2010;16(28):8446-65.

85. Balbina M, Santos I. tetraazacyclododecan-1-yl] acetic Acid (H 7 DOA3P): Multinuclear-NMR and Kinetic Studies. *Helvetica Chimica Acta*. 2009;92:2398-2413.

86. Gano L, Marques F, Campello MP, et al. Radiolanthanide complexes with tetraazamacrocycles bearing methylphosphonate pendant arms as bone seeking agents. *Quarterly Journal of Nuclear Medicine*. 2007;(March):6-15.

87. Balogh E, Tripier R, Fousková P, et al. Monopropionate analogues of DOTA4- and DTPA5-: kinetics of formation and dissociation of their lanthanide(III) complexes. *Dalton transactions (Cambridge, England : 2003)*. 2007;(32):3572-81.

88. Keire D a, Jang YH, Li L, et al. Chelators for radioimmunotherapy: I. NMR and ab initio calculation studies on 1,4,7,10-tetra(carboxyethyl)-1,4,7,10-tetraazacyclododecane (DO4Pr) and 1,4,7-tris(carboxymethyl)-10-(carboxyethyl)-1,4,7,10-tetraazacyclododecane (DO3A1Pr). *Inorganic chemistry*. 2001;40(17):4310-8.

89. Lima LMP, Delgado R, Esteves CV, et al. Cyclen derivatives with three methylphosphonate pendant arms : synthesis and study of the effect of an additional pendant arm on metal complexation. *Submitted to Inorganic chemistry*. 2011.

90. Delgado R, Félix V, Lima LMP, Price DW. Metal complexes of cyclen and cyclam derivatives useful for medical applications: a discussion based on thermodynamic stability constants and structural data. *Dalton transactions (Cambridge, England : 2003)*. 2007;(26):2734-45.

91. Burai L, Tóth É, Merbach AE. HPLC separation of diastereomers of LnIII-ethylenepropylene-triamine-pentaacetate complexes. Direct assessment of their water exchange rateElectronic supplementary information (ESI) available: Table S1?S4 and Figs. S1 and S2. See http://www.rsc.org/suppda. *Chemical Communications*. 2003;(21):2680.

92. Laus S, Ruloff R, Tóth E, Merbach AE. GdIII complexes with fast water exchange and high thermodynamic stability: potential building blocks for high-relaxivity MRI contrast agents. *Chemistry (Weinheim an der Bergstrasse, Germany)*. 2003;9(15):3555-66.

93. Ruloff R, Tóth É, Scopelliti R, et al. Accelerating water exchange for GdIII chelates by steric compression around the water binding siteElectronic supplementary information (ESI) available: synthesis of TRITA and TRITA-bz-NO2-17O relaxation rates and chemical shifts for GdIII chelates. See ht. *Chemical Communications*. 2002;(22):2630-2631.

94. Vitha T, Kubícek V, Kotek J, et al. Gd(iii) complex of a monophosphinate-bis(phosphonate) DOTA analogue with a high relaxivity; Lanthanide(iii) complexes for imaging and radiotherapy of calcified tissues. *Dalton transactions (Cambridge, England : 2003)*. 2009;(17):3204-14.

95. Polásek M, Sedinová M, Kotek J, et al. Pyridine-N-oxide analogues of DOTA and their gadolinium(III) complexes endowed with a fast water exchange on the square-antiprismatic isomer. *Inorganic chemistry*. 2009;48(2):455-65.

96. Polásek M, Kotek J, Hermann P, et al. Lanthanide(III) complexes of pyridine-N-oxide analogues of DOTA in solution and in the solid state. A new kind of isomerism in complexes of DOTA-like ligands. *Inorganic chemistry*. 2009;48(2):466-75.

97. Polásek M, Rudovský J, Hermann P, et al. Lanthanide(III) complexes of a pyridine N-oxide analogue of DOTA: exclusive M isomer formation induced by a six-membered chelate ring. *Chemical communications (Cambridge, England)*. 2004;2(22):2602-3.

98. Keizers PHJ, Saragliadis A, Hiruma Y, Overhand M, Ubbink M. Design, synthesis, and evaluation of a lanthanide chelating protein probe: CLaNP-5 yields predictable paramagnetic effects independent of environment. *Journal of the American Chemical Society*. 2008;130(44):14802-12.

99. Pellegatti L, Zhang J, Drahos B, et al. Pyridine-based lanthanide complexes: towards bimodal agents operating as near infrared luminescent and MRI reporters. *Chemical communications (Cambridge, England)*. 2008;(48):6591-3.

100. Crich SG, Biancone L, Cantaluppi V, et al. Improved route for the visualization of stem cells labeled with a Gd-/Eu-chelate as dual (MRI and fluorescence) agent. *Magnetic resonance in medicine : official journal of the Society of Magnetic Resonance in Medicine / Society of Magnetic Resonance in Medicine*. 2004;51(5):938-44.

101. Koullourou T, Natrajan LS, Bhavsar H, et al. Synthesis and spectroscopic properties of a prototype single molecule dual imaging agent comprising a heterobimetallic rhenium-gadolinium complex. *Journal of the American Chemical Society*. 2008;130(7):2178-9.

102. Andrews M, Ward B, Laye R, Kariuki B, Pope S â€ ..A. Sensitized Lanthanide-Ion Luminescence with Aryl-Substituted N -(2-Nitrophenyl)acetamide-Derived Chromophores. *Helvetica Chimica Acta*. 2009;92(11):2159-2172.

103. Moore EG, Szigethy G, Xu J, et al. 3-Hydroxypyridin-2-one complexes of near-infrared (NIR) emitting lanthanides: sensitization of holmium(III) and praseodymium(III) in aqueous solution. *Angewandte Chemie (International ed. in English)*. 2008;47(49):9500-3.

104. Toth E, Brucher E, Lazar I, Toth I. Kinetics of Formation and Dissociation of Lanthanide(III)-DOTA Complexes. *Inorganic Chemistry*. 1994;33(18):4070-4076.

105. Quici S, Cavazzini M, Marzanni G, et al. Visible and near-infrared intense luminescence from water-soluble lanthanide [Tb(III), Eu(III), Sm(III), Dy(III), Pr(III), Ho(III), Yb(III), Nd(III), Er(III)] complexes. *Inorganic chemistry*. 2005;44(3):529-37.